

Washington University in St. Louis

Washington University Open Scholarship

All Theses and Dissertations (ETDs)

5-24-2011

The Interaction of Cofilin with the Actin Filament

Diana Wong

Washington University in St. Louis

Follow this and additional works at: <https://openscholarship.wustl.edu/etd>

Recommended Citation

Wong, Diana, "The Interaction of Cofilin with the Actin Filament" (2011). *All Theses and Dissertations (ETDs)*. 902.

<https://openscholarship.wustl.edu/etd/902>

This Dissertation is brought to you for free and open access by Washington University Open Scholarship. It has been accepted for inclusion in All Theses and Dissertations (ETDs) by an authorized administrator of Washington University Open Scholarship. For more information, please contact digital@wumail.wustl.edu.

WASHINGTON UNIVERSITY IN ST. LOUIS

School of Engineering and Applied Science

Department of Biomedical Engineering

Thesis Examination Committee:

David Sept, Chair

Frank Yin, Co-Chair

Anders Carlsson

John Cooper

Vitaly Klyachko

Jay Ponder

The Interaction of Cofilin with the Actin Filament

by

Diana Yi Fei Wong

A dissertation presented to the Graduate School of Arts and Sciences
of Washington University in partial fulfillment of the
requirements for the degree of

DOCTOR OF PHILOSOPHY

May 2011

Saint Louis, Missouri

copyright by
Diana Yi Fei Wong
2011

ABSTRACT OF THE DISSERTATION

The Interaction of Cofilin with the Actin Filament

by

Diana Yi Fei Wong

Doctor of Philosophy in Biomedical Engineering

Washington University in St. Louis, 2011

Research Advisor: Professor David Sept

The regulation of filamentous actin (F-actin) production from the polymerization of globular actin (G-actin) within the cell is critical for many cell functions. Since actin is found in all cells, understanding how actin-binding-proteins (ABPs) bind and how their regulating mechanisms work is not only important to the basics of cytoskeletal pathways, but also to understanding associated diseases and creating possible therapeutics to combat them.

Cofilin is an ABP that plays an important part in the regulation process and in recent times, has come to be known as a player in maintaining a cell's homeostasis. It's activity has been shown to have implications in many diseases, such as Alzheimer's and certain cancers. Cofilin binds and severs actin filaments, leading to depolymerization as well as the creation of new barbed ends. Although some of the details of cofilin's interaction with G-actin have been illuminated through a range of experimental studies, the specific interactions with F-actin have remained much more elusive. As of yet, there are only cryoEM models of cofilin-bound F-actin (where the binding occurs

at a 1:1 ratio), which are not high enough resolution and do not show molecular interactions. The focus of this research is to build a model of how cofilin binds F-actin and understand the mechanism of severing.

Computational methods, such as protein-protein docking, all atom molecular dynamics (AA MD) simulations, and Coarse Grain MD (CG MD) can help in understanding the interactions between cofilin and F-actin. Iteratively combining these methods with biochemical and mutagenesis experiments to reach a consensus offer a guide towards a more cogent answer. Here in this dissertation, I describe how I built a cofilin and F-actin binding model, with the aid of empirical data. This work allowed me to create several filament models with varying number of bound cofilin, which replicates different binding states of the filament. I also simulated the dynamics of these filaments models to gain insight into filament behavior, particularly twist.

Acknowledgments

The text of this thesis is about the science of proteins. Let us take a break for some momentary blasphemy. For me, the molecular interactions I studied were just as important as the human interactions over the last seven years. This phase of my life and career have in large part been about the countless good people with whom I have had the privilege of sharing my life and experiences. I have tried to live the life of a good scientist, skeptical as always, but I would not be the person I have become without mentors and friends. Here I hope to pay homage to them:

I want to first thank Dave, the captain of our ship, whose mentorship led the way to this body of work. His kind friendship and laissez-faire style has helped me developed into a scientist in my own right. I deeply appreciate that he allowed my outrageous displays of self-expression (even in science) when it would have been much easier (and less embarrassing) to curb my dynamic personality.

My fellow shipmates, past and present, have been good company on this adventure. Thanks to all of them—particularly Akansha, Karthik, Hoon, and Frank who have seen me to the other side of the Ph.D. The CCB has been the nexus of some great times, especially Hoang T., Matt W., Sunjoo L., Mike S., and Chuanjie W. whom I have learned so much with and from. Our group may be dissolved but the hilarity won't be so easily forgotten.

While I took orders from one captain, there have been others who had other lessons to offer. Jay Ponder selflessly taught me and anyone else who wanted to learn, regardless of what he was doing at the time. Garland Marshall, when I was an unsure first year, guided me to a laurel that gave me the confidence to keep going. Dr. Yin, Gary Stormo, and a handful of other unnamed professors have put the scientific world in a different perspective for me and I thank them for their honest conversations. Also, I am grateful to the National Science Foundation for allowing me to be a Graduate Research Fellow and supporting me in more ways than one.

The Usual Suspects have been a great source of happiness and camaraderie. Dick Wu, has been a true supportive friend from the beginning to the end. He is the pinnacle of reliability and understanding, and a quintessential example of the best of friendships. A number of other friends have also been great sources of encouragement (Dan K., Christina C., Alice H., Glen R., Karen T., Kaoru H., Ben T., Kavitha K.). Also, thank you all my Aikido friends

who have given me a family away from research, where I could rest my weary head—in an arm pin on the dojo floors or near head-on collision with someone twice my size.

Our re-stationing to Michigan surprisingly opened my eyes to a new world that I had forgotten existed. While we may have been on an island, in terms of research colleagues, new friends unexpectedly brightened my life. Robinson, David, and Katharine, the first of newfound kindness, along with many others have been the light during cloudy days.

Thank you, everyone from Missouri to Michigan, and everywhere else whom I can't fit in this already long declaration, for fighting all those pirates and dodging canon balls with me!

I want to give a special note of gratitude to Akansha Saxena, my best friend, loyal lab mate and source of meaningful discussion, who from day one of our graduate studies has been my most supportive companion, through even my darkest of times. Without her—my compass—I most certainly would have been lost and alone (and at times, starving).

My bright beacon of light in the stormiest of seas has been my other best friend, my confidant, my beloved anchor of hope—Tony C. Yang. Voluntarily staying up late nights with me on the phone so I could work with company, he has also offered me the greatest solace and encouragement during the final battles that only I could fight. Through him, I am reminded each day what joy is.

While they could only watch me struggle on the high seas from afar, my parents and sisters—Khim, Ooi, Jenny and Linda—have offered the best ammunition to keep fighting: their unconditional love and never-ending support. They are the lighthouse and home base to which I can always return. BaBa made a scientist out of me. As an impressionable five year old, I thought, “If a poor village boy with nothing could get a Ph.D., surely I could, too?” MaMa made great sacrifices so that her children may live a better life than her—a gift I try not to squander. I can only hope that I managed to learn the virtues of strength, resolve, and fortitude from her.

May the adventure continue for me with all my loved ones by my side!

Diana Yi Fei Wong

Washington University in Saint Louis
March 2011

This dissertation is dedicated to my mother and father

親愛的媽媽爸爸

Khim and Dr. Ooi,

typical immigrant parents who worked hard and sacrificed for the ultimate goal that their children
have better lives than they did.

Contents

Abstract	ii
Acknowledgments	iv
List of Tables	x
List of Figures	xi
Preface	xiii
1 Introduction	1
1.1 Actin	1
1.1.1 Dendritic Nucleation Model of F-actin	2
1.1.2 Structure of G-actin	4
1.1.3 Structure of F-actin	6
1.2 ADF/Cofilin Proteins	9
1.2.1 Other ADF Homology (ADF-H) Domain proteins	10
1.2.2 Structure of Cofilin	11
1.3 Actin and Cofilin Interactions	13
1.3.1 Binding Surface	13
1.4 Regulation of Cofilin	15
1.4.1 On and Off: Ser3 Phosphorylation	16
1.4.2 When to throw the switch? pH Regulation	17
1.4.3 Oxidative Stress/Oxidation	19
1.5 Cofilin's Effects on F-actin	20
1.5.1 Twist and Destabilization	20
1.5.2 Structural Effects	21
1.5.3 Concentration Modulation	23
1.6 Previous Modeling	25
1.7 Medical Significance: Alzheimer's Disease, etc.	25
1.8 Synopsis of Thesis	28
1.8.1 Specific Goals	28
2 Computational Methods	29
2.1 Molecular Docking	29
2.1.1 Basic components	30
2.1.2 Choosing the correct tool	31

2.1.3	Preparing the molecules	32
2.1.4	Iterative docking and analysis	34
2.1.5	Post analysis	35
2.2	Coarse Grain Molecular Dynamics (CGMD)	36
2.2.1	Shape-Based Coarse Graining: SBCG	36
2.2.2	Residue-Based Coarse Graining: RBCG	37
3	The Interaction of Cofilin with the Actin Filament	38
3.1	Introduction	38
3.2	Methods	40
3.2.1	Secondary Structure Alignment	40
3.2.2	Docking and Refinement Simulations	40
3.2.3	Molecular Dynamics Simulations	42
3.3	Results	42
3.3.1	Secondary Structure Alignment	42
3.3.2	Model for the Cofilin/F-actin Complex	43
3.3.3	Analysis of Known Cofilin Mutations	47
3.4	Discussion	59
4	Short-Ranged Dynamics of Cofilin-Bound Actin Filaments	61
4.1	Introduction	61
4.2	Methods	62
4.2.1	Building Filament models	62
4.2.2	All-Atom (AA) Molecular Dynamics (MD) Simulation	62
4.3	Results	64
4.3.1	Maintaining Binding Contacts	65
4.3.2	Contact Analysis	68
4.3.3	Root Mean Squared Fluctuation (RMSF)	69
4.3.4	Principle Component Analysis (PCA)	72
4.4	Discussion	74
4.4.1	RMSD	74
4.4.2	Contact Points	74
4.4.3	RMSF	74
4.4.4	PCA	75
5	Long-Ranged Dynamics of Cofilin-Bound Actin Filaments	76
5.1	Introduction	76
5.2	Methods	77
5.2.1	Building Coarse Grain Models	77
5.2.2	Coarse Grain Molecular Dynamics (CGMD) Simulation	79
5.2.3	Defining Metrics	82
5.3	Results	85
5.3.1	Maintaining Contacts (Relative RMSD)	85

5.3.2	Twist	85
5.3.3	Distance Measurements	93
5.4	Discussion	95
6	Conclusions and Future Work	99
6.1	Part 1: The Interaction of Cofilin with the Actin Filament	99
6.1.1	Future Work	99
6.2	Part 2: Short-Ranged Dynamics of Cofilin-Bound Actin Filaments: . .	100
6.2.1	Future Work	100
6.3	Part 3: Long-Ranged Dynamics of Cofilin-Bound Actin Filaments . .	100
6.3.1	Future Work	101
	References	103
	Curriculum vitae	117

List of Tables

1.1	Kinetics Data from Kuhn and Pollard 2005	2
1.2	Data from Mutagenesis Studies	15
1.3	Filament Twist Data	20
3.1	PDB IDs	44
3.2	Salt Bridge Contacts of Known and New Residues	48
3.3	Complete Annotated Table of Human Cofilin	55
4.1	All Atom Simulation Details	65
4.2	Solvent Accessible Surface Area (SASA) Analysis	69
5.1	Coarse Grain Simulation Details	82
5.2	Average Twist	89

List of Figures

1.1	Treadmilling	3
1.2	Actin Structures and Some Actin Binding Proteins (ABPs)	3
1.3	Apr2/3 Dendritic Model	4
1.4	Structure of G-actin	5
1.5	Structure of F-actin	7
1.6	ADF-H Domain	11
1.7	Human and Yeast Cofilin	12
1.8	Bare (F-actin) and Decorated (Cofilactin) Filament	13
1.9	pH Regulation	18
1.10	F-actin's Conformational States	22
1.11	Model of Cofilin Binding and Severing	25
2.1	The Standard Docking Protocol	34
3.1	Structural Alignment	43
3.2	A structure-based sequence alignment for seven ADF/cofilin proteins and homologs	44
3.3	A structural alignment of human cofilin and yeast cofilin.	45
3.4	RMSD of Best Docked Models	46
3.5	Molecular details of the interaction between cofilin and the actin filament.	47
3.6	Comparison of our cofilin/F-actin complex	47
3.7	Actin-P and Actin-B	49
3.8	Contact residues that match cofilin mutagenesis	49
3.9	New binding model contact residues on cofilin	53
4.1	All Atom Filament Models	63
4.2	RMSD of Filament	66
4.3	Actin Contacts	68
4.4	Cofilin Contacts	69
4.5	RMSF of Bare and Decorated Filaments	70
4.6	RMSF of Sparse and Split Filaments	71
4.7	Distribution of PCA	73
5.1	Coarse Graining Protocol	78
5.2	Lennard-Jones Potential of AA and CG	79
5.3	Coarse Grain Filament Models	80
5.4	CG Simulation Protocol	82

5.5	Definition of Metrics	83
5.6	Twist	84
5.7	RMSD of CG Decorated and Sparse Filament	86
5.8	Example of Filament Twist from Trifurcating Simulation	87
5.9	Coarse Grain Filaments	88
5.10	Average Twist of 3 Simulations of 3 Filaments	89
5.11	Trifurcating Simulation	90
5.12	Distribution of Twist	91
5.13	Twist Over Time	92
5.14	Filament Lengths over Time	94
5.15	Distribution of Bare Filament Twist	96

Preface

The research described in this dissertation concerning cofilin and F-actin began in Spring 2008 but the bulk of the work did not really take flight until our move to University of Michigan, Ann Arbor. As alluded to in the Acknowledgments section, UMich has been a great environment to work in and I will never forget the nearly two years spent there.

There are two other major projects that I worked on during my tenure on the WashU campus. While they have not produced publications, the experiences I gained from them have had a deep impact on my graduate student learning. In the first project, I reparameterized docking software for the purpose of predicting protein-protein binding. In the second project, I employed the polarizable force field, AMOEBA, from Jay Ponders lab to find binding energy between Serine proteases and their respective drugs in an effort to adapt the force field for docking purposes. I am grateful for all the time and patience that Jay, Chuanjie Wu, and Mike Schnieders took to teach me about force fields and the grueling accompanying task of parameterizing new molecules.

Ideally I would like to discuss these projects in more detail so that the years of work I put into them does not go by the wayside, but time and energy do not permit it. At the very least, hands on experience with docking software has enabled a more knowledgeable approach when performing such endeavors on the cofilin-actin work.

The following will be a discussion of how a specific biological question about a particular protein system can be answered using computational methods. The first chapter is a primer on actin filaments that will help establish the problem, with more attention focused on directly relevant literature. The following three chapters describe the story of how I tried to answer that question in a sequence of steps that lead from one to the next. Finally, in the last chapter I make final conclusions and remarks of the

process. And should there be a confusion of voice, sometimes it is the royal we who is speaking.

Chapter 1

Introduction

Actin is a protein found in all eukaryotic cells, first isolated by Straub from muscle in 1942. (Kabsch and Vandekerckhove 1992) It is essential to many cellular functions, such as mitosis, motility and migration, and cell signaling. As an important part of cytoskeleton, it has the job of supporting cell structure by forming filaments made up of actin monomers. In order for it to be dynamically changing, to satisfy the needs of the cell, it also has to exert forces or go to different parts of the cell. It does so by growing and shrinking. As vital as actin filaments may be, it is the whole system of proteins involved and their proper regulation of how they work that is integral to function. Cofilin is one actin-binding protein (ABP) responsible for protein policing. Preferentially binding to ADP-actin, it not only aids in depolymerization at the pointed end and works to bring actin monomers to the barbed end for elongation, but also severs filaments, giving rise to more sites of depolymerization. The exact details of how cofilin binds (Wriggers et al. 1998, Kamal et al. 2007, Paavilainen et al. 2008) and severs remains controversial and is only conjectured upon. The molecular mechanism of this process is the focus of this dissertation.

1.1 Actin

A single monomer of actin, or **globular actin**, is known as G-actin. When these monomers polymerize, they become **filamentous actin**, or F-actin. As one pillar of three components in the cytoskeleton, filaments offer a structural support system to the cell. Actin has high sequence identity and conservation across eukaryotic cells and high protein expression is testament to its profound importance. (Doolittle 1995)

1.1.1 Dendritic Nucleation Model of F-actin

In order for filaments to form, there must be a concentration of available G-actin to allow for binding and polymerization. A filament begins to grow either due to nucleation or branching from an existing filament and continues in its *elongation* phase. Polymerization occurs favorably at one end, the barbed end, and preferentially with ATP-actin; this can also be an indication that the end with ATP-actin is newer in age. As a filament ages, the ATP is dephosphorylated to become ADP-actin, which associates at negligible rates. (Kuhn and Pollard 2005) Kinetics dictate that the barbed end will grow and the pointed end will depolymerize.

The **rate of polymerization** has been observed in real-time measurements using TIRF (total internal reflection fluorescence microscopy). (Kuhn and Pollard 2005) The association and dissociation rates were measured for barbed and pointed ends about the critical actin concentration levels and can be seen in Table 1.1. The ADP-

Table 1.1: Kinetics Data from Kuhn and Pollard 2005

	k_a ($\mu\text{M}^{-1}\text{s}^{-1}$)	k_d (s^{-1})
ATP @ Barbed	7.4	0.89
@ Pointed	0.56	1.4
ADP @ Barbed		1.4
@ Pointed		0.16

actin that is most likely to dissociate rejoins the pool of G-actin available to re-polymerize at the barbed end of a filament again, often with the aid of a chaperone and phosphorylation. Cofilin is one such ABP that aids in this recycling of G-actin (to be discussed in detail later). (Didry et al. 1998, Carlier and Pantaloni 1997)

This phenomenon of growth at one end and recycling is known as **treadmilling** (See Figure 1.1) and first observed from gelsolin-capped actin *in vitro*. (Lanni et al. 1981, Selve and Wegner 1986) It is elegant and simple how the differences of association and dissociation rates make this possible. As an example, this process allows for filaments to grow toward the edge of a cell and push the membrane in creating filopodia or lamellipodia. Pollard and Borisy 2003 is a good review on this type of assembly/disassembly driven cell motility. Capping proteins cap the barbed end and prevent elongation while Arp2/3 complexes allow for branching in the middle

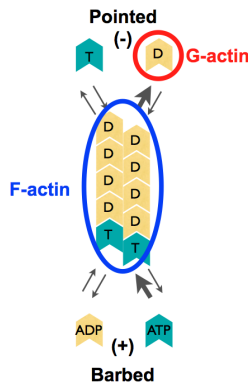


Figure 1.1: Treadmilling

of a filament, as can be seen in Figure 1.2. (Pollard and Cooper 2009) The Arp2/3 nucleation model, Figure 1.3, shows how a number of proteins play together as a system.

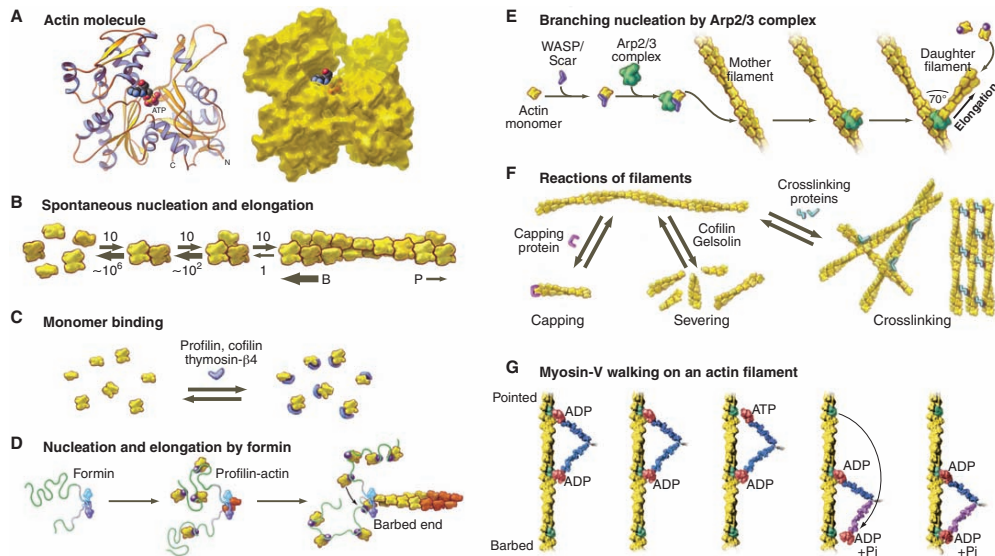


Figure 1.2: Actin Structures and Some Actin Binding Proteins (ABPs): Figure reprinted from Pollard and Cooper 2009.

The **Arp2/3 complex**, comprised of 2 actin-related proteins and 5 other proteins, nucleates new filaments at a 70° angle from the existing filament—this dendritic network can be found in lamellipodia, for example. (Robinson et al. 2001) Cofilin can modulate this ebbing and flowing of the dendritic network, at least *in vivo*, since

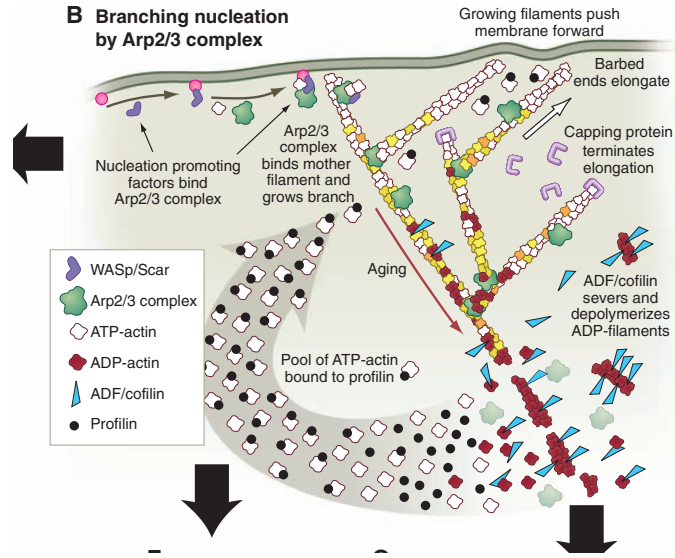


Figure 1.3: Arp2/3 Dendritic Model: Figure reprinted from Pollard and Cooper 2009.

cofilin severing allows for actin to be recycled by acting as a chaperone to ADP-actin, getting it phosphorylated, and bringing it to the elongating edge. (Bernstein and Bamberg 2010) Cofilin competes with Arp23, decreasing Arp2/3's affinity for actin filaments and according to *in vitro* studies, also decreases branch stability and enhances branch removal. (Chan et al. 2009)

Tropomyosin binds F-actin and stabilizes the filament but also inhibits cofilin binding because part of tropomyosin's binding site overlaps with that of cofilin. (Kuhn and Bamberg 2008)

1.1.2 Structure of G-actin

An actin monomer is approximately 42 kDa and 375 residues long. Because G-actin so readily polymerizes (especially in crystallization concentrations), its structure was resolved in the 1990 Kabsch et. al. atomic crystal structure model of rabbit skeletal muscle actin complexed to pancreatic deoxyribonuclease I, with a resolution of 2.8 Å in the ATP form and 3.0 Å in the ADP form. (Kabsch et al. 1990) It was only later when actin was modified by tagging with a tetramethylrhodamine (TMR) at C374, which inhibits actin treadmilling, was a 1.54 Å resolution ADP-actin monomer

crystal structure was resolved (PDB ID 1J6Z). See the translucent shadow G-actin in Figure 1.4 for structure. (Otterbein et al. 2001)

In the structure (Figure 1.4), there are **four subdomains (SD)**, clockwise from the top right quadrant in the order of SD2 (blue residues 32-69), SD1 (red residues 1-31, 70-144 , 338-375), SD3 (yellow residues 145-180, 270-337), and SD4 (green residues 181-269). There is a nucleotide binding cleft at the center of all four domains to which ATP or ADP, when dephosphorylated, may bind.

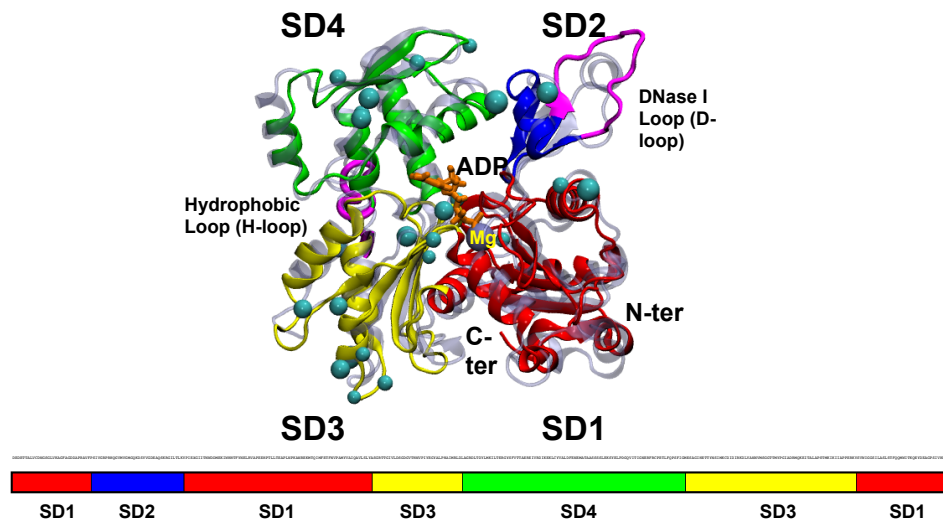


Figure 1.4: Structure of G-actin: Oda’s 2009 2ZWH model is opaque, Otterbein’s 2001 1J6Z is the translucent shadow. Oda’s DNase I loop is more loop than helix. Cyan beads correspond to mutagenesis that is lethal to cofilin binding. (Rodal et al. 1999)

The structure of G-actin makes little sense without putting it in context with F-actin as specific parts of the globular form are structurally important to understanding how F-actin can be as strong of a building block it is. F-actin can be either viewed as a double-stranded helix or two unit spiral, as seen in Figure 1.5. SD3 and SD4 interact with other protomers (monomers in bound in filament form) and make up the core of the filament. Residues 262-274, between SD3 and S4 are known as the **hydrophobic plug or H-loop**. Along with the C-terminal, it may be essential to stability and account for lateral contacts within the filament. (Owen and DeRosier 1993) As the name implies, it is a buried portion of actin that locks itself with a protomer on the other double strand.

Another component extremely important to stability is the **DNase I loop or D-loop**, in residues 38-52. In the Holmes and Lorenz F-actin models (to be covered in the next section), it was first proposed to be important to longitudinal contacts, as in the between the protomers within the two strands. (Holmes et al. 1990) Being very flexible, there have been many observed conformations of D-loop that range from disordered loops to helices. (Muhlrad et al. 1994, Orlova and Egelman 1993, Strzelecka-Gołaszewska et al. 1995, Kim et al. 1996, Khaitlina and Strzelecka-Gołaszewska 2002)

The nucleotide in actin has been found to be of importance to stability since Nucleotide-free actin (NFA), created by using denaturants (e.g. urea) to remove the ADP/ATP and stabilized by sucrose, quickly denature. (Asakura 1961) In high concentrations of sucrose, NFAs can polymerize, showing that nucleotides are not necessary for filament formation, but ADP is needed for monomer stabilization, regulating mechanics and dynamics (to be covered in the Section 1.2 about ATP hydrolysis), and as an indicator for filament age (for depolymerization purposes). (De la Cruz et al. 2000)

1.1.3 Structure of F-actin

While actin monomers can be crystallized, filaments polymerize to irregular lengths and have not been crystallized. X-ray fiber diffraction can result in structures but are not very high resolution and do not show atomic, much less side chain, interactions. Using such techniques in combination with fitting the Kabsch 1990 G-actin structure, the Holmes 1990 F-actin filament model was created and used for many years. (Holmes et al. 1990) The structure of F-actin turns out to be a 13 actin monomer per turn helix that repeats with a rotation of 166° , *on average*, per protomer. As seen in the Figure 1.5, there is directionality to the filament, with the top end being the **pointed “-” end** (SD2 and SD4) and the bottom end being the **barbed “+” end** (SD1 and SD3). (Top and bottom are non-conventional terms.) The implications of non-symmetrical ends, with regards to polymerization and depolymerization, will be discussed in the Section 1.2.

It was not until the Oda 2009 (PDB ID 2ZWH) model, using X-ray fiber diffraction on F-actin from rabbit skeletal muscle with a resolution of 3.3 Å in the radial direction and 5.6 Å along the equator, that a higher resolution model that described an the

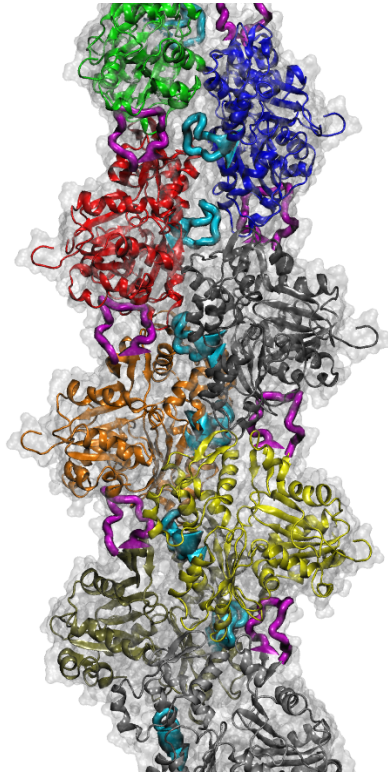


Figure 1.5: Structure of F-actin: 2ZWH from Oda et al. 2009. The DNase I loop is highlighted in magenta while the Hydrophobic plug is highlighted in cyan.

structure of a true filament was obtained. (Oda et al. 2009) The difference between G- and F-actin monomer was that in F-actin, there is a rotation of SD3 and SD4 by 20° about the SD3-SD1 axis—namely F-actin monomers are flatter. This flatness may contribute to a more stable helical filament.

Another high resolution electron cryomicroscopy derived structure with 3 \AA resolution of rabbit skeletal muscle was resolved by Fujii et. al. (Fujii et al. 2010) that generally agrees with Oda 2009. While other methods used averaging of 10,000's of images (Holmes et al. 2003, Galkin et al. 2008, Oda et al. 2009), they were able to obtain higher contrast resolution because of energy filtering. They find that F-actin is not as flexible as previously thought with only 1° twist variability and the D-loop conformation depends on what is bound, in agreement with the Oda and Holmes models. That needs to be taken with a grain of salt since they used highly oriented actin gels in which the filaments were stretched. The “axial” (longitudinal) contacts are tight between the D-loop and SD1 and SD3 of the monomer towards the

pointed end, binding mostly through electrostatic and hydrophilic interactions (at V45-Y143 and H40-T169). The “**interprotofilament**” (**lateral**) interactions are “modest” hydrophilic contacts at the hydrophobic-plug (Q263-G273) of SD3 to the D-loop of the protomer one unit upstream to the barbed end. This paper reiterates past implications (McGough and Chiu 1999, Bobkov et al. 2004) that lateral contacts are the weak link to filament strength, as will be discussed later.

The flexibility of F-actin may depend on each protomer, deriving its motion from the D-loop. (Orlova and Egelman 1993) There is apparently modulation by the metals, Ca^{2+} or Mg^{2+} , and nucleotides (ADP or ATP) changes SD2 and thereby affects filament flexibility in general. (Bobkov et al. 2002)

A recent study (Galkin et al. 2010) has produced cryomicroscopy structures, with a 10 Å resolution, which quantifies the structural states of F-actin, insinuating that past structures are simply wrong because they only capture one conformation, although it is obvious that filaments are flexible and can take different forms. They show six main modes of “polymorphisms” in which the D-loop takes on helical and coil conformations (a notion that has not been previously denied) and have different rotations with respect to the actin protomer. The claim is that actin’s high sequence conservation may be derived from the need for its many structural states in filamentous form such that mutations and other changes render it less efficient in accomplishing all its tasks. The paper further categorizes 63,000 segments of F-actin segments into six classes of structure, including a “tilted state” encompassing 24% of the samples where the nucleotide cleft is open and correlated to D-loop conformations. The D-loop is thus named an “allosteric switch.” See Figure 1.10 for states.

It is with these advancements of resolving actin structures that we are able to further our knowledge of cofilin and other actin-binding proteins. At the time when the work in this dissertation was performed, the Oda 2009 filament model was the best structure available and thus used as the basis of the model we present here.

1.2 ADF/Cofilin Proteins

Since the polymerizing and depolymerizing of actin filaments is so important to F-actin function, proteins that regulate such a process are profoundly vital to cell function. There are a plethora of ABPs that do this, but in recent times, the family of **ADF/Cofilin Actin-Depolymerizing-Factor** proteins have come to be credited with more importance than initially thought, playing a significant role in pathways and biosystems as an “agent of cellular homeostasis.” (Bamburg and Bernstein 2010)

The ADF/cofilin family, known as “Cofilin/tropomyosin-type actin-binding protein” and identified as PF00241 in the PFam database (Finn et al. 2010), is part of the ADF clan along with the gelsolin family. This family, with about 40% sequence identity, consists of ADF, cofilin, destrin, actophorin, coactosin, depactin and glia maturation factors (GMFs) beta and gamma. (Paavilainen et al. 2008) The defining characteristic is it is made up of a domain, the **ADF-H (ADF-Homology) domain**, which is also found in a more extensive protein family that includes three classes: ADF/cofilins (made up of one domain), twinfilins (two tandem domains), and drebin/Abp1s (made up of one ADF-H domain, a variable region and an SH3 domain). (Lappalainen et al. 1998)

Initially first found in porcine kidneys (Nishida et al. 1984), **cofilin binds to actin and enhances depolymerization at the pointed end, thus speeding activity.** It has been known to **cause twisting in the filament when bound and can sever mid-filament, thereby creating more pointed and barbed ends for depolymerization and elongation.** (Bamburg and Bernstein 2010) Porcine cofilin, identical to human cofilin except there is S109 instead of Cys109, and at merely 21 kDa and 166 amino acids long, is a small unassuming protein. ADF, on the other hand, was originally found in embryonic chick brains and unlike cofilin, does not have a β -strand at the C-terminus. (Bernstein and Bamburg 1982)

ADF and cofilin proteins, both non-muscle isoforms, have been greatly compared in their activity rates. (Yeoh et al. 2002) At saturating concentrations, both can **bind to actin stoichiometrically** at a 1:1 ratio at the same site, appearing to wedge itself between two protomers near their lateral contact. Both lead to severing and activation. Both show about the same affinity to G-actin as well as rates of association

to the barbed and pointed ends. The main difference is that cofilin nucleates ADP-actin into polymerization at a rate two times that of ADF, which already nucleates ADP-actin twice that of ATP-actin. ADF also depolymerizes more at a pH of 8 than cofilin, but both have low depolymerization at a pH of 6.5. Yeoh et al. further asserts that ADF has greater depolymerizing ability at the pH of 8 not from tighter binding/severing/dissociation rates but because cofilin simply has a better balance of polymerization and depolymerization kinetics. (Yeoh et al. 2002)

1.2.1 Other ADF Homology (ADF-H) Domain proteins

As the founding member, ADF/cofilin binds both G- and F-actin. In general, binding to G-actin inhibits a spontaneous nucleotide exchange. (Carlier and Pantaloni 1997, De la Cruz 2005, Andrianantoandro and Pollard 2006) In the case of F-actin, cofilin induces a destabilizing structural change that leads to disassembly, especially in aged filaments. (Okreglak and Drubin 2007) An exact molecular model for how the binding occurs in F-actin remains to be debated upon. (Wriggers et al. 1998, Kamal et al. 2007, Paavilainen et al. 2008)

Taking a further step back, there is a sort of “modular structure” to the actin-regulatory (i.e. binding) proteins in which the gelsolin family contain structurally similar segments that bind to G- or F-actin. (Puius et al. 1998) The gelsolin family consist of proteins such gelsolin, severin, and villin, that may not share that much sequence conservation with ADF/cofilin, but certainly look very structurally, when superimposed. (Pollard et al. 1994) See Figure 1.6. See Figure 3.1 for more structural alignments.

Yet another outlying set of proteins contain the WH2 domain, which shows some similarity to the ADF-H domain. Indeed, the ADF/cofilin and gelsolin families, as well as WH2 domain containing proteins, inhibit spontaneous nucleotide exchange in actin monomers by putting SD2 and SD4 in a “closed” state—the exact mechanism remains unknown. (Tellam 1986, Bamberg 1999, Hertzog et al. 2004, Paavilainen et al. 2004, Paavilainen et al. 2008)

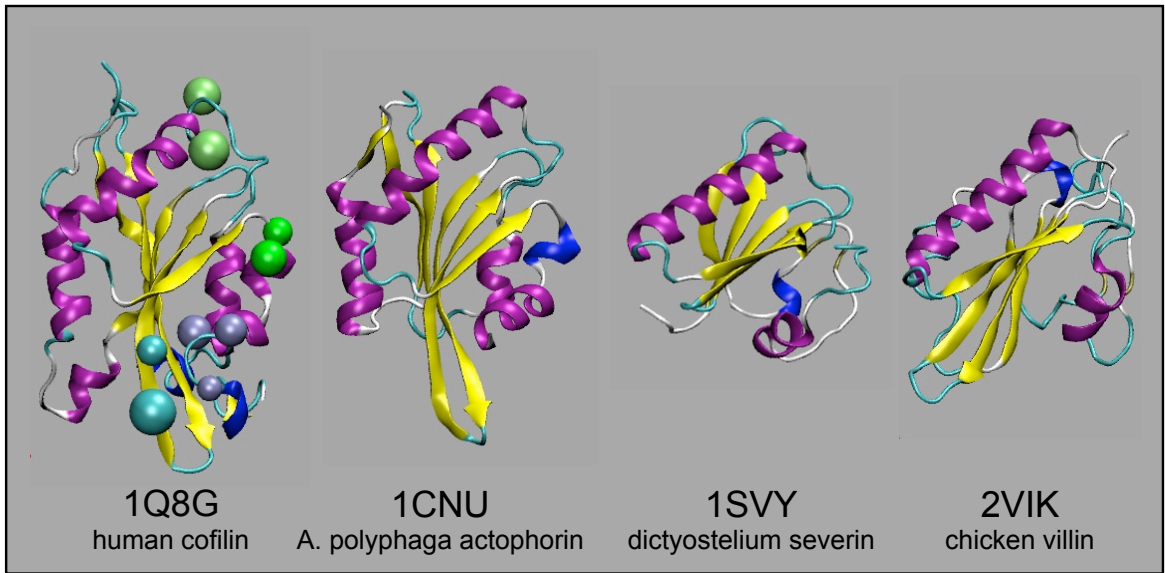


Figure 1.6: ADF-H Domain: Examples of differing ADF-H Domain proteins include human cofilin, *Acanthamoeba polyphaga* actophorin, *dictyostelium* severin, and chicken villin. Note the a common helix at the top of each protein that is consistently aligned.

1.2.2 Structure of Cofilin

Yeast cofilin was first crystallized by Fedorov et. al in the most updated structure, PDB ID 1CFY. (Fedorov et al. 1997) Human cofilin (PDB ID 1Q8G) was resolved later with NMR by Pope et al. (Pope et al. 2004) Many of the mutagenesis experiments have been performed on yeast cofilin. See Figure 1.7 for structural comparison. As seen in the figure, there are two extra loops in human ($\alpha 2$ and $\alpha 3$) that are not found in yeast (yeast at G22K23 and E43T44) are in green cartoon representation. GFP/RFP tags were placed in those yeast sites for tagging purposes and the E43T44 yielded a functional cofilin while the G22K23 lost function. (Lin et al. 2010)

Since we are more interested in human cofilin for egocentric human reasons (medical and otherwise narcissistic ones), the work here will focus on a human model. With both structures, we can easily structurally align human to yeast and interpolate known experimental results to human cofilin. The protocol for this process will be discussed in Chapter 3.

While much work has been done in this area, there is still no high-resolution structure of cofilin bound to F-actin. The closest structure that shows how cofilin binds G-actin

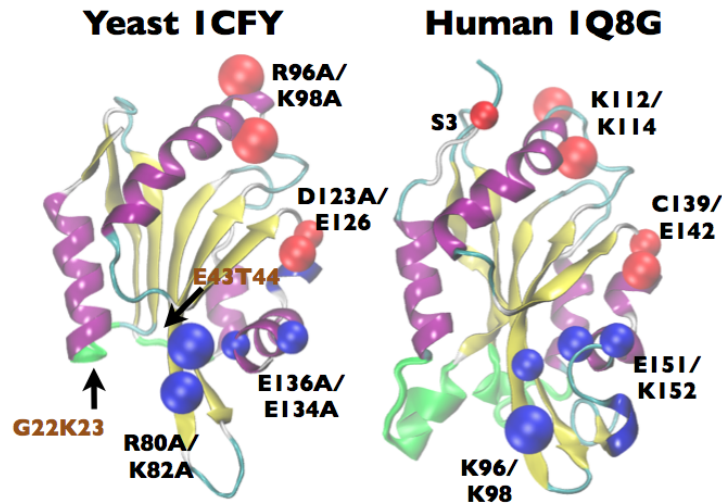


Figure 1.7: Human and Yeast Cofilin: Human (IQ8G) and yeast (ICFY) structures compared. G-/F-sites are in red beads. F-sites are in blue beads. Extra loops found in human that are not found in yeast (yeast at G22K23 and E43T44) are in green cartoon representation, in the back of the protein. The right of the two loops, E43T44, (occluded) is where the insertion can take place without loss-of-function consequences.

is the mouse twinfilin (C-terminal ADF-H domain) and G-actin crystal structure (PDB ID 3DAW) which was only recently resolved. (Paavilainen et al. 2008) Though twinfilin has high structural and some sequence homology with cofilin, it is nevertheless a protein with different function and binding than cofilin. Since twinfilin consists of tandem ADF-H domains (like two cofilins in a row), the N-terminal ADF-H caps the barbed end of actin while the C-terminal ADF-H binds approximately at the same site as ADF/Cofilin. (Paavilainen et al. 2007) Similarly to cofilin, twinfilin has a high affinity to ADP-actin monomers and filament barbed ends which allows it to prevent elongation. (Ojala et al. 2002, Helfer et al. 2006) However, glaringly different, twinfilin has much weaker binding to F-actin and a less extent of disassembly than ADF/cofilins (Paavilainen et al. 2008), thus making it a model that may not grant sufficient understanding of the severing mechanism.

1.3 Actin and Cofilin Interactions

To reiterate, cofilin preferentially binds ADP-actin and can bind both G- and F-actin. When it binds F-actin, it can aid in depolymerization (perhaps by chaperoning ADP-actin and lowering the critical concentration) or cause severing to occur mid-filament. Cryo-EM images show a comparison between F-actin (bare filament) and F-actin with cofilin bound stoichiometrically (fully decorated filament) in Figure 1.8. The structural differences of these filaments will be discussed in Section 1.5.1.

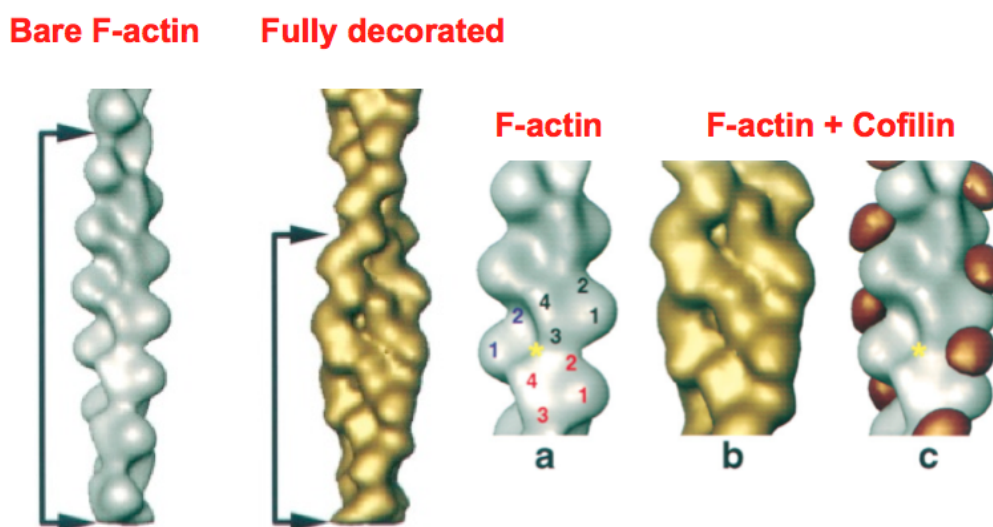


Figure 1.8: Bare (F-actin) and Decorated (Cofilactin) Filament: Figure reprinted from McGough et al. 1997.

1.3.1 Binding Surface

Mutagenesis Studies

The initial binding surface was found through systematic mutagenesis, prior to the availability of a structure, by changing charged residues to alanine when two or more were present in a sliding window of five residues. (Lappalainen et al. 1997) This is the most thorough biochemical characterization study to date, laden with information. Lappalainen et. al. tested 20 mutants for their growth phenotype (wt, ts-, or lethal)

and went on to characterized the temperature sensitive and lethal mutations with G- and F-actin binding as well as depolymerization activities. (See Table 1.2) Of those, five mutations are either F/G-sites that lethal to both G- and F-actin binding (cof1-17, cof1-20 D123/E126, cof1-28 Δ N5) or F-sites that are lethal to only F-actin binding (cof1-16 R80A/K82A, cof1-22 E134A/R135A/R138A). All these mutations will be important for confirming a binding model. Also, N-terminus is conserved for function and when the first five residues are deleted result in a lethal mutation, but it is not the target of protein kinases.

A few other important important mutagenesis studies have been done on yeast and porcine cofilin (Moriyama et al. 1992, Moriyama et al. 1996) that are also summarized in Table 1.2. Select mutagenesis studies on human cofilin have suggested that the N-terminus corresponds to G-site and C-terminus to the F-site. (Pope et al. 2000)

On the actin front, a systematic series of residues that affect cofilin binding have been tested and found for actin. (Rodal et al. 1999) These lethal mutations may eliminate binding, but the list cannot be assumed to be exhaustive since mutating actin is difficult because changes on the monomer can affect folding or filament assembly, actin mutagenesis effects on cofilin binding are not straight forward.

Cross-linking Studies

A number of cross-linking studies have been performed (e.g. Kudryashov et al. 2006, Benchaar et al. 2007, Kamal et al. 2007, Mannherz et al. 2007, Grintsevich et al. 2008) but because disulfide bonds are artificially introduced, it is hard to decipher how much credence to put into the binding interactions observed.

Mannherz et al.'s cross-linking and peptide array studies suggests that the G-actin site should include residues: 34-44, 52-62, 136-143, 328-338, and 346-353.

Kamal et al.'s radiolytic oxidative protein footprinting and mass spectrometry suggests that there is a hydrogen bond between H87 in actin and S89 in cofilin, but also goes on to aggressively challenge models by other groups.

Table 1.2: Data from Mutagenesis Studies

Mutation	Binds G-actin	Binds F-actin	Depoly- merizes	Severs	Actin turnover
Porcine cofilin, Moriyama and Yahara 2002					
WT pH 8 (pH \geq 7.5)	+	+	++	++	++
WT pH 7 (pH < 7)		++	\pm		
S120A pH 8		+	\pm	+	+
S120A pH 7		-	\pm		
S94D pH 8		-	++	-	++
S94D pH 7		-	+		
Δ N5 7/8		+	\pm	-	\pm
Porcine cofilin, Moriyama et al. 1996					
WT S3 (pH \geq 7.5?)		+	+	+	
WT pS3 (pH < 7.5?)	-	-		-	
S3D (like lo pH, pS3)	-	-		-	
S3A (like hi pH, wt)	+	+	+	+	
Yeast cofilin, Lappalainen et al. 1997					
WT	+++	+++	+++		
Δ 1-5 lethal (cof1-28)	+	+	+		
D10A, E11A ts- (cof1-5)	+++	+++	++/+++		
D34A K36A E38A lethal (cof1-9)	+++	+++	++/+++		
D68A E70A E72A lethal (cof1-14)	nd	++	++		
R80A K82A lethal (cof1-16)	++/+++	+	+		
R96A K98A lethal (cof1-17)	+	+	+		
D123A E126A lethal (cof1-20)	+	+	+		
E134A R125A R138A ts- (cof1-22)	++/+++	++	++		
Human Cofilin, Pope et al. 2000					
K95Q/K96Q	Yes	No	weak		
K96Q	Yes	No			
S3D/K96Q	No	No	No		
S3D pH 6.3		No	No		
S3D low salt		Yes	Yes, wt	Yes, probably	Induces twist like wt

1.4 Regulation of Cofilin

Although the main goal is elucidate how cofilin interacts with F-actin, it is still important to understand how cofilin is modulated, most often by interactions with other proteins. There are already a number of great reviews that discuss this subject.

(Bamburg et al. 1999, Ono 2003, Troys et al. 2008, Oser and Condeelis 2009, Bamburg and Bernstein 2010)

1.4.1 On and Off: Ser3 Phosphorylation

In a proteolytic study of porcine cofilin, **Ser3 was identified as the site of phosphorylation**. (Moriyama et al. 1996) Cofilin with pSer3 is unable to bind to G- or F-actin while Ser3 can. The S3D mutation emulates the behavior of pS3 while S3A behaves like wild type cofilin. The mutations S2A/S4D and S2D/S4D in yeast cofilin are also lethal to binding, indicating that bulk in either Serine at the N-terminus impairs binding. (See Table 1.2.)

Clearly, a site that can deactivate cofilin is a key regulatory switch and other proteins can capitalize on their signal pathways. In fact there are growth factors that can activate multiple pathways to promote phosphorylation or dephosphorylation; this activation of cofilin can ultimately affect cell morphology and neuronal outgrowth. (Meberg et al. 1998)

Deactivation of Cofilin

LIM Kinase 1 (LIMK1) can inactivate cofilin by directly phosphorylating Ser3. (Arber et al. 1998, Yang et al. 1998, Bernard 2007) LIMK2 also has the same behavior, but mice without both LIM kinases are healthy and fertile even though they cannot phosphorylate ADF/cofilin—perhaps TES kinase (TESK) compensates. (Meng et al. 2004) Even further upstream of regulation is the Rho family of GTPases, also kinases, which can activate LIM kinase. (Kuhn et al. 2000)

Activation of Cofilin

There are also proteins that can activate cofilin through dephosphorylation such as, slingshot and chronophin. (Bamburg and Bernstein 2010) While dephosphorylation is the key to cofilin activation, PIP2 also needs to dissociate, if it is bound. (Song et al.

2006, Yonezawa et al. 1990, Ojala et al. 2001, Gorbatyuk et al. 2006, van Rheenen et al. 2007)

1.4.2 When to throw the switch? pH Regulation

Environmental **pH** is another way to control cofilin, perhaps again having to do with phosphorylation, although there is a chick ADF mutant that cannot be phosphorylated but is still pH dependent so that remains to be clarified. (Agnew et al. 1995) It was first found in porcine cofilin that at **high pH (>7.3)**, **depolymerization occurred at a higher rate than low pH**, even when there was an excess concentration of cofilin. (Yonezawa et al. 1985) Most ADF/cofilin (including human cofilin and human ADF) are pH sensitive, although *Acanthamoeba actophorin* (a member of the ADF/cofilin family) is pH insensitive. (Hawkins et al. 1993, Maciver et al. 1998, Chen et al. 2004). In wounded fibroblasts, the pH needs to be increased for actin dynamics to occur for healing. (Bernstein et al. 2000) In many cases, this pH regulation makes sense because there is significant pH change near the plasma membrane, where filament restructuring often occurs. (Bernstein et al. 2000)

Regulation by pH has been greatly studied in ADF, which is similar enough to cofilin. ADF is more sensitive than cofilin to pH shifts, with comparatively less binding at pH <7.1. (Hawkins et al. 1993, Hayden et al. 1993) When increasing the pH, ADF preferentially co-localizes with G-actin, more than F-actin, which encourages depolymerization. Cofilin, on the other hand, does not co-localize with G-actin and is only comparatively weakly enhanced by increasing pH. (Bernstein et al. 2000) See Figure 1.9

ADP- vs ATP-actin and phosphate release

As mentioned earlier, cofilin binds preferentially to ADP-actin (i.e. older portions of a filament or monomers not yet ready for polymerization) over ATP-actin (i.e. newer parts of the filament). Inorganic phosphate (Pi) stabilizes SD2 in F-actin but cofilin increases disorder and accelerates treadmilling. (Galkin et al. 2003) Pi also lowers the rate of cofilin binding at physiological Pi concentrations, especially at low pH (6.5);

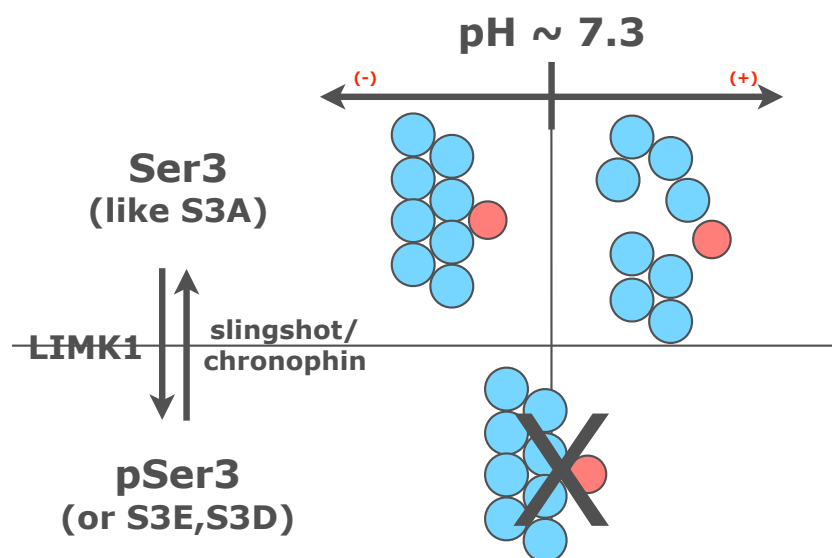


Figure 1.9: pH Regulation

cofilin in turn induces a conformation change to SD2 thereby reducing the Pi's affinity to actin's nucleotide cleft. (Muhlrad et al. 2006) Indeed, cofilin depolymerization occurs at high pH perhaps because phosphate (Pi) release is also pH dependent. (Pavlov et al. 2006) This seems like a double check in the case of pH sensitive cofilin since low pH conditions imply Ser3 would be phosphorylated and less likely to bind F-actin anyway. Also, cofilin bound ADP-actin should not spontaneously bind Pi and become ATP-actin again since its fate is either to be severed or depolymerized.

His133

Deprotonating His133 was assumed to be required to activate cofilin. (Pope et al. 2004) In an *in vivo* study by Frantz et al., both human H133A cofilin and pH insensitive actophorin are able to restore the first phase of actin free barbed ends in fibroblasts that lack H⁺ efflux by the Na-H exchanger (NHE1) but S3A cannot. (Frantz et al. 2008) In the mutant H133A, **human cofilin remains pH sensitive in NMR spectra and severing *in vivo***. Frantz et al. also found that PIP2 inhibits cofilin activity by binding, with decreased binding at higher pH (7.5 vs 6.5) but is pH *insensitive* for H133A. They claim through their MD that the salt bridge between H133 and D98 observed by Pope et al. 2004 weakens at high pH.

1.4.3 Oxidative Stress/Oxidation

Reactive oxygen species (ROS) can induce oxidative stress on cells and potentially exacerbate cancer. Oxidants include taurine chloramine (TnCl) and hydrogen peroxide (H_2O_2), for example. When cofilin is oxidized, it forms intramolecular disulfide bonds and **dephosphorylates pS3**, rendering it into a form that **can bind F-actin but cannot depolymerize F-actin**; as follows, T-cells that are under oxidatively stress cannot modulate F-actin in response to chemotaxis or co-stimulation. (Klemke et al. 2008) In a series of mutations in human cofilin (C39G, C80G, C139G, C147G), Klemke et al. finds that C39 and C80 are critical to regulation and function because they can only be weakly or not at all phosphorylated, respectively, nor do they have the same migrating pattern as a wild type cofilin in a non-reducing SDS-PAGE. The results have to be taken with a grain of salt because they are *in vitro* experiments that look at conformation via gel assays.

Klamt et al. furthers the work and creates Cys to Ala mutations at all four cysteine sites (as mentioned in Klemke et al. 2008) and finds that oxidations of every Cys is required to make cells apoptotic. This comes from the observation that when oxidized cofilin at the Cys residues along with dephosphorylation of Ser3 loses its affinity for actin, it translocates to mitochondria where it mediates the opening of permeability transition pore (PTP) thereby induces swelling and cytochrome C release—this causes apoptosis.

Self Association—Cofilin Oligomers

When oxidized, cofilin can also self associate but in its dimerized state, it can neither depolymerize nor sever. (Bamburg and Bernstein 2010) There are a number of agents that instigate this reaction (*in vitro*), such as water-soluble carbodiimide, Ellman's reagent, or glutathione disulfide, which induces disulfide bond formation, but can be reversed with dithiothreitol. (Pfannstiel et al. 2001) While single cofilin encourages severing, oligomerized cofilin induce highly ordered actin bundles to form, which are groups of ADF/cofilin bound actin filaments, in oxidative stress. Pfannstiel et al. further proposes that oligomers are stabilized by high cofilin concentrations and PIP2—not by disulfide bonds. (Pfannstiel et al. 2001)

1.5 Cofilin's Effects on F-actin

An even more exhaustive discussion of cofilin interactions and its ramifications would be a great academic exercise, but unfortunately might continue indefinitely, given its invasion of neurobiology. Instead, the previously discussed molecular details may be sufficient to understand the original goal of understanding the mechanics involved when cofilin severs F-actin.

1.5.1 Twist and Destabilization

In a bare actin filament, two values are necessary for a transformation matrix to turn the coordinates of one monomer into a perfectly symmetrical filament. In the case of Oda et al.'s bare filament, the single monomer from PDBID 2ZWH only needs to be translated 27.59 Å up (towards the pointed end) and -166.4° around the z-axis. This rotation around the axis is the angle of twist. (Oda et al. 2009)

One of the first seminal papers on the observation of yeast cofilin inducing twist, in a stoichiometric fully decorated filament, was done by McGough et al. using electron cryomicroscopy and helical reconstruction, finding that cofilin binds cooperatively with maximum binding of 1.16 cofilin and Hill constant of 6.4. A fully decorated filament is stabilized by the cofilin and has a mean twist of 162° , which is approximately a decrease of over 4° from a bare filament, as well as shorter long-pitch helix, increased diameter, and the loss of the phalloidin binding site. (McGough et al. 1997) The angle of twist is also 162° for ADF-saturated actin. (Galkin et al. 2001) A fully decorated filament is squatter/fatter and more twisted than a bare one, as seen in Figure 1.8. This is like an over twisted Slinky. See Table 1.3 for a summary.

Table 1.3: Filament TwistData:
from † Hanson et. al. 1967, * McGough et al. 1997, ‡ Fujii et al. 2010

	Rotation between monomers	Subunits per turn	Crossover length (Å)
Bare	166.4° ‡	2.160*	385-358†
Decorated	162° *	2.222*	269*
Mixed (bare)			371*
Mixed (decorated)			278*

1.5.2 Structural Effects

Examining the contacts has provided some insight into the the affects of cofilin binding and has been done by a number of groups for the case of fully decorated filaments. The **lateral contacts** between protomers have been shown to be disrupted. (McGough and Chiu 1999, Bobkov et al. 2004) The hydrophobic plug, which bridges the protomers across opposite strands, is the site of a S265C to C374 crosslinking that occurs in the filament but is inhibited by cofilin. (Bobkov et al. 2004)

Longitudinal contacts are also weakened upon cofilin binding. (Galkin et al. 2003, Bobkov et al. 2002) Yet again through cross-linking and FRET studies, Bobkov et al. shows that cofilin changes the structure of the SD1 and SD2 interface of two protomers when the DNase I loop shifts away from the adjacent SD1 and Q41C (in the D-loop) cross-links to C372 (of the H-loop) instead and effectively weakens the longitudinal contact. EM studies show that the contacts become weak because SD2 and D-loop simply have a conformational change, which is more extreme on the pointed than the barbed end (Galkin et al. 2003), where there is more depolymerization.

At high pH, a condition for severing, ADF has the ability to induce a **12° tilt**—a change within each protomer subunit with respect to the filament—and that may cause breakage in longitudinal contacts. (Galkin et al. 2001) Orlova et al. finds that after making three types of unstable filaments (either from forcing a disulfide bond between the H-loop and to the subunit, putting a TMR label on the C-terminus of actin, or examining very newly formed filaments) induces the same “tilted state” observed in ADF/cofilin decorated actin filaments. There are even different tilted states in which SD2 does not interact with SD1 in the upstream protomer (towards the the pointed end) and instead interacts with SD3; the other less common state is where SD4 interacts with SD1 on the opposite strand. (Orlova et al. 2004)

Destabilization happens at the older, ADP-actin, pointed end, as expected (Galkin et al. 2003, Orlova et al. 2004), but it seems that new polymerizing filaments also shrink more at the barbed ends (1.8/s) than older filaments that have become stable at the pointed ends (0.1/s) *in vitro*. (Kueh et al. 2008) Cofilin on aged filament accelerate the shrinking to 5.9/s (Kueh et al. 2008) and perhaps halts the process of

changing disordered new filaments into stable ones in a “time reversal” (Orlova et al. 2004).

Indeed, the D-loop seems to be key to stability. Although the function of cofilin is to twist and sever, ADF (and presumably cofilin as well) stabilizes certain “helical variations” in F-actin. (Galkin et al. 2001) Paavilainen et al. proposes that the D-loop does not contribute to actual contacts but does rearrange when the ADF-H domain (of twinfilin in their case) binds and weakens the inter-filament contacts. The hydrophobic loop (residues 262-274), which is important for filament growth and stability, weakens due to this D-loop change. (Paavilainen et al. 2008)

In the recent F-actin polymorphism paper (Galkin et al. 2010) and from personal discussion, the author claims that filaments must first twist into a conformation where the D-loop is disordered (mode 4 or 5 in Figure 1.10) before cofilin can bind. Since EM images are not of high enough resolution, this proposal is still a proposal and not fact. In Chapter 5, this will be further explored.

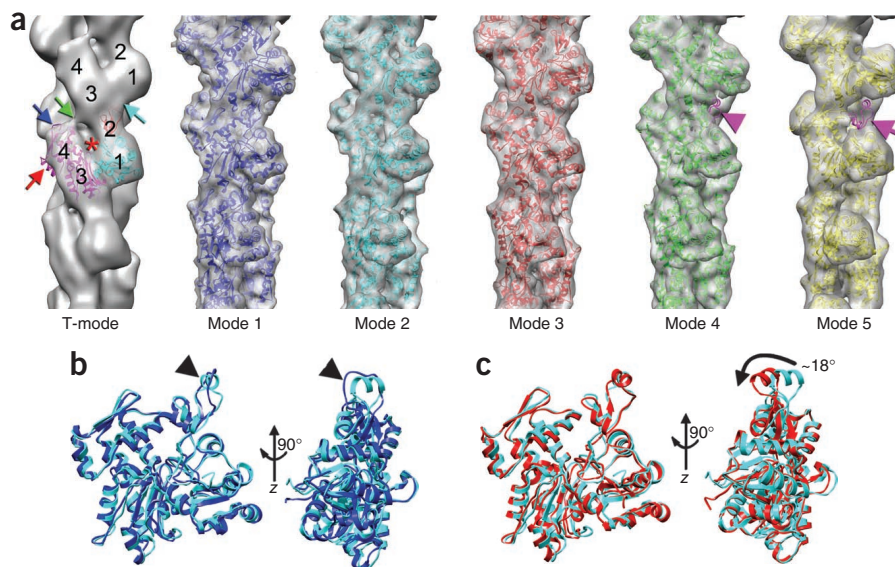


Figure 1.10: F-actin’s Conformational States: (a.) Cryomicroscopy show F-actin in six main structural states. These “polymorphisms” are 10 Å and show that SD2 can be disordered and was not even resolved in some of the mode states. (b.) The D-loop can be a loop (mode 1) or helix (mode 2). Figure reprinted from Galkin et al. 2010.

In studies that examine mechanical properties, cofilin also affects bending stiffness of actin. In bare actin, the persistence length is 9.8 μm and the flexural rigidity is

0.040 pN μm^2 , but a cofilin decorated filament has a persistence length of 2.2 μm and flexural rigidity of 0.091 pN μm^2 . (McCullough et al. 2008) Saturating cofilin causes the filament to be more flexible, in addition to its over-twisting characteristic. From this, the authors propose that cofilin weakens and stabilizes subunit interactions and increases flexibility, inducing change in SD2's structure leads to “mechanical asymmetry.” (McCullough et al. 2008)

Through numerical and analytical experiments, De la Cruz et al. have found that there is a strong twist-bend coupling that the interconversion of energy and stress between bending and twist is essentially conserved. In their mesoscopic model of F-actin, 60% of elastic energy comes from this bend-twist coupling and is due to the double protofilament, helical structure. (De la Cruz et al. 2010) This implies that cofilin increases twisting and thus increases bending, or vice versa.

1.5.3 Concentration Modulation

The concentration of cofilin greatly changes how it affects actin. The amount of cofilin in a system can make the difference in disassembly, stability, and even disease (as will be discussed in Section 1.7). Whereas the previous section was under the assumption of saturating concentrations, this section discusses the implications of how varying concentrations implies modulating cofilin-actin activity.

At high concentrations of cofilin, actin severs rapidly but it quickly stabilizes in a twisted form. (Bamburg and Bernstein 2010) Saturated filaments are not only stable, but can nucleate and elongate filaments especially when monomers are already bound to cofilin. (Yeoh et al. 2002, Chen et al. 2004, Andrianantoandro and Pollard 2006) Crosslinking studies have shown the L180C/L269C/C374 mutant, which crosslinks the H-loop to SD3/SD4 region, inhibits nucleation and elongation (Shvetsov et al. 2008), although one should be wary of the such forced pinning.

Differential scanning calorimetric (DSC) studies have shown that it is actually the actin to cofilin ratio that determines stability of the filament. At sub-saturating concentrations (i.e. 100:1), F-actin is significantly destabilized, but at saturating concentrations (i.e. 1:1), F-actin is “thermally stable”—cofilin stabilizes the protomers

it is directly bound to but destabilizes parts of the filament that it does not contact. (Dedova et al. 2004)

Severing and Cooperativity

Severing is most efficient at $<1 \mu\text{M}$ by porcine cofilin (Moriyama and Yahara 1999, Moriyama and Yahara 2002) and 10 nM by *S. pombe* cofilin (Andrianantoandro and Pollard 2006) which is below K_d , confirming that its performance is best when few cofilin are bound (De la Cruz 2005). Pavlov et al. proposes that cofilin severs using allosteric and cooperative destabilization by restricting flexibility in cofilin-unstable regions. (Pavlov et al. 2007)

Since cofilin phosphorylation and Pi binding is pH dependent, it is reasonable to say that cofilin's ability to sever is as well. Cofilin binding is pH sensitive (occurring at a rate 2 to 3 times faster at pH 6.8 than pH 8.0) and depolymerization occurs at a higher rate at high pH, but in the case of **severing, yeast cofilin is actually pH independent**. (Pavlov et al. 2006) However, yeast twinfilin induces filament severing at low pH. (Moseley et al. 2006)

Cooperativity is a very important aspect of cofilin binding. Cofilin's cooperative binding and Arp2/3's subsequent decreased affinity for filaments results in debranching, where cofilin directly competes with Arp2/3 even in lower cofilin concentrations. (Chan et al. 2009)

Building on previous studies (e.g. De la Cruz 2005, Andrianantoandro and Pollard 2006), De la Cruz and Sept propose a one-dimensional Ising model that describes the cooperativity kinetics. On a bare filament, cofilin activity is high in binding. When filaments age (or dephosphorylate) and cofilin bind cooperatively in patches, at a certain concentration when there are the maximum number of boundaries between decorated and bare regions, the conditions are prime for severing. When cofilin saturate all sites, severing ceases and the filaments are stable. But over a longer period of time when cofilin dissociate, the number of boundaries begin to increase again and the conditions tip toward severing again. (De la Cruz and Sept 2010) See Figure 1.11.

Finally, De la Cruz details how cofilin may sever actin filaments. (De la Cruz 2009)

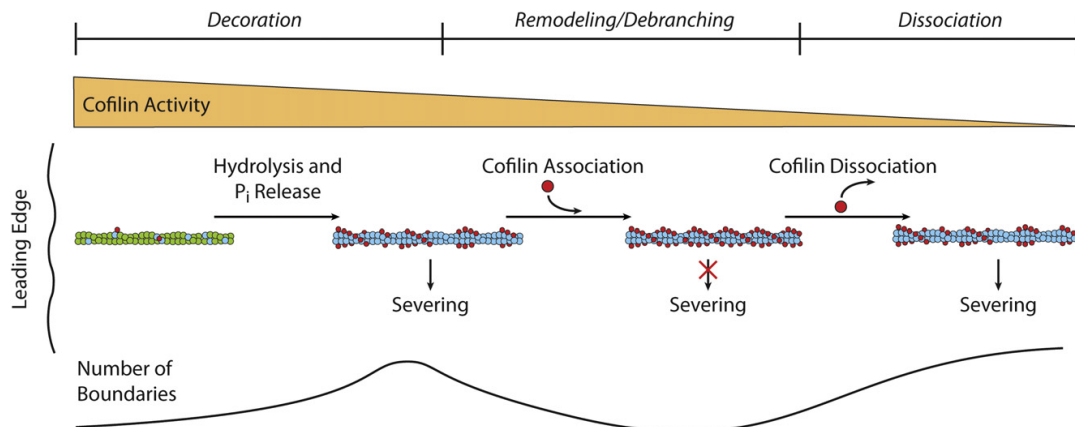


Figure 1.11: Model of Cofilin Binding and Severing: Reprinted from De la Cruz and Sept 2010, Elsevier.

1.6 Previous Modeling

There have been a few computational models that have tried to make sense of the vast data of cofilin twist and severing activity. As mentioned before there is the Ising model of kinetics (De la Cruz and Sept 2010) and the twist-bend coupling model (De la Cruz et al. 2010) along with De La Cruz's other work in process that describe decorated and bare boundaries. Pfaendtner et al. simulate a periodic native/bare (with a twist of 166° or 36 nm helical repeat) and decorated/cofilactin (with a twist of 163° or 30 nm helical repeat) filament and find that lateral contacts of the H-loop are disrupted in cofilin binding and that the D-loop reorganizes. (Pfaendtner et al. 2010) Unfortunately, due to the periodicity nature of the model, the bending and twisting would not be readily captured.

1.7 Medical Significance: Alzheimer's Disease, etc.

Cofilin has moved into the limelight as its significance to diseases have become more apparent—it is not merely an “academic exercise” to study this protein. There are

implications that it has an effect on inherited cancers, Carney syndrome (cardiac tumors), HIV-1 infections, CD4 T-cells, and most notably, Alzheimer's disease. (Bamburg and Bernstein 2010)

As always, there is such thing as too much of a good thing. When filaments are saturated with ADF/cofilin, the decorated filaments bundle into large rod structures (often discussed in the neurobiology), which can occur with overactive cofilin, often caused by mediators of neurodegeneration. (Minamide et al. 2000, Bernstein et al. 2006) These rods disrupt microtubules and axonal transport. (Bernstein et al. 2006) Rods can form in axons and dendrites of stressed neurons and can cause synaptic dysfunction and eventually cognitive impairments, such as Alzheimer's Disease. (Minamide et al. 2000, Minamide et al. 2010) Moreover, mitochondria in proximity to rods also malfunction which leads to neurite degeneration. (Bernstein et al. 2006)

When ADF/cofilin are overly active (e.g. in their dephosphorylated state) and in high concentrations, they lead to an accumulation of fully decorated actin filaments, or rods, many times stimulated by existing neuronal degenerating conditions (e.g. oxidative stress, ischemia, or β -amyloid peptides). (Bamburg et al. 2010) These rods or bundles have been described with great detail in a recent review on their influence in neuronal dysfunction and degeneration. (Bamburg et al. 2010)

Soluble $A\beta_{1-42}$ amyloid peptides, the culprit of Alzheimer's that aggregates as plaques in brains and causes cognitive defects, induce rod formation because of its affects *cdc42*, which is an upstream regulator of cofilin. (Davis et al. 2009) Also, with cellular stress or oxidative (i.e. Alzheimer's), there is a decline of ATP and since cofilin binds to ADP-actin well, it fully decorates the filament, resulting in rod development. (Minamide et al. 2000, Maloney et al. 2005, Davis et al. 2009) Cofilin may also affect the brain in that rods with activated ADF/cofilin can recruit phosphorylated MAPs (micro-tubule-associated proteins); during mitochondrial inhibition these rods and inclusions containing hyper-phosphorylated MAP/tau accumulate and imitate neurophil threads, eventually leading to disease progression and more neurodegeneration. (Whiteman et al. 2009)

Rod formation is not only a player in Alzheimer's, this event has repercussions in Huntington's Disease when huntingtin proteins are unable to clean out the abundant rods in heat-shocked neuronal cells. (Bernstein et al. 2006)

While this discussion of medical implications just skims the surface, it is apparent how important cofilin can be to other pathways with which actin has interaction. Rod formation happens under stress and occurs early on during neurodegeneration, making the cofilin and actin interaction a recently identified hot therapeutic target. (Bamburg et al. 2010)

1.8 Synopsis of Thesis

With previous ground work laid out, I can now address the three questions I have sought out to answer about cofilin and F-actin interactions.

1.8.1 Specific Goals

The work in this thesis can be summarized in the following three goals, which comprise Chapters 3, 4, and 5 respectively:

- **Part 1: Structural binding model of cofilin and F-actin:** How does cofilin structurally bind to F-actin?

Here, we use sequence alignments, homology modeling, and docking techniques to propose a model as to how cofilin binds actin because of the lack of structure data.

- **Part 2: Short-ranged dynamics of cofilin-bound actin filaments:** What are the important domains that affect binding or mechanics?

To answer this question, we build different filament models so that we may use all atom molecular dynamics (AA MD) to gain insight into the molecular interactions.

- **Part 3: Long-ranged dynamics of cofilin-bound actin filaments:** What are the long ranged behaviors (e.g. twist, bend, persistence length) of filaments with cofilin bound at varying concentrations and what are the characteristics that may induce severing?

To make finding the dynamics of this large filament system into a more surmountable task, we use coarse graining techniques. With access to longer time scales, we can tease out interesting characteristics like twist that may contribute to severing.

Chapter 2

Computational Methods

This chapter outlines some of the computational methods we use in this work. First we will discuss Molecular Docking strategies that can be used, although we only use a subset of them to accomplish the goals we put forth. Molecular Dynamics is also very important, but will not be covered in this dissertation. Please refer to Leach 2001, Chapter 7 for an excellent review of the topic. There are many ways to accomplish Coarse Graining of a model but the specific methods we use will be discussed at the end of this chapter.

2.1 Molecular Docking

As difficult as it is to obtain structures for every protein we could possibly want, getting the co-crystal structure of two bound proteins is often a greater challenge. Since solving such bound structures may not always be experimentally possible, there has been significant effort in the simulation community to predict them. The previous sections covered protocols to obtain structures, whether from x-ray crystallography or through ab initio prediction, and how to sample dynamics of these structures. This section will show how to take these results and use them to predict bound complexes with drugs, ligands or other proteins. As discussed before, the confidence in binding models obtained from docking methods is only as good as the experimental information we have a priori. The more information that is available (mutagenesis data, sequence or structure conservation, etc.) the more reliable docking simulations will be.

2.1.1 Basic components

While an end-user of various tools available for docking does not have to understand the minutiae of all the algorithms under the hood, it is still important to appreciate some details so as to know which software is suitable for different situations. Every docking program has two essential components: a search algorithm and an energy scoring function. (Leach 2001) The details and interdependence of these two components varies greatly among the different pieces of software and some of these details are discussed below. The issue of search space deals with sampling the different possible orientations, or poses, that the macromolecule and ligand can bind. In rigid docking, where the internal coordinates of the macro and ligand are held static, there are six relative degrees of freedom for two molecules: three translational and three rotational degrees of freedom. This can lead to hundreds of thousands or millions of possibilities, depending on the size of molecules, but this problem is further compounded in the case of flexible docking. Once bonds are allowed to rotate and side chain or backbone conformations are explored, the size of the search space increases exponentially. There are many different search algorithms, ranging from brute-force conformational searches or more effective and efficient stochastic-based algorithms. In general, better sampling of the different possible poses will lead to a higher probability of finding the correct binding structure.

With so many poses generated from the search step, we need a system to rank them according to their likelihood of being the binding answer(s), whether it be by energetics, binding affinity, or some other metric. Scoring functions (Jain 2006) to evaluate these structures must not only be accurate in calculating the energy of a pose, but also efficient to rank a large number of structures in a timely matter. The binding score or energy resulting from various scoring functions can be based on first principles (like molecular mechanics force fields), empirical data (functions fitted to experimental data), semi-empirical (a combination of the two), or knowledge based (statistics and heuristics). There are programs that show good performance, although they may be optimized to the selected benchmarks and may only prove to make good predictions for systems for which they are parameterized. (Huang et al. 2006) Since the difficulties in predicting absolute binding energies are great, it is often more desirable and effective to predict the correct relative affinities of a group of compounds.

In reality, the entire procedure to generate a single docked complex needs to be repeated tens, hundreds or thousands of time. To analyze this large ensemble of predictions, many protocols use cluster analysis, looking for structures that are repeatedly predicted as a measure of confidence. Of course, any result needs to be compared to known experimental data as a sanity check. Additional analysis would be recommended, as well as further experimental validation in an iterative cycle to improve any docked model.

2.1.2 Choosing the correct tool

The first step is to select the appropriate docking software for the system of interest. Some programs are parameterized for specific kinds of protein structures or particular ligands (such as only small molecules), while others are more widely applicable. At the same time, some programs are free for academic use, while others charge a nominal or substantial fee, even for academic use. Unfortunately it is not possible in this limited space to provide details on each software package and the user will need to investigate each package on an individual basis. Table 1 contains a list of software and web addresses, but some of the more widely used packages are: AutoDock (Goodsell and Olson 1990), FlexX (Rarey et al. 1995), GLIDE (Friesner et al. 2004; Halgren et al. 2004), GOLD (Jones et al. 1995), HADDOCK (Dominguez et al. 2003), and RosettaDock (Schueler-Furman et al. 2005b,a).

Although every software package will claim to have certain advantages, the best method in assessing their quality is in head-to-head comparisons, hopefully completed by some independent third party. For small molecule docking, there have been several published comparison published in recent years. (Leach et al. 2006, Cross et al. 2009, Cummings et al. 2005, Sousa et al. 2006) In the case of protein-protein docking (Leach et al. 2006, Bonvin 2006, Ritchie 2008, Vajda and Kozakov 2009), the best resource for evaluating the most current docking methods is the results gathered from the bi-annual Critical Assessment of PRedicted Interactions (CAPRI). (Lensink et al. 2007; Mendez et al. 2005) Like the CASP competition for structure prediction, CAPRI evaluates blind predictions of protein-protein interactions. In the latest round (of which results were published in 1997), there is an additional component for assessing scoring functions. Additionally, there are evaluation tests (Schulz-Gasch and Stahl

2003, Tiwari et al. 2009, Warren et al. 2006) with decoy benchmarks (Huang et al. 2006, Irwin 2008) or evaluative reviews (Moitessier et al. 2008) that are released whenever a new tool has been developed.

2.1.3 Preparing the molecules

The ligand of choice impacts how the search step should be carried out. In general, docking protocol can be divided into protein-small molecule docking and protein-protein. Each category will be covered in this section, where the smaller molecule (e.g. drug) is defined as the ligand and the larger protein defined as the macromolecule.

Macromolecule

Regardless of the ligand, the macromolecule protein is usually dealt with in the same way. The sheer size of a protein and the potential degrees of freedom usually means that exhaustive sampling is not possible. Many programs have some limited sampling capability, especially for the side chains through the use of rotamer libraries, but they tend to not adequately sample backbone conformations. To facilitate whichever program the reader uses, it can be very beneficial to sample an ensemble of structures from a molecular dynamics or other type of simulation. Alternatively, if there is NMR structure data, the ensemble of models can be used in independent docking runs. In essence, a series of snapshots will give the docking search algorithms a different starting structure from which to sample, and this may aid in a better holistic representation of the conformational space.

Once a series of macromolecule structures are chosen, they need to be prepared for docking. The details of this are specific to the program being used, however there are several general considerations that need to be kept in mind. Just as with MD simulations, these would include the protonation state of the protein and particular residues, the proper treatment of any non-standard amino acids and post-translational modifications, and the inclusion of any required ligands, nucleotides, ions, etc. If the sites of these modifications is known or thought to be close to the binding site, these

may be critical for success if they are more distal from the binding site, they may be able to be ignored.

Less of a formatting issue and more of a technical one, the charge state of the macromolecule is very important and needs to be thoroughly considered as it is often the driving force of many intermolecular interactions. Experimental information, such as pH or salt dependency can help in deciding what a charge state of particular groups should be. Some programs require an active hand in making this determination. There may be other steps for preparing the macromolecule, such as defining flexible regions and rotatable bonds, which are important to consider.

Small Molecule Ligands

Drugs and small peptides tend to have more limited degrees of freedom and can therefore be treated in a more systematic approach. In short, the fewer the rotatable bonds, the easier it is to sample completely. Depending on the software, docking packages that allow the user to define fixed or rotatable bonds are usually sufficient, although caution would still be advised to make sure if enough conformations are used in docking and that they are not sterically hindered. Just as for the macromolecule, the electrostatics on the ligand is very important in driving interactions, and if not correctly represented, the results could be drastically affected.

Protein Ligands

Peptides with secondary structure and proteins being docked as ligands have a slightly different treatment than drugs or small molecules. While certain parts may be locked into helices or sheets and thus have somewhat restrictive motions, there could be unstructured loops or more dynamic regions. Just as we saw before, it is not possible to fully capture these degrees of freedom, and these protein ligands are treated in the same fashion as the macromolecule. Again, if there is an NMR structure, those models can be used or the ligand could be subjected to simulation studies. Ultimately, we would ideally generate an ensemble of structures for the macromolecule and ligand and perform docking for every combination of the two. As will be covered in the

virtual screening section, some have found that combining methods to converge at a docked model may be more necessary for protein-protein docking. (Vajda and Kozakov 2009)

2.1.4 Iterative docking and analysis

With the ligand and macro prepared, we can begin the process of generating docked models (see Figure 2.1). To find the best model, an iterative method is typically the most successful approach. A general, first pass, docking may help to find a region on the macromolecule where the ligand is most likely to interact. This is a blind run docking, meaning that the macro and ligand are allowed to randomly pair with no bias in any region. To save in time in this step, it is usually best to allow limited or no flexibility.

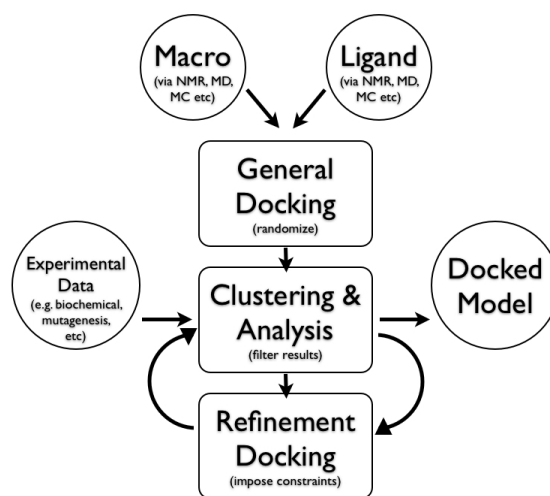


Figure 2.1: The Standard Docking Protocol: Reprinted from Saxena et al. 2009, Elsevier.

The second step would be to cluster the results from the blind docking, grouping the ligands based on location and examining their energetic, or ranking, score. Ideally this would identify one particular area on the macromolecule, but if there are several locations, a highly ranked representative structure of each cluster (or binding site) can be used for finer docking runs. As always, the use of experimental data here is crucial in determining probable sites as well as in corroborating the selection of the

best model. Using these filtered results, we can perform refinement docking where the ligand is restricted to a specified region based on the blind docking results. How this restriction is imposed depends on the software being used, but most programs possess this capability. There are often more fine grained tuning options for more exact exploration, including side-chain sampling or repacking that allow for flexible docking. (Bonvin 2006) The user should make use of these capabilities as appropriate.

2.1.5 Post analysis

If an iterative docking methodology is used, analysis needs to take place intermittently to maximize docking success. Clustering coupled with score ranking is the most basic analysis to find potential good poses. Particularly in the case of protein-protein docking, the use of experimental data, such as mutagenesis data, may be required. Such data can be used to filter out false positives and improve the overall results. Also, although the search and scoring steps of most docking protocols are highly intertwined, one can easily re-score a set of poses using a different scoring function or functions. Some programs have multiple and easily manipulated scoring functions. Although usually requiring extra effort, re-scoring aids in enriching the results and converging at a consensus result with which other methods agree.

Virtual screening

So far the methods described here assume that the ligand to be docked is already identified. In the case of drug discovery, the small molecule of interest that binds a given target may be what we are trying to determine. In such cases, a whole gamut of small molecule data bases (such as Available Chemicals Directory, ChemACX, Maybridge Database, Zinc, NCI Diversity Set (Voigt et al. 2001), can be docked against the target protein for screening purposes. This kind of virtual screening can aid in narrowing down potential inhibitor candidates before vast resources are devoted to testing them at the bench. High-throughput virtual screening is obviously very popular with pharmaceutical companies since it would not only save money from actual testing but also help in lead drug discovery. With 1,000-100,000 compounds in each database, high-throughput methods are required to accomplish such screening in

a timely matter. Usually this simply means using multiple computer processors with a reasonably fast docking tool and performing docking with a database of molecules. Many times it is advantageous to use a combination of several docking software for both the search and scoring algorithms in order to find a consensus subset of the best docking small molecules. (Vajda and Kozakov 2009) While the details of this protocol are out of the scope of this chapter, we list some literature to further elucidate virtual screening. (Cross et al. 2009, Irwin 2008, Jain 2004, Kitchen et al. 2004, Kontoyianni et al. 2008, Shoichet 2004, Zoete et al. 2009)

2.2 Coarse Grain Molecular Dynamics (CGMD)

There are many groups that have tried to develop coarse grain models, but Schulten's group implemented a rather robust version that comes ready-to-use in the VMD/NAMD package (Humphrey et al. 1996, Nelson et al. 1996). The protocol for a protein-lipid CG model, based on Marrink et. al.'s CG model for lipids (Marrink and de Vries. . . 2004), is well documented on the websites:

(<http://www.ks.uiuc.edu/Research/CG/> and

<http://www.ks.uiuc.edu/Research/vmd/plugins/cgtools/>).

2.2.1 Shape-Based Coarse Graining: SBCG

In the case of SBCG, the user must determine the number of beads that will represent the all-atom structure. The center of mass of whichever atoms are grouped together becomes the site of the bead that represents them. The fewer beads used, the coarser the representation. Each of these need to be parameterized and that requires an MD simulation of the all-atom structure. The longer this all atom MD is, the better the parameterization, assuming more conformations are represented. Like typical force fields, a term for intramolecular interactions (bond length, angle, and di-hedrals) as well as intermolecular interactions (van der Waals and Lennard-Jones potential) are required. This has been done for a number of protein-lipid models. (Arkipov et al. 2006, Freddolino et al. 2008)

2.2.2 Residue-Based Coarse Graining: RBCG

RBCG, on the other hand, requires much less parameterization since we are using values that have been tested in a number of simulations that include both proteins and lipids. (Shih et al. 2006a, Shih et al. 2007) Residues are represented with two beads: one for the back-bone and one for the side chain (or just one in the case of Alanine).

Chapter 3

The Interaction of Cofilin with the Actin Filament

This chapter will describe the work in accomplishing all the goals in Part 1 and a subset of the goals in Part 2. The first task is to determine how cofilin structurally bind to F-actin and then find the contacts points and important sites that affect binding or mechanics. Here, I give details of how to build a model to achieve this end and present the results of molecular docking and dynamics studies using a muscle actin filament and human cofilin I. Guided by extensive mutagenesis results as well as other biophysical and structural studies, I arrived at a model for cofilin bound to the actin filament. This predicted structure agrees very well with cryo-electron microscopy results of cofilin-decorated filaments, provides molecular insight into how the known F- and G-actin sites on cofilin interact with the filament, and also suggests new interaction sites that may play a role in cofilin binding. The resulting model also helps to understand the molecular function and regulation of cofilin and will provide a starting point for larger scale simulation work.

3.1 Introduction

The regulation of actin polymerization is vital for cellular function, particularly in processes such as cell division and migration where rapid reorganization of the cytoskeleton is required. Cofilin plays a key role in this regulation process. Cofilin was first implicated for its function as a filament severing protein (Hawkins et al. 1993, Hayden et al. 1993), but it has subsequently been shown to have a much broader

physiological role (see (Bernstein and Bamberg 2010) for a recent review). In order to understand the molecular function of this protein, the past two decades have seen an extensive array of biochemical and genetic studies (Lappalainen et al. 1997, Moriyama et al. 1992, Moriyama et al. 1996, Moriyama and Yahara 2002, Pope et al. 2000, Rodal et al. 1999), x-ray, NMR and cryo-EM structural work (Fedorov et al. 1997, McGough et al. 1997, Galkin et al. 2001, Pope et al. 2004), numerous biophysical studies (Blanchoin and Pollard 1999, De la Cruz 2005, Andrianantoandro and Pollard 2006, Grintsevich et al. 2008, McCullough et al. 2008, Michelot et al. 2007), as well as computer simulation work (Pfaendtner et al. 2010, Wriggers et al. 1998, Carlsson 2006, De la Cruz and Sept 2010, Frantz et al. 2008). Collectively, these studies have given us critical pieces of information about the interaction of cofilin with the actin filament.

One complicating factor in this system is that cofilin binds both to monomeric or G-actin as well as polymerized actin filaments or F-actin. The generation of numerous cofilin and actin mutations has provided molecular details on how these proteins interact with each other. (Lappalainen et al. 1997, Moriyama et al. 1992, Moriyama et al. 1996, Moriyama and Yahara 2002, Pope et al. 2000, Rodal et al. 1999) Through these studies it has been determined that the G- and F-actin binding modes have some common features; however there are some intrinsic differences and a number of amino acids appear to only affect one of the two interactions. Along with this mutagenesis work, structural studies have provided significant insight into the interaction of cofilin with actin. Here again, cryo-EM work has characterized the filament interactions, such as the twist induced by cofilin binding (McGough et al. 1997) as well as changes in the orientation of the protomer (Galkin et al. 2001), and our knowledge of the interaction with G-actin with cofilin is informed by co-crystal structures with two ADF/cofilin homologs: gelsolin segment 1 (McLaughlin et al. 1993) and more recently, twinfilin (Paavilainen et al. 2008). These structural data are invaluable, however we still lack a detailed understanding of the direct molecular interactions between cofilin and F-actin.

Here we present the results of molecular docking and molecular dynamics studies aimed at deriving a molecular model for the cofilin/F-actin complex. Recent work from Pfaendtner et al. (Pfaendtner et al. 2010) illustrated the utility of such types of simulations in studying this system. Using the cofilactin structure derived from

electron microscopy by Galkin et al. (Galkin et al. 2001), the authors simulated the dynamics of the cofilin-bound filament and thus were able to gain insight into the dynamics and mechanics of this system. The methods we employ in this work are similar, however our objective here is very different, namely to derive an independent structural model for the cofilin-bound filament that agrees with the biochemical and structural data detailed above.

3.2 Methods

3.2.1 Secondary Structure Alignment

Multiple sequence alignments (MSA) using standard alignment tools do not account for secondary or tertiary structure and this has been shown to lead to incorrect alignments for ADF/cofilin family proteins (Lin et al. 2010). Here, a secondary structure MSA was built from a selection of relevant ADF/cofilin family proteins as well as ADF Homology Domain (ADF-H) homologs. The VMD plugin tool, MultiSeq (Humphrey et al. 1996), was used for the initial alignment of sequences. The structures used were for human cofilin (PDB 1Q8G, also the seed structure), *S. cerevisiae* cofilin (PDB 1CFY), *S. pombe* cofilin (PDB 2I2Q), chicken cofilin (PDB 1TVJ), *A. thaliana* ADF (PDB 1F7S), *A. polyphaga* actotrophin (PDB 1CNU), and human coactosin (PDB 1T3Y). Some minor manual corrections to the alignment were necessary particularly at the anchor points near the loops (between human R21 to R32 as well as V57 to D65), which would not be done correctly based on sequence alone. Porcine cofilin was used in some mutagenesis work, but since there is no solved structure and it has nearly 100% sequence identity with human cofilin (a single C108S substitution), we did not include it in our alignment.

3.2.2 Docking and Refinement Simulations

In order to prepare for molecular docking studies, we first constructed an 8-protomer actin filament using the recent model from Oda et al. (PDB 2ZWH) (Oda et al. 2009). The filament was simulated using molecular dynamics (MD) as detailed in the

following section. A series of 6 filament structures were then extracted at 0, 5, 10, 15, 20 and 25 ns for use in docking studies. For cofilin, instead of performing additional MD simulations, we were able to use 10 models from the NMR structure of human cofilin I (PDB 1Q8G) (Pope et al. 2004).

Docking was carried out using RosettaDock (Gray et al. 2003). Each combination of filament and cofilin structure was used resulting in 60 different pairs. An initial unbiased docking was performed, where the cofilin was given full freedom to bind anywhere along the actin filament. All bound complexes were ranked by their docking score and their general correspondence to the cryo-EM structure of the decorated filament, and the top 20 scoring models were chosen as the starting structures for refinement dockings. In this next round of docking, more restrictive parameters (e.g. allowing 10 Å translation, 30° rotation from the starting structure) were applied; the top cofilin models that had the most buried surface area and the greatest number of F- and G- sites (S3, K96/K98, K112/K114, C139/E142 and E151/K152) in contact with the actin filament were chosen for each of the six binding sites along the filament. The 25 ns filament snapshot had the best representation of these top binding models and became the basis for our fully decorated filament.

(Note that the process of finding the best metric to find the best model was a very involved process. An exhaustive search for correlations amongst Rosetta Energy, RMSD, number of contact points, solvent accessible surface area, as well as calculated energies were explored.)

In order to test the stability of the models, the fully decorated filament, with 6 cofilin bound in 6 different binding models, was simulated using MD for more than 80 ns. Using contact analysis and RMSD, two of the six models appeared to be more stable than their counterparts and maintained better contact with the actin filament. These two conformations ended up with very similar structures and contacts, and formed the basis for the final model, and this structure was replicated at all six binding sites on the filament. This new, decorated filament was used for analysis and further MD simulation as detailed below.

3.2.3 Molecular Dynamics Simulations

The bare and decorated filaments were simulated with all atom molecular dynamics (MD). Simulations were performed in an isothermal-adiabatic (NpT) ensemble with the CHARMM27 force field and TIP3P water model, under periodic boundary conditions. Each actin protomer had ADP as the bound nucleotide. Bonded interactions were computed every 2 fs using SHAKE, short-ranged non-bonded electrostatic and van der Waals (with a 10 Å cutoff and smooth switching function beginning at 8.5 Å, and pair-list distance of 11.5 Å). Long-ranged, full electrostatic interactions were computed every 4 fs with the Particle Mesh Ewald method with grid points at least 1/ Å in each dimension. Using Langevin Dynamics, NpT conditions were maintained at 1 atm and temperature of 300 K with a damping coefficient of 1 ps⁻¹ and a Langevin piston oscillation period of 200 fs and decay of 100 fs for the production run (200 fs and 500 fs respectively for both heating and equilibration). Following minimization, the system was heated in 50 K steps with 40 ps per step and restraints on the C α atoms. At 300 K, the restraints were removed and the system was allowed to equilibrate for approximately 1 ns before the production run was started.

3.3 Results

3.3.1 Secondary Structure Alignment

In order to correlate all of the published experimental mutagenesis results, our first task was to generate an accurate alignment of the ADF/cofilin sequences. Structural conservation within this family is high, although sequence conservation is variable depending on which proteins are chosen (average of 32% across the sequences presented here). There are many insertions and deletions that occur, and this presents real challenges for alignment methods that only consider sequence similarity. Structure-based methods produce better sequence alignments in situations like this, but automated methods that consider both structure and sequence still face difficulties (Kim and Lee 2007). For this reason, we started with a sequence-based alignment and manually adjusted the gaps based on secondary and tertiary structure. This method

brings more regions of the proteins into register and we see a much higher degree of correlation between the secondary structure and the individual mutagenesis results (see Figure 3.2). Obviously the alignment of human and yeast cofilin is of primary interest in this effort since these two systems formed the basis for the majority of the mutagenesis work (Figure 3.3). The difficulties of aligning the yeast and human cofilin sequences has been noted in the past (Lin et al. 2010). Our manually curated alignment solves these ambiguities, and we now see proper alignment, for example, between K22-R32/G58-D66 in human cofilin with the regions K23-K26/D47-S49 in the yeast protein.

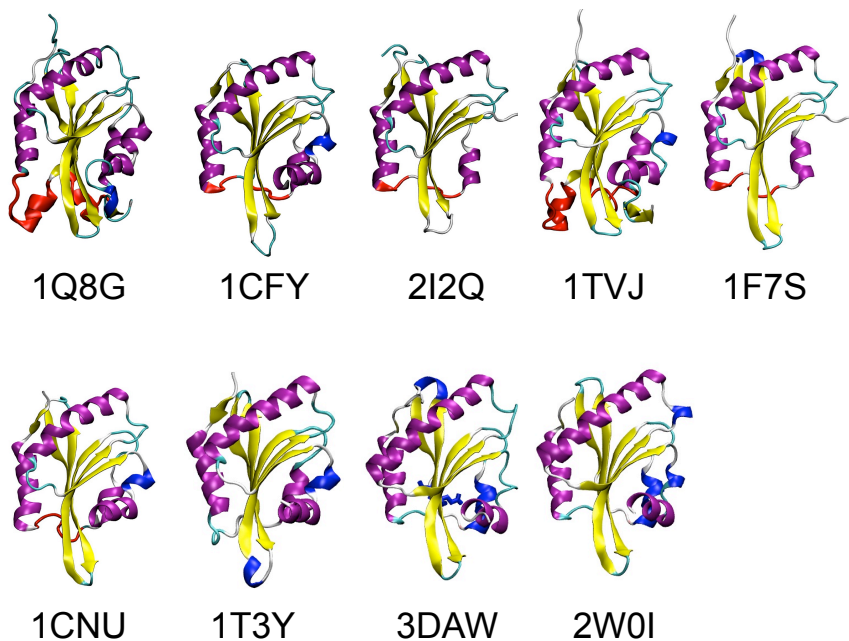


Figure 3.1: Structural Alignment

3.3.2 Model for the Cofilin/F-actin Complex

As described in the Methods, we performed several iterations of molecular docking, using both the mutagenesis results and the stability of the cofilin/F-actin complex in MD simulations as a quality metric for a given model. The results can be seen in

Table 3.1: PDB IDs: PDB IDs and associated proteins.

PDBID	Species	protein
1Q8G	human	cofilin
1CFY	<i>S. cerevisiae</i> (yeast)	cofilin
2I2Q	<i>S. pombe</i> (yeast)	cofilin
1TVJ	chicken	cofilin
1F7S	<i>A. thaliana</i>	ADF
1CNU	<i>A. polyphaga</i>	actotrophin
1T3Y	human	coactosin
3DAW	mouse	twinfilin (C-ter)
2W0I	human	twinfilin (C-ter)



Figure 3.2: A structure-based sequence alignment for seven ADF/cofilin proteins and homologs (see Methods for details on the sequences). Shaded regions of the sequences indicated secondary structure elements and colored bars above the sequence denote regions of contact in our model and the location of lethal mutations (red), mutations with a WT phenotype (green) and novel mutations suggested by our model (blue) (see text for mutation references).

Figure 3.4. See Chapter 4 Results Section 4.3.1 for an explanation of analysis, but briefly, two of the flanking actin protomers (i and $i+2$) to a cofilin are fitted for the entire trajectory and the **relative RMSD** is calculated for the cofilin (or actin $i+1$ as a baseline control). See Figure 3.7 for a diagram of this indexing. Four of the models

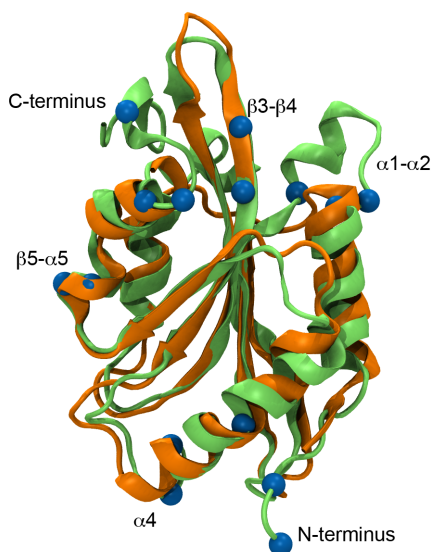


Figure 3.3: A structural alignment of human cofilin (green) and yeast cofilin (orange). The secondary structure elements discussed in the text are labeled and the locations of lethal point mutations explained by our docking model are shown as blue spheres.

(Cofilin 2, 3, and 4) have relative RMSD values of greater than 1 nm (or 10 Å) which suggests they are not tightly bound, although observing the trajectory would have been insufficient to observe the subtle difference between bound and unbound. Two of the binding models (Cofilin 5 and 6) show the lowest relative RMSD values (under 7 Å), not much greater than their actin counterparts; they also have the greatest number of residues in contact. Not only are the relative RMSD values low but their fluctuations are also low, like the actin controls. Cofilin 6 was used as the best docked model for subsequent filament models. See Figure 3.4, purple line (Act6-8Cof6) for Cofilin 6's relative RMSD.

The final model showed very good interaction with the filament, appeared to maintain its contacts with the filament when subjected to MD simulation, and the binding interfaces explain mutations on both the cofilin and actin sides. Figure 3.5 shows details of our cofilin/F-actin model where the binding surfaces have been highlighted in yellow and mutations known to affect cofilin binding are shown in red. This model was used as a template to produce a fully decorated cofilactin filament consisting of 8 actin protomers and 6 cofilin molecules. MD simulations were then performed using this cofilactin model and we analyzed buried surface area as well as the statistics of atomic contacts, salt bridges and hydrogen bonds formed during the course of the

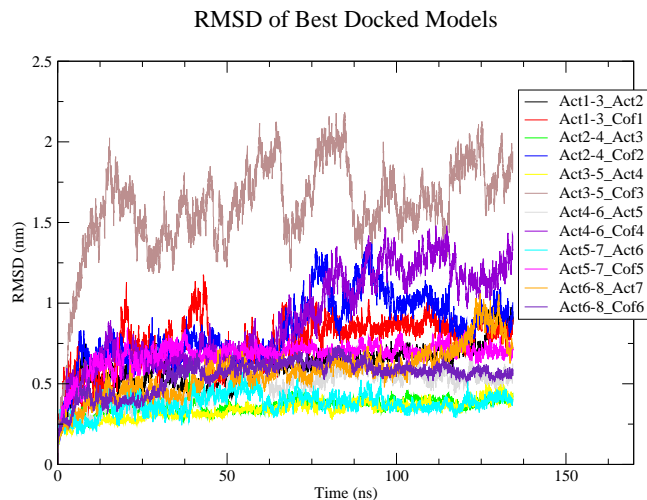


Figure 3.4: Relative RMSD of Best Docked Models: Flanking actins (Actin i and Actin $i+2$) are fitted with least squares and the RMSD of the bound Cofilin i or Actin $i+1$ on the opposing side is calculated over the course of the trajectory. Note the low fluctuations for the opposing actin, signifying consistent binding. Some cofilin show the same low fluctuations (as if bound) and others do not (as if not bound well). Cofilin 6 appears to be the best model, with its lowest RMSD values like that of the actin, and was thus used as the best docked model. All frames are sampled at 0.02 ns.

simulation. There is an average of about 700 \AA^2 of buried surface area per bound cofilin as well as 4-5 salt bridges at any given point in the simulation. The molecular details of these interactions will be discussed in more detail in the following section. (The frequency of salt bridge contacts can be seen in Table 3.2.)

Our model complex obviously matches well with mutagenesis results since a subset of these results were used to rank and filter our docked models, but it also is in very good agreement with available structure information. Figure 3.6 shows a comparison of our cofilin/F-actin complex with the cryo-EM structure from Galkin et al. (Galkin et al. 2003) as well the twinfilin/G-actin crystal structure (Paavilainen et al. 2008). In Figure 3.6a, the molecular model fits extremely well within the envelope of the EM density map. It is also interesting that although complex with monomeric actin, the twinfilin/G-actin complex also shows good correspondence with our docked model when put in the context of the full filament (Figure 3.6b). There are some minor clashes between twinfilin and the Actin-B protomer, but since this crystal is with G-actin, this is perfectly understandable.

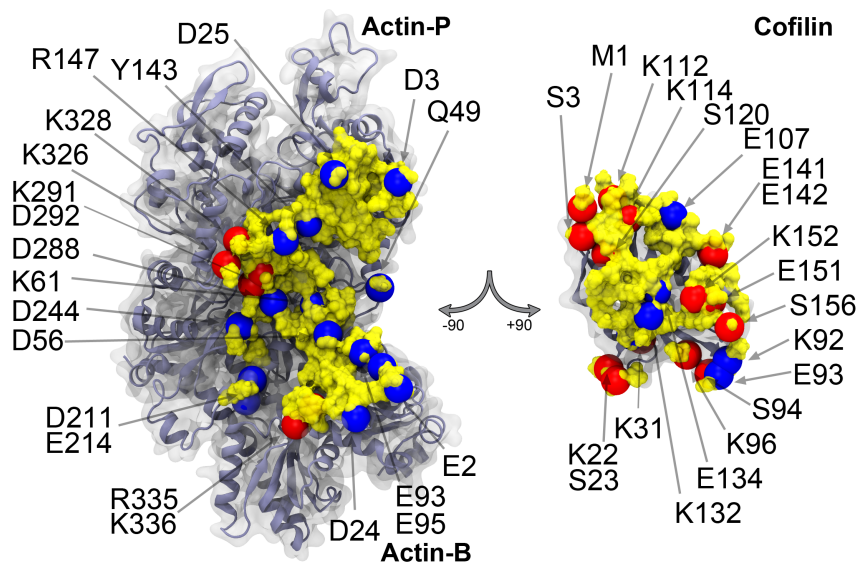


Figure 3.5: Molecular details of the interaction between cofilin and the actin filament. On the left is an actin trimer where we have labeled the two actin protomers that contact cofilin (Actin-P and Actin-B). The contact surfaces within 5 Å of the binding partner have been highlighted in yellow. Lethal mutations for both proteins are shown as red spheres while other contact points predicted by the model are shown in blue.

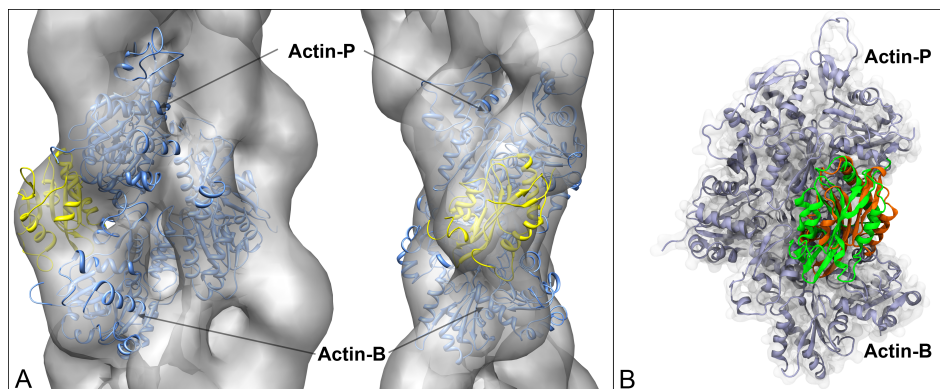


Figure 3.6: Comparison of our cofilin/F-actin complex with (a) the EM volume reconstruction of Galkin et al. (Galkin et al. 2003) and (b) the twinfilin/G-actin structure of Paavilainen et al. (Paavilainen et al. 2008). For the EM comparison in (a), our model depicts the actin trimer in blue and cofilin in yellow, and the position and orientation was determined by optimizing the fit between our model and the electron density map using Chimera (Pettersen et al. 2004). In (b), our model cofilin is shown in orange and twinfilin in green, and the relative orientation was determined by fitting the G-actin in the twinfilin structure to our Actin-P protomer.

3.3.3 Analysis of Known Cofilin Mutations

Having a detailed molecular model allows us to perform equally detailed analysis of the interactions between cofilin and the actin filament. In the following section some of the

Salt Bridge Analysis of AA Decorated Filament, 0-170 ns, dt=0.2 ns, 850 frames

COF	ACT	Actin	Cofilin Chain						Avg
			CF1	CF2	CF3	CF4	CF5	CF6	
Experimental									
K96	D56	3	34%	77%	60%	0%	75%	0%	41%
	E93	3	0%	0%	0%	12%	23%	0%	6%
K112	D25	1	26%	4%	13%	23%	10%	16%	15%
E141	K326	1	19%	51%	13%	6%	20%	25%	22%
	K328	1	5%	0%	7%	3%	22%	0%	6%
E142	K328	1	36%	80%	48%	67%	49%	66%	58%
	R147	1	93%	0%	24%	96%	88%	59%	60%
E151	K291	1	78%	0%	63%	70%	23%	45%	47%
K152	R292	1	70%	60%	17%	58%	0%	33%	40%
Exp Average			40%	30%	27%	37%	34%	27%	33%
NEW Residues									
K19	E93	3	0%	0%	86%	16%	16%	6%	21%
K22	D24	3	0%	0%	7%	47%	2%	11%	11%
	E2	3	36%	0%	7%	0%	7%	10%	10%
K92	D211	3	0%	58%	2%	0%	14%	13%	15%
	E214	3	46%	86%	0%	3%	82%	0%	36%
E93	R335	3	14%	80%	0%	0%	0%	28%	20%
	K336	3	14%	0%	0%	91%	0%	5%	18%
E107	R147	1	50%	1%	47%	2%	3%	0%	17%
	K328	1	35%	2%	25%	0%	5%	12%	13%
K132	E93	3	99%	99%	86%	77%	18%	64%	74%
	D56	3	86%	85%	84%	75%	17%	85%	72%
E134	K61	3	45%	74%	39%	19%	0%	9%	31%
Total Average			38%	36%	30%	33%	23%	24%	26%

Cofilin Residues Key

1	binds to Actin-P (Act i)
3	binds to Actin-B (Act i+2)
known F site	
known FG site	

Actin Residues key

ts- or cs-/ts- actin mutation (Rodal)
lethal mutation for cofilin binding (Rodal)
new actin residue identified

Table 3.2: Salt Bridge Contacts of Known and New Residues: The frequency of salt bridge formations are presented in this table. Note that as expected, many of the new residues found are from binding to Actin-B, an “F-site”.

key interactions between cofilin and actin and how these compare with experimental findings are discussed. We have adopted the convention where Actin-B/Actin-P refers to the actin protomer directly adjacent to the bound cofilin on barbed/pointed side (see Figure 3.7). Further, the amino acid numbers and the locations of secondary structure elements all use the human cofilin sequence/structure as the reference (see Figure 3.3). Table 3.3 shows exhaustive annotation of the known mutations.

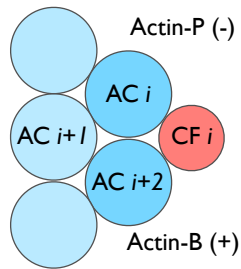


Figure 3.7: Actin-P and Actin-B: Actin-P is downstream towards the pointed end (aka AC i) and Actin-B is upstream towards the barbed end (aka AC $i+1$).

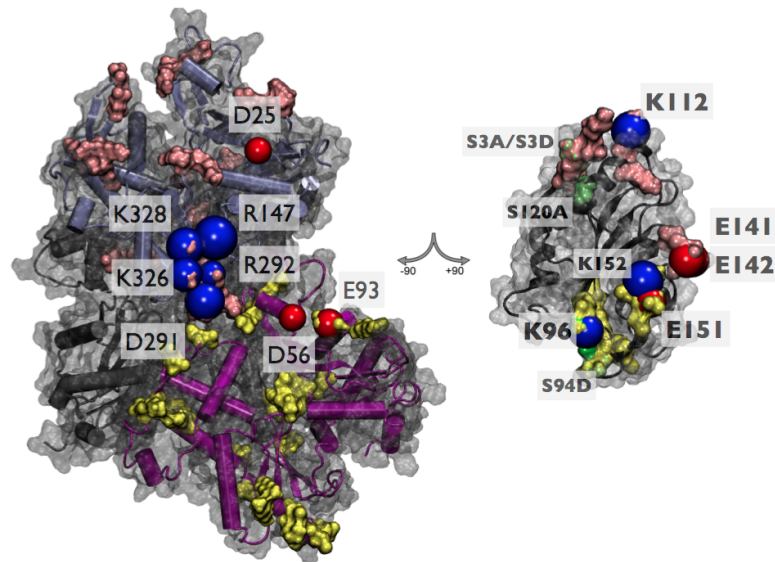


Figure 3.8: Binding model contact residues that match **cofilin** mutagenesis: The pink and yellow surfaces correspond to mutagenesis from Rodal et al. 1999. Blue and red beads are basic and acidic residues, respectively, from known mutagenesis studies that are found in salt bridge formation in our model.

N terminus and Ser3

The deletion of the first five residues in the N-terminus (*cof1-28*) prevents binding to both G- and F-actin (Lappalainen et al. 1997, Moriyama and Yahara 2002). Similarly, mutation of S3 to D/E, a known phosphorylation site, also eliminates binding (Lappalainen et al. 1997, Moriyama et al. 1996, Pope et al. 2000). We see significant interactions with this region of cofilin in our model with M1 making contact 100% of the time, often with D3 on Actin-P, and S3 contacting with actin about 78% of the time, with no specific hydrogen bonding.

Alpha 1 – Alpha 2

The *cof1-8* yeast mutation K23A/K24A/Y25A aligns to K22/S23/K31 in human cofilin. This is a temperature sensitive mutation, however it has not been tested in vitro for F-actin binding (Lappalainen et al. 1997). K22 has 71% contact with the filament and forms intermittent salt bridges with D24 and E2 of Actin-B while S23 has 63% contact. Interestingly, the *cof1-8* mutation occurs around a loop region where human cofilin has a short α -helix inserted. This will be covered later in the Discussion.

Beta 3 – Beta 4

The R80A/K82A mutation in yeast (*cof1-16*) is lethal and weakens binding to F-actin (Lappalainen et al. 1997). Further, both the S94D mutation (Moriyama and Yahara 2002) and the K96Q mutation (Pope et al. 2000) appear to eliminate binding of human cofilin to the actin filament. In many sequence alignments, R80/K82 in yeast are aligned with K96/D98 in human cofilin (Pope et al. 2004, Paavilainen et al. 2008, Bamberg et al. 1999, Gorbatyuk et al. 2006) however based on function and interactions we see, it seems more appropriate to equate these amino acids with S94/K96 in human cofilin even though they are not aligned. There is a sustained interaction between both S94 and K96 with Actin-B, with K96 on cofilin forming a persistent salt bridge with D56 on actin, while D98 on cofilin has only 34% contact and no observable hydrogen bonding or salt bridge interactions. Alternatively, it may be that only R80A is necessary to lose F-actin binding.

Alpha 4

Yeast R96A/K98A (*cof1-17*) is a lethal mutation (Lappalainen et al. 1997) that appears to align with human K112/K114. Just two turns along this same helix, S120A also decreases F-actin binding as compared to WT cofilin (Moriyama and Yahara 2002). There is very good interactions between K112 and D25 on Actin-P with a salt bridge formed about 82% of the time. K114 also forms consistent contacts with Actin-P, but appears to be nonspecific. S120 makes some contact with the filament

(13% of the time), but S119 has 100% contact, and D122 makes 85% contact with Q49 on Actin-B and Y143 on Actin-P.

Beta 5/Alpha 5 Loop

The yeast D123A/E126A (*cof1-20*) mutation is lethal and results in weaker filament binding (Lappalainen et al. 1997). These yeast residues align with C139/E142, however the human protein has an additional glutamate at position 141. C139 does make consistent contacts in our model, but both E141 and E142 make salt bridges: E141 with K326 and K328 on Actin-P, and E142 with R147 and K328, also on Actin-P. It seems highly probable that E141 is matching the interactions of D123 in yeast while E142 matches those of E126, but this discrepancy underlines the difficulties of making simple assignments based on sequence alignments.

C-terminus

Yeast E134A/R135A/R138A (*cof1-22*) is a temperature sensitive mutation that leads to reduced F-actin binding (Lappalainen et al. 1997). Based solely on sequence, these three yeast residues would align with E151/K152/G155 (Pope et al. 2004, Paavilainen et al. 2008, Bamberg et al. 1999, Gorbatyuk et al. 2006) and indeed there is good interactions between E151 and K291 on Actin-P, and K152 with D292 also on Actin-P. G155 obviously appears as a weak candidate for an interaction site based on our knowledge of protein biochemistry, however the neighboring residue S156 seems like a much more promising equivalent since it makes contacts more than 75% of the time and forms hydrogen bonds with residues D211 and D244 on Actin-P.

WT mutations

In addition to the many mutations that affect F-actin binding, there are numerous cofilin mutations that appear to have WT binding. As seen in Figure 3.2, the vast majority of these mutations fall outside of our contact regions with the filament. In this sense they do support our binding model as negative controls, but mutation of

contact residues does not always have an effect on binding (Bogan and Thorn 1998) and thus we cannot place too much weight in this correspondence.

New Putative Cofilin Contacts

Although there has been extensive mutagenesis performed on cofilin, our model has several points of interaction that appear to be novel, namely K19, K92, E93, E107, K132 and E134. K22 was previously identified, but K19, which aligns to K20A in yeast, looked to be like wild type (*cof1-6* D18A/K20A), but was never tested for filament binding. In our model K19 forms a salt bridge with E93 on Actin-B, and the E93A/E95A mutation on actin is lethal to cofilin binding (Rodal et al. 1999). Similarly, there are interactions between K92 and E214 on Actin-B, as well as E93 with R335/K336 on Actin-B. Although K92 and E93 have not been mutated, the E334A/R335A/K336A mutation on actin is lethal to cofilin binding (Rodal et al. 1999). E107 on cofilin interacts with both R147 and K328 on Actin-P, and the K326A/K328A actin mutation affects cofilin binding (Rodal et al. 1999), but E141/E142 on cofilin interacts with this same site. Finally, K132 and E134 show interactions with D56/E93 and K61 respectively, both on Actin-B. Interestingly, these two residues flank H133 that was tested for its ability to confer pH dependent severing (Frantz et al. 2008), however these interaction sites have not been directly tested. These new putative cofilin contacts can be seen more clearly in Figure 3.9.

Unmatched Cofilin Mutations

Our model matches a large group of mutagenesis results, however there are a few cofilin mutations that are not readily explained. Yeast D10A/E11A (*cof1-5*) and D34A/K36A/E38A (*cof1-9*) align to human D9/G10 and E42/K44/N46 respectively, and both are temperature sensitive mutations. (Lappalainen et al. 1997) Neither region of cofilin shows contact with the filament in our model, but since these mutations also show no change in F-actin binding in in vitro assays, they may be affecting some other aspect of cofilin structure, dynamics or interactions that would not be captured in our binding model. Another mutation, D68A/E70A/E72A in yeast (*cof1-14*), is lethal and lowers stability and slightly decreases F-actin binding. (Lappalainen et al.

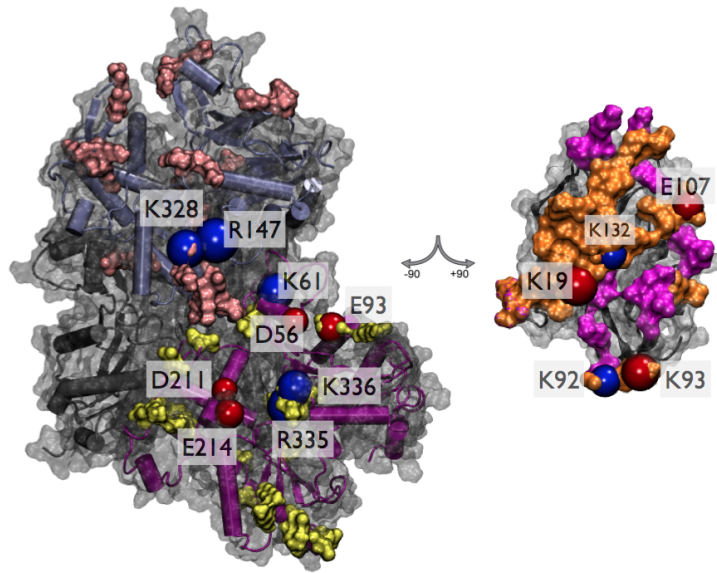


Figure 3.9: New binding model contact residues on cofilin: The pink and yellow surfaces correspond to mutagenesis from Rodal et al. 1999. Blue and red beads are basic and acidic residues, respectively. The magenta surface on cofilin correspond to residues on the model's binding surface also seen in experimental data. The orange surface are residues seen only on the model's binding surface (within 5 Å of actin averaged over the 50-100 ns of the trajectory).

1997) This mutation maps to D86/T88/E90 on human cofilin, but since it makes no contact in our model the phenotype is difficult to account for.

Analysis of Actin Mutations

Apart from change to cofilin, there have also been mutagenesis performed with actin. (Wertman et al. 1992) This series of mutations were tested for cofilin activity with a mixture of results. (Rodal et al. 1999) Some of the mutations (*act1-107*, *act1-130*, *act1-127*, *act1-128* and *act1-108*) failed to show interaction with cofilin or any other actin binding protein, suggesting that there may be changes to the structure or stability of the actin. However, three mutations, *act1-103*, *act1-106* and *act1-126*, exhibited binding defects specific for cofilin. The *act1-103* mutation is E334A/R335A/K336A, and we see ionic bonds formed between both R335 and K336 with E93 on cofilin. Similarly, the *act1-106* mutation involves R290A/K291A/E292A, and salt bridges form between K291 and E151 on cofilin as well as E292 and K152 on cofilin. Finally, the *act1-126* mutation site has multiple interactions. This mutation is K326A/K328A

and there are several interchangeable salt bridges between K326A and E141/E151 on cofilin plus K328 and E107/E141/E142 on cofilin. Several salt bridges also form with E93 on Actin-B and D288 in Actin-P, but since these amino acids are part of the *act1-130* and *act1-107* mutations, respectively, we cannot draw any firm conclusions. As a potential new contact site, we see significant interactions between R147 on Actin-P with both E107 and E142 on cofilin.

Table 3.3: Complete Annotated Table of Human Cofilin: Red mutagenesis affects F/G-binding, orange affects F-binding only, yellow lowers F-binding, green exhibits wild-type in F-actin binding, and purple is undetermined in F-actin binding.

Resid	Res	Freq Contact w/ in 5 Å, dt10 50-170 ns	Model Results: Binding interactions to F-actin			Yeast Mutation (Lappalainen 1997) Alanine Muth Phenotype	Mutagenesis		Other Annotation from Literature	
			match experimental	new residues	does not match experimental		Yeast Mutations	Porcine or Human Mutations		
1	M	1.00	X high contact			FG	<i>cof1-28</i> : del M1-G5 lethal	porcine ΔN5 binds F moderately (+), depol weakly (±), no sever (-) (Moriyama 02)		
2	A	0.86	X high contact				yeast S2A/S4D & S2D/S4D lethal (Moriyama 96)			
3	S	0.78	X high contact			S3E, S3D no bind	<i>cof1-3</i> : S4E lethal; <i>cof1-4</i> : S4A;	S3D lethal & pS3 does not bind (Moriyama 96); S3D lethal, like pS3 (Pope 2000); porcine S3A binds/form rods (Moriyama 96)	*pH < 7.5, binds but does not sever (Moriyama 2002) *unphosphorylated Ser makes N term unstruct & flexible (Frantz 08, MD)	
4	G	0.40								
5	V	0.15								
6	A	0.06								
7	V	0.00								
8	S	0.00								
9	D	0.00	X			ts-	<i>cof1-5</i> : D10A, E11A			
10	G	0.00	X				D10A, E11A			
11	V	0.00								
12	I	0.08								
13	K	0.00								
14	V	0.00								
15	F	0.33								
16	N	0.47								
17	D	0.05	X			wt	<i>cof1-6</i> : D18A, K20A WT			
18	M	0.01								
19	K	0.96		E93 (Actin 3)	X		D18A, K20A			
20	V	0.88								
21	R	0.75								
22	K	0.71	X ND	D24 or E2 (Actin 3) (low confidence)	?	ts-, nd	<i>cof1-8</i> : K23A, K24A, K26A ts-, not determined			
23	S	0.63	X ND		?		K23A, K24A, K26A			
24	S	0.32								
25	T	0.14								
26	P	0.00								
27	E	0.04								
28	E	0.01								
29	V	0.00								
30	K	0.00								
31	K	0.00								
32	R	0.06	X ND		?		K23A, K24A, K26A			
33	K	0.00								
34	K	0.00								
35	A	0.00								
36	V	0.00								
37	L	0.00								
38	F	0.00								
39	C	0.00						C39 & C80 critical to reg & function; C39G weakly phos S3; C39G same conf change as oxidized (Klemke 08)	may disulfide bond w/ C147 to self assoc. as oligomers dimerization, in vitro w/ oxidative stress (eg glutathione) (Pfannstiel 2001)	if all oxidized, disulfide bond as C39-C80; can disulf bond w/ C139 but C80 "ties it up" (Klamt 09)
40	L	0.00								
41	S	0.00								
42	E	0.02	X			WT to F	<i>cof1-9</i> : D34A, K36A, E38A lethal			
43	D	0.09								
44	K	0.50	X				D34A, K36A, E38A			
45	K	0.24								
46	N	0.01	X				D34A, K36A, E38A			
47	I	0.00								

96	K	0.84	D56 or E93 (Actin 3); should be aligned to K82A in yeast?			F	cof1-16: R80A, K82A lethal	K95Q/K96Q in loop, yes G, no F; S3D/K96Q yes F, no D (Pope 2000); K96Q yes G, no F, alters chem environ B3 & B6-Cter; strong wt pH CSP; hbond w/ Y89 (Pope 2004)	in low pH = 6, interact with D98 in actin, MD (Frantz 08)	95-102 homologous to C-ter villin headpiece, KKEK for F-actin binding; yst 79-KRSKIV (Pope 2000)	
97	E	0.43									
98	D	0.34		should not be aligned to K82A in yeast?	X	F	R80A, K82A lethal				
99	L	0.04									
100	V	0.00									
101	F	0.00									
102	I	0.00									
103	F	0.27									
104	W	0.00							104-115: PIP2 binding site (Kusano 1999)		
105	A	0.69									
106	P	0.46									
107	E	0.93		R147 (Actin 1)	X						
108	S	0.50									
109	A	0.39									
110	P	0.22									
111	L	1.00									
112	K	0.82	D25 (Actin 1)			FG	cof1-17: K96A, K98A lethal	K112Q inhibits PIP2 binding, better with K114Q (Moriyama 92)			
113	S	0.01									
114	K	1.00	X high contact			FG	K96A, K98A lethal	K114Q inhibits PIP2 binding (Moriyama 92)			
115	M	1.00									
116	I	0.50									
117	Y	0.18									
118	A	1.00									
119	S	1.00									
120	S	0.13			X			porcine S120A lower F @ pH7, weaker D @ pH 8, no sever/weak turnover (Moriyama 02)			
121	K	0.86			X	WT	cof1-18: K105D, D106A WT				
122	D	0.85			X		K105D, D106A				
123	A	0.39									
124	I	0.00									
125	K	0.77			?	WT	cof1-19: R109A, R110A WT				
126	K	0.80	? X high contact; BB2010		?		R109A, R110A				
127	K	0.06	? BB2010		?						
128	L	0.26									
129	T	0.86									
130	G	0.83									
131	I	0.87									
132	K	1.00	X NMR CSP	E93 or D56 (Actin 3)							

133	H	0.91						hum H133A pH Insens./ salt br. weakened when H133 deprotonated @ higher pH , D98 to K96 instead (Frantz 08)	"confers pH sensitivity to PIP2" (BB2010, Leyman 2009)
134	E	0.79	X NMR CSP	K61 (Actin 3)					
135	L	0.07							
136	Q	1.00							
137	A	0.31							
138	N	0.97							
139	C	0.87	X high contact			FG	<i>cofi-20: D123A, E126A lethal; less stable; low G, low F, low D</i>	C139G still gets oxidized like wt (Klemke 08)	if all oxidized, C139-C47 (Klamt 09)
140	Y	0.05							
141	E	0.67		K326 or K328 (Actin 1); should be aligned to D123A in yeast?	X not noted as FG site in human				
142	E	0.98	K328 or R147 (Actin 1)	should be aligned to E126A in yeast?		FG	D123A, E126A lethal		
143	V	0.02							
144	K	0.08							
145	D	0.45							
146	R	0.12			X	WT	<i>cofi-21: D130A WT</i>		
147	C	0.41						C147G still gets oxidized like wt (Klemke 08);	if all oxidized, C139-C47 (Klamt 09)
148	T	0.54							
149	L	0.00							
150	A	0.02							
151	E	0.88	K291 (Actin 1)			Ts-, F	<i>cofi-22: E134A, R135A, R138A ts-</i>		
152	K	0.83	R292 (Actin 1)				<i>E134A, R135A, R138A ts-</i>		
153	L	0.44							
154	G	0.35							
155	G	0.63	X high contact				<i>E134A, R135A, R138A ts-</i>		
156	S	0.75	X high contact	should be aligned to R138A in yeast	X		should be R138A		
157	A	0.44							
158	V	0.06							
159	I	0.23							
160	S	0.00							
161	L	0.01							
162	E	0.00							
163	G	0.00							
164	K	0.00							
165	P	0.00							
166	L	0.00							

3.4 Discussion

We have developed a molecular model of human cofilin bound to F-actin by utilizing a combination of experimental data and iterative docking and molecular dynamics studies. Our model explains numerous mutagenesis results on both cofilin and actin, and the binding site matches extremely well with available structural data.

One feature that our results highlight is the challenge associated with aligning the sequences of various cofilin homologs. Sequence conservation is moderate within this family of proteins ($\sim 32\%$), but apart from amino acid substitutions, there are numerous insertions and deletions in the protein, making it very difficult to translate point mutations in one system to another. Human and yeast cofilin are great examples of this since the human protein has two insertions in the N-terminal portion of the protein (Figure 3.3). Based on the protein structures, we would place these insertions such that the stretch K22-R32 in human cofilin would align with K23-K26 in yeast, and G58 to D66 in human would correspond to D47-S49 in yeast. Since the function of these two proteins is very similar, one might expect that these two insertion points are not critical for filament binding, however this does not appear to be the case. First, the *cof1-8* allele (K23A/K24A/Y25A) spans the first insertion site and produces a temperature sensitive phenotype in yeast. (Lappalainen et al. 1997). Second, an attempt to insert fluorescent proteins into the yeast protein produced a loss of function phenotype at the first insertion site, but resulted in a function protein at the second site. (Lin et al. 2010) Although our manual alignment fixes discrepancies in these insertions, there is still some ambiguity in interpreting mutations made in other regions of the protein, particularly in some of the central β sheets such as S94 or E142. In this sense, a given sequence alignment does not provide a one-to-one correspondence, but simply is a guide to understanding the relationship between sequence, structure and function.

A key interaction point between cofilin and the filament is the DNase-I loop (D-loop) of the actin protomer. Cryo-EM observations (Galkin et al. 2003), cross-linking studies (Kim et al. 2000), and molecular dynamics simulations (Pfaendtner et al. 2010) have provided significant evidence that the D-loop, as well as other portions of subdomain-2, become disordered upon cofilin binding, thus breaking the contacts between protomers along the long-pitch helix. There are significant interactions with

subdomain-2 in our model. The α -helix containing E93/E95 in Actin-B makes sustained ionic bonds with cofilin, and this was one of the regions of actin that was found to be remodeled in previous MD simulations. (Pfaendtner et al. 2010) We also see hydrogen bonding interactions with Q49 at the C-terminal end of the D-loop and D56/K61 directly below the D-loop. These interactions appear to alter the dynamics and conformation of the D-loop enough that its interactions with subdomain-1 of Actin-P are reduced by about 10% over the course of our MD simulation. The length of our simulation is clearly a limiting factor and we have not had sufficient time to observe the twisting of the filament that would further disrupt these interactions, but this is still consistent with the previous observations mentioned above.

The phosphorylation of S3 on cofilin is a key method of regulating cofilin activity. In our model S3 makes consistent contacts with the actin filament, but we do not see any specific hydrogen bonding interactions. Interestingly, through a series of MD simulations Frantz et al. found that pS3 forms salt bridges with K126/K127 on cofilin. (Frantz et al. 2008) We see that the α -helix containing K126/K127 makes significant contact with the filament, and although mutation of these two basic residues (R109A/R110A in yeast *cof1-19*) has no discernible phenotype in yeast (Lappalainen et al. 1997), the interaction of pS3 would cause the N-terminus of the cofilin to mask several other interaction points along the helix (e.g. K112, K114, S120) and that would likely be enough to eliminate filament binding.

In summary, we have derived an independent model for cofilin bound to the actin filament that agrees well with structural and biochemical data, and further provides insight into filament remodeling and regulation by phosphorylation. This model also suggests new potential sites of interaction on both cofilin and actin that could be tested experimentally and will serve as a starting point for larger-scale simulation studies.

Chapter 4

Short-Ranged Dynamics of Cofilin-Bound Actin Filaments

This chapter will discuss my results for Part 2, to simulate the short-ranged dynamics of cofilin decorated F-actin and explain important contact points that affect binding or mechanics. I have performed a series of molecular dynamics studies using muscle actin and human cofilin I. After determining a model for bound cofilin from the previous chapter, I performed an all-atom molecular dynamics simulations on bare actin filaments, fully decorated filaments, and filaments with cofilin bound at isolated sites and explain how I characterize each filament model.

4.1 Introduction

Much work has been done to understand the motions of actin filaments. Not only are structures insufficiently high enough resolution, they do not capture the full dynamics of filaments. Moreover, they often involve the inclusion of stabilizing agents that may introduce artifacts. When studying cofilin-bound F-actin, one can only reliably find structures for two concentration states: no cofilin and saturating cofilin. Here, we employ Molecular Dynamics (MD) tools to bridge the gap between experimental data and the unobservable to understand how, on the molecular level cofilin interacts with actin.

4.2 Methods

4.2.1 Building Filament models

A **bare, 8-protomer actin filament** was built by using the PDB ID 2ZHW (Oda et al. 2009) and the associated transformation matrix, shifting from one protomer to the next by translating 27.59 Å up the z-axis and rotating -166.4°. (In this dissertation, this angle will be described with a positive value, rotating the other direction on the axis.) A second, **fully decorated filament** was built using the bare filament and fitting the best docked model (derived in Chapter 3) at each of the six available binding sites. To simulate the effects of non-stoichiometric binding conditions, where the concentration of cofilin is **not** saturating, two other filaments were also created.

The third model is a **sparse filament** where a single cofilin is bound at the center of the filament, between Actin 4 (AC4) and Actin 6 (AC6) (designated Cofilin 4 or CF4). The intention of this model is to simulate the best conditions for severing, as described in De la Cruz (2005) and Andrianantoandro and Pollard (2006), where the most efficient filament severing occurs at low concentrations of cofilin. While it may be overly optimistic to observe different twisting or possible severing behavior, especially in an all-atom MD on such low time scales (of hundreds of nanoseconds), this simulation was nevertheless run.

The fourth model is the **split filament** had Cofilins 1, 2, 5, and 6 bound (CF1, CF2, CF5, CF6), but the two center positions (CF3 and CF4) did not. The split filament models a filament with two domains of decorated filament separated by a bare region. While this represents sub-stoichiometric conditions, the intention of this filament was to see if such a scenario would introduce more instability or not.

See Figure 4.1 for filament models.

4.2.2 All-Atom (AA) Molecular Dynamics (MD) Simulation

All four of these filament models were simulated with all atom molecular dynamics (MD) using the same conditions described in Chapter 3:

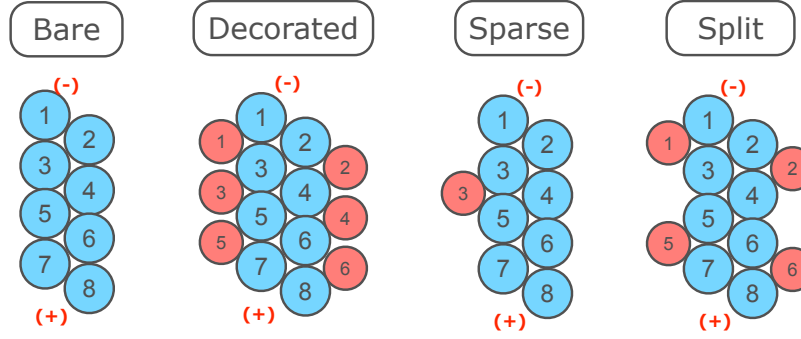


Figure 4.1: All Atom Filament Models: Cartoon representations of bare, decorated, sparse, and split filament models. Actin protomers are represented with blue circles, designated AC1 to AC8. Cofilin are in pink circles, designated CF1 to CF6 for the 6 possible sites. Pointed end (-) at top.

Simulations were performed in an isothermal-adiabatic (NpT) ensemble with the CHARMM27 force field and TIP3P water model, under periodic boundary conditions. Each actin protomer had ADP as the bound nucleotide. Bonded interactions were computed every 2 fs using SHAKE, short-ranged non-bonded electrostatic and van der Waals (with a 10 Å cutoff and smooth switching function beginning at 8.5 Å, and pair-list distance of 11.5 Å) every 2 fs. Long-ranged, full electrostatic interactions were computed every 4 fs with the Particle Mesh Ewald method with grid points at least 1/ Å in each dimension. Using Langevin Dynamics, NpT conditions were maintained at 1 atm and temperature of 300 K with a damping coefficient of 1 ps⁻¹ and a Langevin piston with an oscillation period of 200 fs and decay of 100 fs for the production run (200 fs and 500 fs respectively for both heating and equilibration). Following minimization, the system was heated in 50 K steps with 40 ps per step and restraints on the C α atoms. At 300 K, the restraints were removed and the system was allowed to equilibrate for approximately 1 ns before the production run was started.

Simulations were run at varying times: 90 ns for bare, 170 ns for decorated, over 110 ns for sparse, and over 130 ns for split.

The detailed MD protocol is as follows, with the varying parameters highlighted and remaining the same in the next step unless otherwise noted:

1. **Solvate (explicit) and Ionize** filament. Solvate package (or plugin) with 12 Å padding around the protein and boundary of 2.4. Autoionize package (or plugin) using 0.060 M (with Na⁺ and Cl⁻).
2. **Energy Minimization** until gradient of (minLineGoal) $1.0e^{-1}$ at 0 K. 1 fs timesteps (2 fs for nonbonded and 4 fs for full electrostatic evaluation, 20 steps per cycle), margin of 5 Å, Langevin dynamics on (damping of 10 ps⁻¹, temperature of 75K), Langevin piston off. (6,000 steps for non-backbone atoms (constraining backbone) and 10,000 steps for all atoms.)
3. **Heat** from 0 K to 300 K at 50 K intervals with restraints on C α atoms, rigid bonds. 2 fs timesteps. At each temperature, simulate for 21,000 or more steps.
4. **Equilibrate** while constraining C α atoms, rigid bonds. 2 fs timesteps for 40,000 steps. Langevin dynamics on (damping of 10 ps⁻¹, Langevin temperature of 300K). Langevin Piston on (target of 1.01325 bar, period of 200 fs, decay of 100 fs, and temperature of 300 K).
5. **Equilibrate with no C α constraints** using previous parameters. 2 fs for 355,000 steps.
6. **Production Run** with above parameters. Langevin dynamics on (damping of 1 ps⁻¹, Langevin temperature of 300K). Langevin Piston on (target of 1.01325 bar, period of 200 fs, decay of 500 fs, and temperature of 300 K).

There is a consistent error in the simulation where the cell basis vectors (the boundaries) were reset after every restarting of the trajectory. This caused the first few picoseconds of simulation to have wildly behaving pressures, but NAMD quickly corrected itself upon simulation. This does not appear to greatly affect the simulation results, as the system quickly became stable, but upon fixing this parameter file error, the simulations did not crash and need to restart as often.

4.3 Results

The beginning portion of the trajectory is considered equilibration period which has been disregarded in averaging analysis. Although each of the simulations have been

Table 4.1: All Atom Simulation Details

Filament Model	Total Atoms	Protein Atoms	No. Na ⁺	No. Cl ⁻	No. Water	Sim. Time (ns)
Bare	391,596	47,032	120	8	114,812	90
Decorated	529,530	62,838	141	33	155,506	170
Sparse	451,357	49,633	134	16	133,858	110
Split	530,678	57,556	145	33	157,648	130

run for differing lengths of time, we use the last 50 ns of each trajectory for the following analysis, (except for the decorated filament in which we used the last 100 ns).

4.3.1 Maintaining Binding Contacts

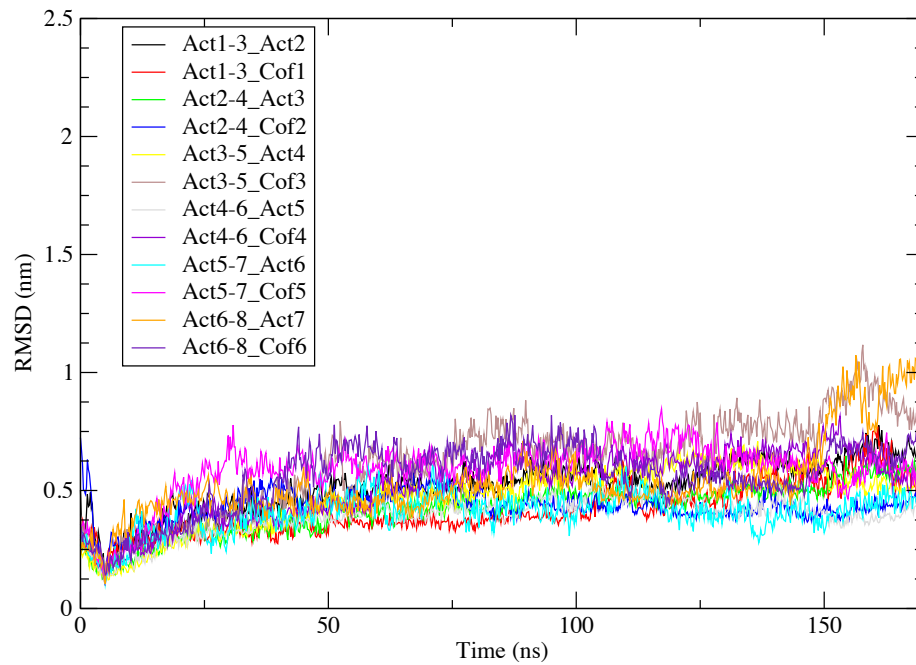
In order to determine how well the cofilin maintained contact with their respective filaments, a Root Mean Squared Distance (RMSD) analysis tracked the distances between the cofilin and of the two flanking actins (Actin-P (i) and Actin-B ($i+2$)) over time. This means the binding distance will be tracked over the course of the simulation. Low fluctuations with low average distance signified binding, high fluctuations with large distances indicate the likelihood of poor binding. The control value is achieved by using Actin i and Actin $i+2$ for the least squares fitting and calculating the RMSD of Actin $i+1$. This value serves as a baseline to compare to when finding the RMSD of Cofilin i because we assume that the actin protomers in the filament will maintain their binding contacts. Observing the trajectory would have been insufficient to observe the subtle difference between bound and unbound.

The RMSD for the decorated filament (Figure 4.3(a)) clearly shows that the values are much lower (mostly under 8 Å) and with low fluctuations. The lines are not as thick due to sampling of every 10 frames, $1/10^{th}$ the rate of the docked models. The reference frame used was from 3 ns time point, which is why the RMSD is not 0 nm at time 0 ns.

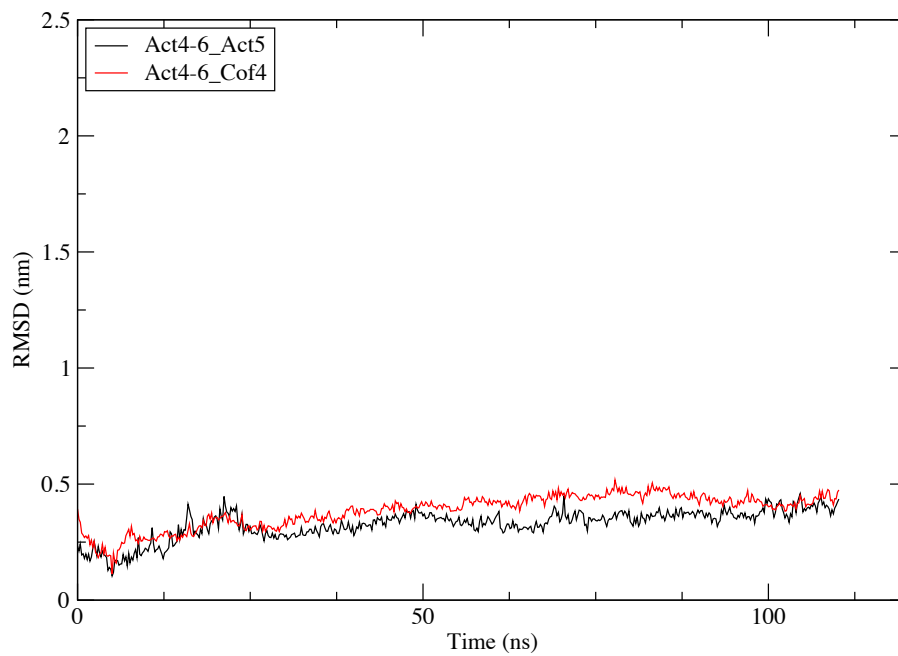
In the sparse filament, only one cofilin was bound so there is only one comparison to its actin control (Figure 4.3(b)). In this case, the RMSD fluctuations and values remain low, below 5 Å. (The reference structure was taken at 6 ns.)

The split filament uses the same starting structures as the decorated filament and most of the RMSD values have a lower average; however, the RMSD values of Cofilin 2 are a bit high, though still below 10 Å. See Figure 4.3(c). (The reference structure was taken at 20 ns.)

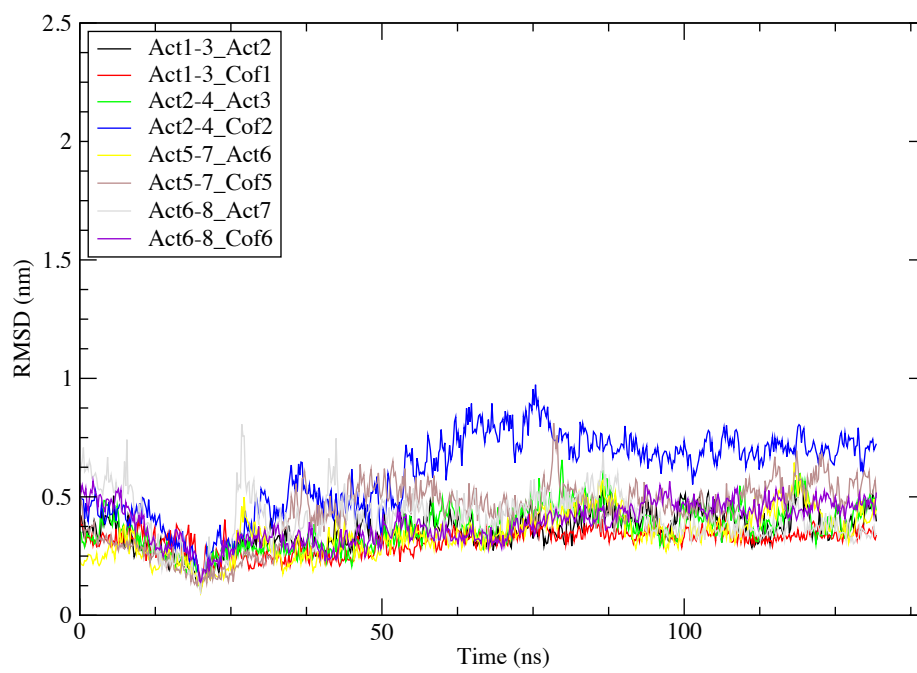
Figure 4.2: RMSD of Filament (Final Models): Overall low fluctuations and low RMSD (with a few isolated cases) show that the contacts, and thus binding, are maintained over time. Frames are sampled at every 0.2 ns.



(a) Decorated Filament



(b) Sparse Filament



(c) Split Filament

4.3.2 Contact Analysis

A contact point is defined when a residue is within 3.5 \AA of the molecule it is binding (cofilin or F-actin), which is more stringent than the analysis presented in Chapter 3. This analysis was carried out on the full 170 ns trajectory, with sampling at every 1 ns.

In the actin contacts (Figure 4.3), cofilin contacts only subdomains 1 and 3 of Actin-P and mostly subdomains (SD) 1 and 2 (occasionally in subdomain 4) of Actin-B. While the contacts appear to be mostly consistent for Actin-P, the peaks tend to be lower, if not more spread out, for Actin-B, which may suggest there is more dynamics occurring.

The cofilin contacts can be seen in Figure 4.4 where there are a mix of very consistent contacts as well as some intermittent ones.

The average solved accessible surface area (SASA) is shown in Table 4.2 for the last 100 ns of simulation, using a 3.5 \AA cutoff to the binding molecule, using a probe radius of 2.8 \AA .

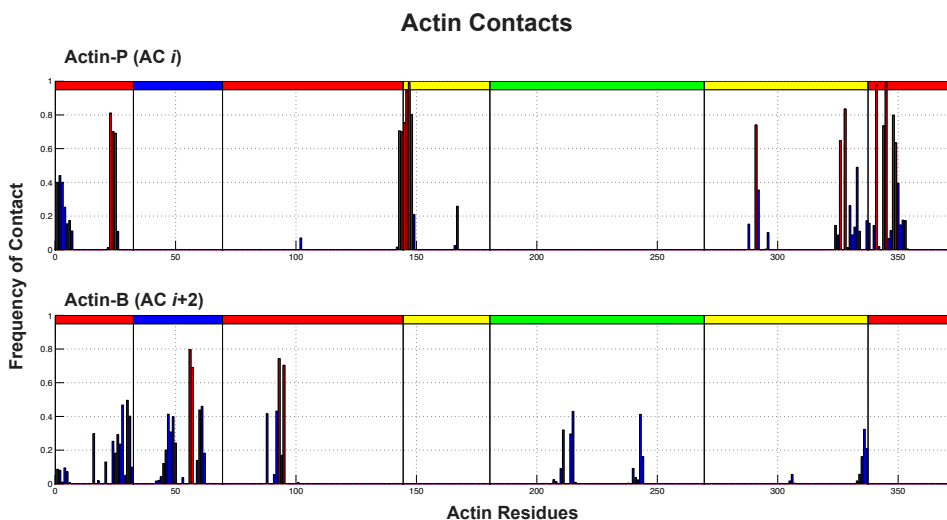


Figure 4.3: Actin Contacts: The frequency of actin contact points for Actin-P (i) and Actin-B ($i+2$) (within 3.5 \AA of cofilin) for each residue (by residue id number) are shown here. The red bars correspond to residues with over 60% contact. The red residue region corresponds to subdomain 1, blue is subdomain 2, yellow is subdomain 3, and green is subdomain 4.

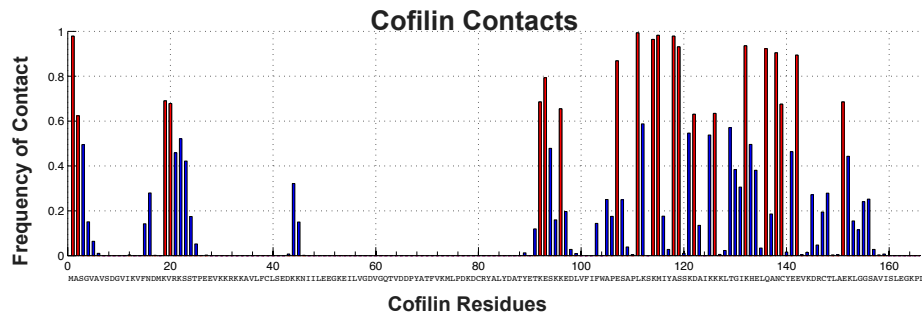


Figure 4.4: Cofilin Contacts: The frequency of cofilin contact points (within 3.5 Å of actin) for each residue (by residue id number) are shown here. The red bars correspond to residues with over 60% contact.

Table 4.2: Solvent Accessible Surface Area (SASA) Analysis: Surface area of binding at each site (Å²) for the actin up and downstream (Actin-P, pointed end, and Actin-B, barbed end) of the bound cofilin (Cofin 1-6).

Monomer	Cof1	Cof2	Cof3	Cof4	Cof5	Cof6	average	avg std
Actin-P	220.9	204.3	130.4	203.3	178.3	208.9	191.0	32.8
Actin-B	160.6	169.3	140.4	197.9	254.5	142.1	177.5	43.2
Cofin	367.6	289.3	308.5	313.4	402.3	304.0	330.9	44.1

4.3.3 Root Mean Squared Fluctuation (RMSF)

Root Mean Squared Fluctuation (RMSF) analysis was used to examine the dynamic regions of the actin protomers to eventually gain insight into filament dynamics. This means the average fluctuation of movement for a given residue was tracked over the course of the simulation. Here, we perform these calculations on the C α of each residue in the actin protomers. Since the filament ends are highly dynamic and would introduce artifacts to the results, only the middle four protomers are examined.

The results for the bare filament, the control filament, as well as the decorated filament can be seen in Figure 4.5. We would expect that since both filaments are uniform, their RMSF profiles across the middle four the protomers would be approximately the same. For the most part, there are few peaks except in subdomain 2, exactly at the DNase I loop, in subdomain 4 around residues 232-234, and subdomain 3 around residues 320-321. The high dynamics about the D-loop matches the conformations observed from EM where the D-loop is highly disordered. The decorated filament

shows marginally more dynamics in subdomain 4 than the bare filament, suggesting that the protomers in a decorated filament may be more flexible. However without statistically significant p-values, it is difficult to be certain of this claim.

The RMSF analysis underlines the fact that these systems are highly dynamic and variable in different conformations. This is particularly true for the sparse and split filaments since these filaments lack uniformity and the each of the four protomers being analyzed are inherently different. The results in Figure 4.6 are merely presented for comparison. With the exception of Actin 4, most of the protomers dynamics seem to be more muted compared to that of bare and decorated.

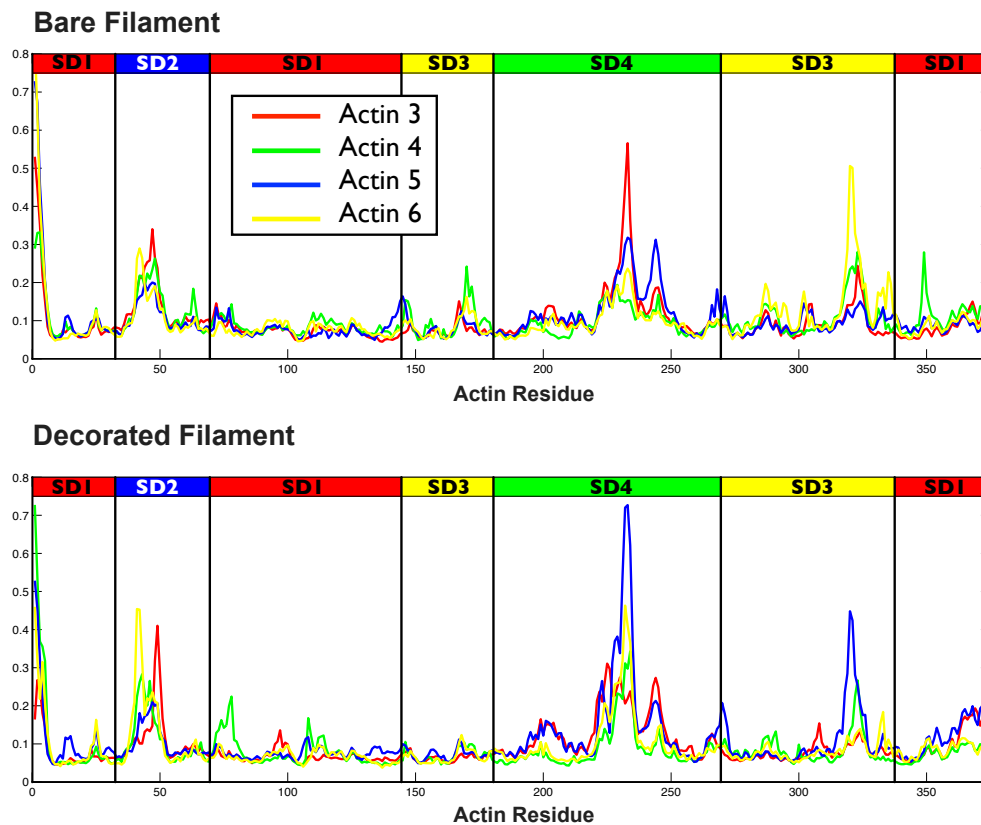


Figure 4.5: RMSF of Bare and Decorated Filaments

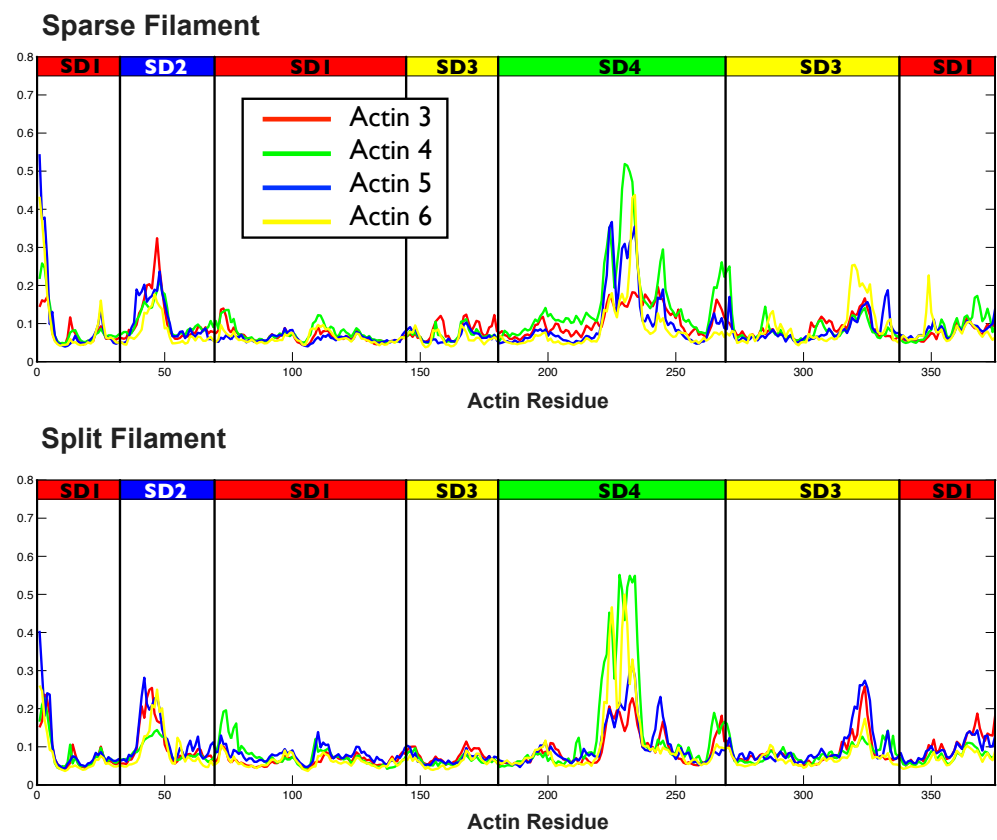
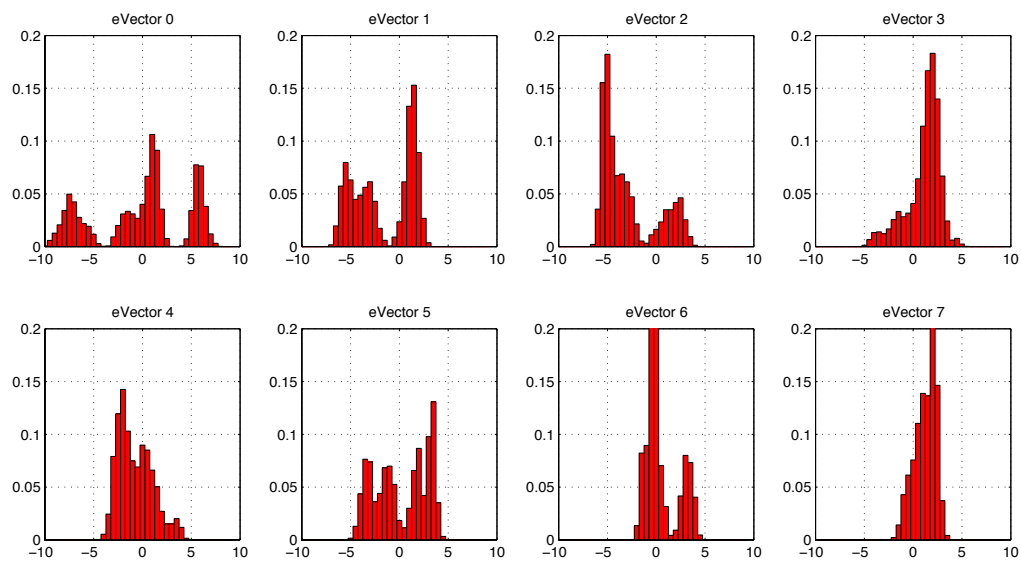


Figure 4.6: RMSF of Sparse and Split Filaments

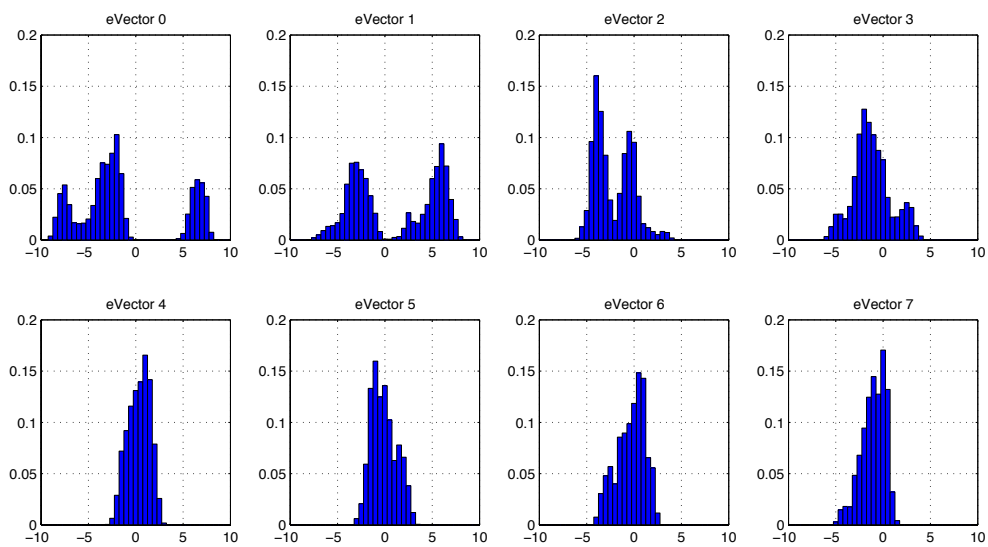
4.3.4 Principle Component Analysis (PCA)

Principle Component Analysis (PCA) can also be used to analyze an MD trajectory. The overall dynamics of a simulation can be decomposed into a basis set of orthogonal modes. Normally the motions of the n $C\alpha$ in a protein are of interest, so there will be $3n$ degrees of freedom and n eigenvectors and eigenvalues to describe the full motion of the simulation. The highest eigenvalues are associated with the eigenvectors that contribute the most to the long-ranging motion. In the case of the filament, we are interested in the intermolecular motion, so trimers of protomers are analyzed together. An 8-mer filament, if we disregard the end protomers, has four sets of trimers: Actin 2-3-4, Actin 3-4-5, Actin 4-5-6, and Actin 5-6-7. These four trimer sets can be concatenated as one contiguous trajectory, which is in turn, converted to one basis set of motion. Analysis for how a trimer of actin protomers behaving about a cofilin binding set can be done.

PCA of the four trimer sets was performed on bare and decorated filaments by combining both simulations for a basis set that is comprised of eight trimer set trajectories. See Figure 4.7. The four trimer trajectories for both bare and decorated filaments were combined to form the basis set dynamics onto which both filaments (for the middle four protomers) were projected. The modes between bare and decorated filaments differ, but it is difficult to fit distributions since some are not very gaussian or bimodal, or trimodal. After creating a porcupine plot of the first top two modes, where the vectors of each mode's movement is depicted as quills on the average actin trimer structure, there does not seem to be much signature of twist. (Data not shown.)



(a) Bare Filament



(b) Decorated Filament

Figure 4.7: Distribution of Bare and Decorated Filaments PCA: The basis set is comprised of the bare trajectory (25-95ns) and the decorated trajectory (to 125 ns). The first eight modes are shown here.

4.4 Discussion

4.4.1 RMSD

In our use of RMSD to determine if a bond is maintained, we have gained more information than simply checking to see if a simulation has plateaued (which is not necessarily the case even when RMSD has reached a equilibrated value). This analysis is particularly useful when the exact binding site or intermolecular bonds are unknown. We saw a significant difference between binding and non-binding models in the original dockings. While good agreement with EM envelopes offer a good check, this provides a more quantitative measure.

4.4.2 Contact Points

Although the contact analysis may only seem relevant to a static observation of contacts, it may offer some insight into the dynamics. There are high frequency peaks in Actin-P, suggesting that these contact points are consistent and long withstanding throughout the course of the simulation. On the other hand, Actin-B also shows a number of peaks but they tend to be lower in frequency of contact. This may suggest that contacts are not as well maintained and are perhaps weaker. Perhaps this is the case because Actin-B contacts are “F-site contacts”. The contacts in Actin-P are “G-site” contacts and may need to be “stronger” because upon severing, which would occur at the “F-site,” these contacts would need to be maintained in order for cofilin to chaperone a G-actin to its next destination.

4.4.3 RMSF

The RMSF analysis did not yield obvious signatures that indicate bare or decorated behavior. It did however confirm the flexibility of the D-loop. This region varied in behavior between all four filament models and while we were unable to obtain solid statistical values, it is still informative because Galkin et al.’s and Orlova et al.’s

work which categorizes thousands of filament conformations show that different conformations of the D-loop allow for different behaviors of the filament; a disordered conformation favored cofilin binding and thus severed more easily. (Galkin et al. 2003, Orlova et al. 2004, Galkin et al. 2010) The differences in D-loop fluctuations may be the key to good binding. On the other hand, these conformational changes may not be observable due to time and filament length limitations and the EM images are, again, of insufficient high resolution to make absolute all-sweeping conclusions.

4.4.4 PCA

Bare and decorated filaments have different distributions of motion. Unfortunately, this changes depending on which part of the simulations are being sampled. This is more likely due to our only sampling a subset of conformational space (a computational limitation) than the cofilin's inability to affect filament dynamics. Since it was difficult to obtain a clear signature difference between bare and decorated filaments, we could not extract a definitive mode of motion that may describe a twisting motion.

Overall, an AA MD of an 8-mer actin filament model is useful for predicting detailed molecular contacts. Unfortunately, it does not reasonably yield clear signatures of more intermolecular dynamics. In our work to characterize twisting behavior in bare and decorated filaments, RMSF and PCA analysis may ultimately be hindered by insufficiently long simulation time-scales and filament length, which are restricted by computational bounds. There are too many atoms to simulate not only for the time in order for an event, such as severe twist or severing, to occur. Additionally, the simulation box for the filament needed to be sufficiently large such that F-actin would not be affected by its periodic image—this prevents building a filament much longer than 8 protomers which makes our model suffer from edge effects or artifacts during simulation.

In order to overcome these limitations, we simulated filaments using coarse grain MD. This work will be discussed in the next Chapter.

Chapter 5

Long-Ranged Dynamics of Cofilin-Bound Actin Filaments

Finally, Part 3 will be discussed in this chapter. After determining an all-atom model for cofilin-bound F-actin (see Chapters 2 and 3), we performed a coarse-grain molecular dynamics simulations on bare actin filaments, fully decorated filaments, and filaments with cofilin bound at isolated sites. We find that the binding of cofilin as domains or in isolated sites affects the average twist angles as well as the twist fluctuations. Decorated filaments not only have a greater average twist, in agreement with cryo-EM studies, but also a lower local fluctuation of twist angle. Additionally, we show how cofilin introduces local disorder in a filament. These results illuminates cofilins effects on F-actin twisting and bending and provide some clues about cooperative binding kinetics and filament severing.

5.1 Introduction

Much work has been done to understand the motions of a actin filaments. While the knowledge of the structures have mostly been obtained through NMR studies where thousands upon thousands of conformations have been sampled, they do not show high resolution molecular details of the structure. (Oda et al. 2009, Fujii et al. 2010) Moreover, finding a specific conformation that is not uniform to the filament, particularly twisting that will lead to severing, cannot be done when the images used to reconstruct a structure require the averaging of many filaments. Also, when studying cofilin-bound F-actin, one can only reliably find structures for two concentration

states: no cofilin and saturating cofilin. Here, we employ Molecular Dynamics (MD) tools to bridge the gap between experimental data and the unobservable to understand how cofilin interacts with actin in terms of twisting and severing, and if we are lucky, cooperativity.

5.2 Methods

5.2.1 Building Coarse Grain Models

Coarse Grain (CG) MD does not only allow us to explore longer time scales but also extend the size of our filament without incapacitating our computational resources (even if there are 96 processors working around the clock running simulations); moreover, there are already established parameters for proteins, though they have mostly been used for lipid-embedded proteins. (Shih et al. 2006b, Shih et al. 2007, Arkhipov et al. 2006, Freddolino et al. 2008)

A **bare, 20-protomer actin filament** was built by using the PDB ID 2ZHW (Oda et al. 2009) and the provided transformation matrix, shifting from one monomer to the next by translating 27.59 Å up the z-axis and rotating -166.4° . The VMD *CG Builder* plugin requires a protein and water database to convert the all atom filament into coarse grain bead representations when using the Residue-Based Coarse Grain (RBCG) model. The conversion maps backbone and side chain atoms to one bead each while four water molecules are mapped to one bead. (Shih et al. 2006b, Shih et al. 2007) See Figure 5.1.

Since the ADP-Mg in actin is a non-standard molecule (heterogeneous atoms, neither protein nor water), we must create a Shape-Based Coarse Grain (SBCG) model with the *Shape-based Coarse Grain Builder* plugin. (Arkhipov et al. 2006, Freddolino et al. 2008) Four beads were used to coarse grain the ADP-Mg molecule. While the bond lengths, angles, and torsions derived from the plugin were adequate, but the electrostatic and the Lennard-Jones potential needed to be adjusted. First, the charges were scaled down from -1.0 to -0.7 to match the charges of other residues. Secondly, value of $\epsilon = 1.195$ was used to also more closely match that of the residues, but R_{min}

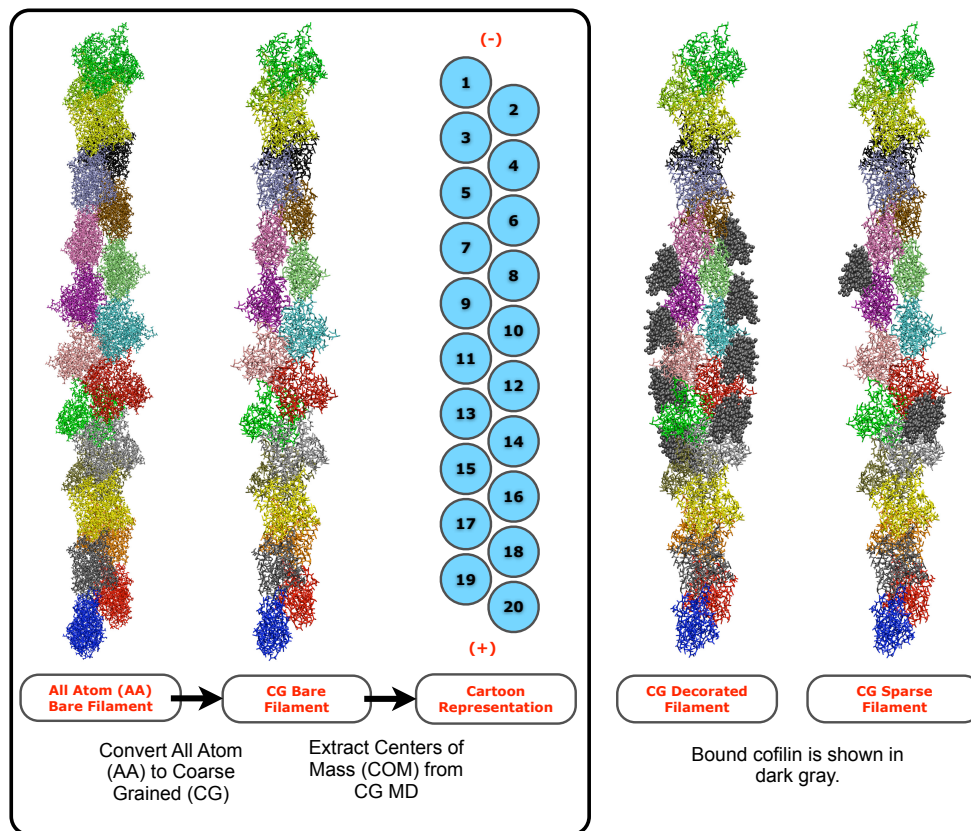


Figure 5.1: Coarse Graining Protocol: Use the VMD CG Builder plugin to convert an all-atom filament to a coarse grain filament for bare, decorated, and sparse models.

comes from the plugin's calculated value. A comparison of the AA, RBCG CG, and SBCG CG (for ADP-MG) Lennard-Jones parameters can be seen in Figure 5.2. The parameters for ADP-MG have slightly longer R_{min} distances but still fall within of reasonable range of the switching distance cutoffs. Part of the curve is curtailed but the values are low enough that it should not affect the simulations greatly.

The rest of the protocol is similar to AA MD in NAMD. Once the structure (PSF) files for the filaments (with or without cofilin bound) have been created, the system is solvated with a CG waterbox and a padding of 20 Å on all sides, which is generous enough so that the protein is not affected by its periodic image. The solvent is ionized with CG ions to 60 mM.

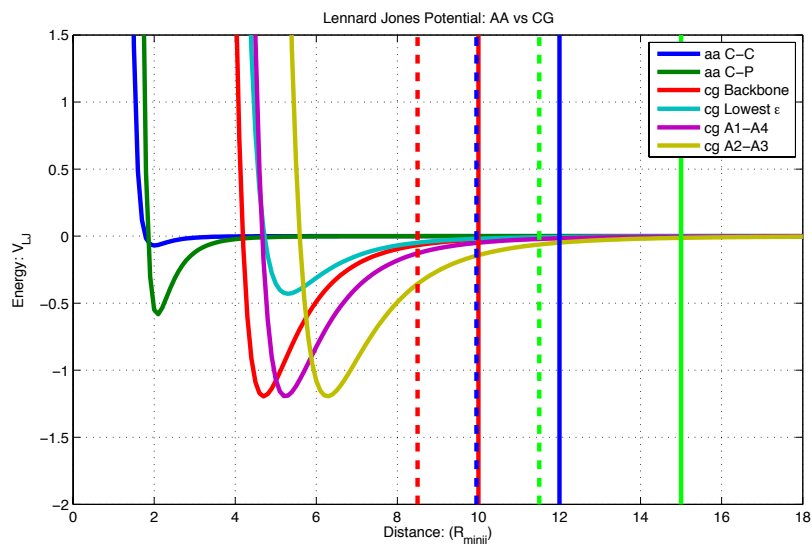


Figure 5.2: Lennard-Jones Potential of AA and CG: The Lennard-Jones potential of all-atom (aa) and coarse grain (cg) are shown. The green and blue curves are two examples of an all atom potential in the backbone (between two carbons, or a carbon and phosphorous). The other curves are either for RBCG (a typical backbone residue ϵ or lowest ϵ values) or the specially parameterized SBCG ADP-MG hetatom (for beads A1-A4 or A2-A3). The vertical lines represent boundary distances; the solid lines are for CG and the dashed lines are AA. The red line represents the start of switching (the distance at which to activate switching/splitting function that smooths the curve to a 0 energy potential for electrostatic and van der Waal calculations). The blue line represents the cutoff distance (the interaction distance at which both electrostatic and van der Waals energies become 0). The green line represents the pair list distance (distance between pairs of atoms for inclusion in pair lists).

The **decorated filament** and **sparse filament** models are built similarly except that the cofilin are included before conversion to CG. The decorated filament has 8 cofilin bound in the center 8 sites (CF6 to CF13) and the sparse filament has 2 cofilin bound at sites CF7 and CF12. See Figure 5.3.

5.2.2 Coarse Grain Molecular Dynamics (CGMD) Simulation

Again, CG MD simulations are similar to that AA MD, as these are run in NAMD. Simulations were performed in an isothermal-adiabatic (NpT) ensemble with the CHARMM-like force field and CG water model mentioned above, under periodic boundary conditions. Each actin protomer had ADP-Mg as the bound nucleotide.

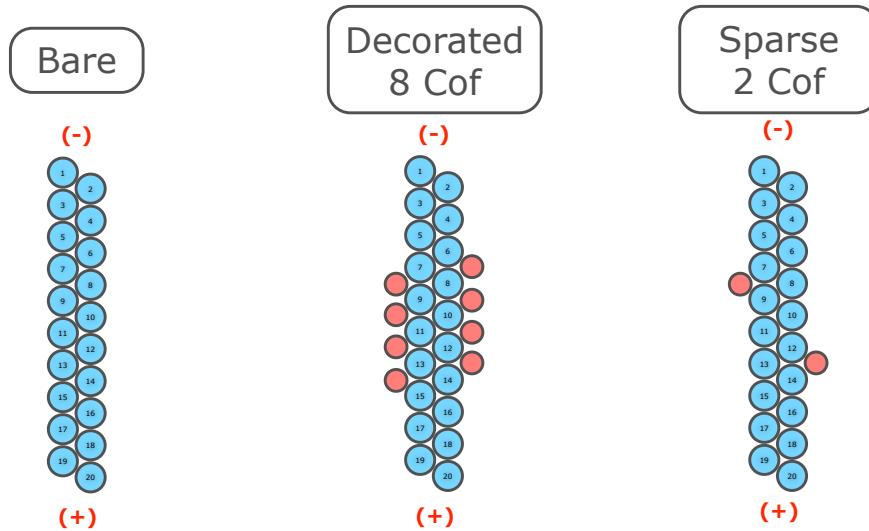


Figure 5.3: Coarse Grain Filament Models: Cartoon representations of bare, decorated, and sparse CG filament models. Actin monomers are represented with blue circles, designated AC1 to AC20. Cofilin monomers are in pink circles, designated CF1 to CF8 for the 8 possible sites in the center of the filament. Pointed end at top (-). The sparse model has cofilin CF7 and C12 bound.

Bonded interactions were computed every 4 fs using SHAKE, short-ranged non-bonded electrostatic and van der Waals (with a 12.0 Å cutoff and smooth switching function beginning at 10.0 Å and pair-list distance of 15.0 Å, and “exclude 1-2” for non-bonded parameters). Long-ranged, full electrostatic interactions were computed every 4 fs with the Particle Mesh Ewald method with grid points at least $1/\text{Å}$ in each dimension. Using Langevin Dynamics, NpT conditions were maintained at 1 atm and temperature of 300 K with a damping coefficient of 5 ps^{-1} and a Langevin piston oscillation period of 200 fs and decay of 100 fs for the production run (200 fs and 500 fs respectively for both heating and equilibration). In the pre-production phase, a damping coefficient of 10 ps^{-1} and time step of 2 fs were used. Following minimization, the system was heated and cooled for two cycles from 100K to 500K in 100K increments at 0.2-0.3 ps each, and finally cooled to 300K so that the CG system could be relaxed back to a non-overlapping conformation. An equilibration time of more than 1 ns was necessary before going to production phase because at higher timesteps and lower damping coefficients, the atoms would move too quickly and the simulation would crash.

The detailed MD protocol is as follows, with the varying parameters highlighted and remaining the same in the next step unless otherwise noted:

1. **Solvate (explicit) and Ionize** filament. Solvate plugin with 20 Å padding around the protein and boundary of 5.0, using CG water beads and solvent water box (cgwat.psf). Autoionize plugin (using cgionize.tcl) using 0.060 M (with CG versions Na⁺ as SOD and Cl⁻ as CHL).
2. **Energy Minimization** until gradient of (minLineGoal) $1.0e^{-1}$ at 0 K for 100,000 steps. 1 fs timesteps (2 fs for nonbonded and 4 fs for full electrostatic evaluation, 20 steps per cycle), margin of 10 Å, Langevin dynamics on (damping of 10 ps^{-1} , temperature of 75K), Langevin piston off.
3. **Simulated Annealing/Heat** from 100 K to 500 K (at 100 K intervals), 500 K to 100 K (at 100 K intervals) and finally 100 K to 300 K (at 50 K intervals). 1 fs timesteps (2 fs for nonbonded and 2 fs for full electrostatic evaluation, 10 steps per cycle). After each temperature change, run for 3,000 – 5,000 steps when heating and 1,000 steps when cooling.
4. **Equilibrate** at 300 K. 2 fs timesteps for minimum of 500,000 steps or until stable to increase steps per cycle. Langevin dynamics on (damping of 10 ps^{-1} , Langevin temperature of 300K). Langevin Piston on (target of 1.01325 bar, period of 100 fs, decay of 100 fs, and temperature of 300 K).
5. **Production Run** with above parameters, using 2 fs or 4 fs depending on system stability (i.e. larger timesteps with longer simulations before crashing and also increasing non-bonding and full electrostatic evaluations with 4 fs). Langevin dynamics on (damping of 5 ps^{-1} , Langevin temperature of 300K). Langevin Piston on (target of 1.01325 bar, period of 200 fs, decay of 100 fs, and temperature of 300 K).

All three filament models followed this protocol. Also, each model was simulated for three independent runs at 500 ns each in which the filament (with or without cofilin) began as a perfectly symmetrical filament built from the Oda model. The first of the simulations was split into three parallel simulations at the 250th ns (Sim 1a, 1b, and 1c), two of which being initiated with new starting velocities. See Figure 5.4.

In Simulation 1 of each model, the cell basis vectors were reset (like the error in the All Atom model simulations). While there does not seem to be much overall behavior differences, eliminating the reset allowed the simulations to run for longer time steps (4 fs) and for longer times without crashing.

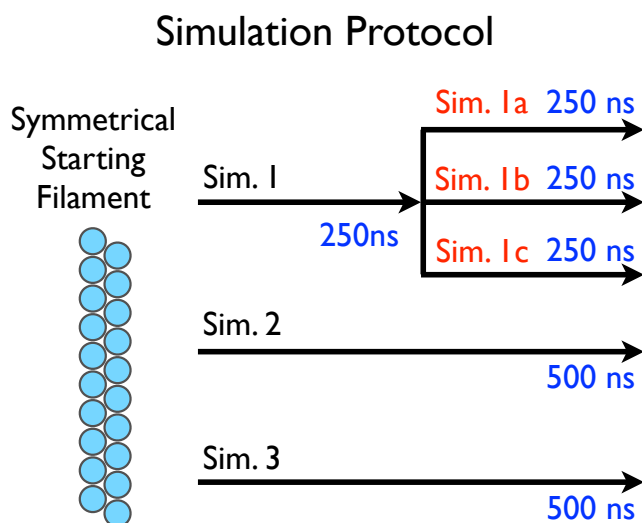


Figure 5.4: CG Simulation Protocol: All three filaments were run in 3 independent simulations for a total of 500 ns. The first simulation was restarted at the 250th ns with two new velocities as three parallel simulations.

Table 5.1: Coarse Grain Simulation Details:

Number of coarse grain atoms are listed for each category. Note that the ions and water are also coarse grain beads.

Filament Model	Total Atoms	Protein Atoms	No. "Na ⁺ "	No. "Cl ⁻ "	No. Water
Bare	109,304	14,520	353	73	94,358
Decorated	113,229	17,104	348	84	95,693
Sparse	110,379	15,166	352	76	94,785

5.2.3 Defining Metrics

Although we can visually observe the movement of the filaments in VMD, it is difficult to see the subtle changes that occur. We have developed a set of metrics to track the behavior of the filaments to compare them quantitatively.

The physical lengths of the filament can be described by the number of values. The **longitudinal distance** is the distance between the **centers of mass (COM)** of actin protomers A_i and A_{i+2} , most associated with the D-loop. The **lateral distance** is the distance between protomers A_i and A_{i+1} , associated with the H-loop. See Figure 5.5.

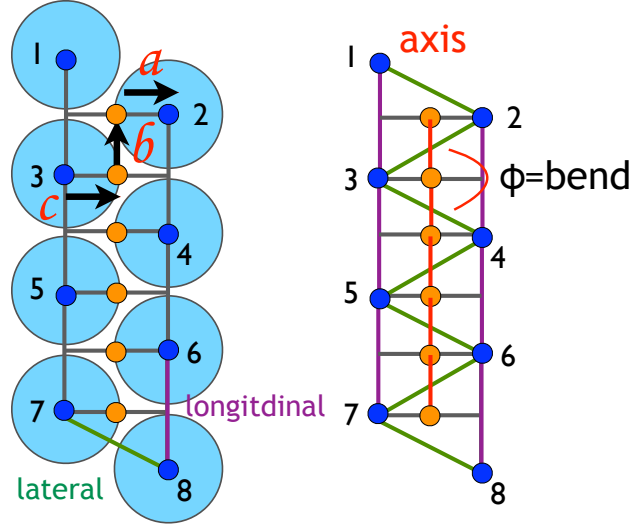


Figure 5.5: Definition of Metrics: Actin protomers are approximated by their centers of mass. This allows for the calculation of axis points. The axis allows for the calculation of twist. Two axis units are sufficient for the calculation of bend.

The axis is determined by first finding where the axis points are. This has been done in other models (e.g. Pfaendtner et al. 2010). Again, using the centers of mass (COM) for all protomers, we find the midpoint between Actin A_i and A_{i+1} and call it point $m1$. The midpoint between the COM of Actin A_{i+1} and point $m1$ is p_1 (orange point) which becomes the **axis point** for the trimer of Actin A_i , A_{i+1} , and A_{i+2} . When this process is repeated for the next set of trimers, Actin A_{i+1} , A_{i+2} , and A_{i+3} , we get the next axis point, p_2 . See Figure 5.6 for these values. If:

$$\vec{a} = \overrightarrow{p_1 A_{i+1}} \quad (5.1)$$

$$\vec{b} = \overrightarrow{p_2 p_1} \quad (5.2)$$

(considered one axis unit)

$$\vec{c} = \overrightarrow{A_{i+2}p_2} \quad (5.3)$$

the effective dihedral angle between them is the **twist** θ of Actin $i+1$ to Actin $i+2$. For purposes of established convention on angles, it is actually $\text{twist} = 180 - \theta$.

$$\text{twist } \theta = \tan^{-1} \left(\frac{|\vec{b}| |\vec{a}| \cdot (\vec{b} \times \vec{c})}{-|\vec{b}|^2 \vec{a} \cdot \vec{c} + (\vec{a} \cdot \vec{b})(\vec{b} \cdot \vec{c})} \right) \quad (5.4)$$

The Oda 2009 bare filament is 166.4° which actually has a negative sign in front, as seen in the transformation matrix, so values less than that (and in our analysis) represent **over-twisting** and values above are **under-twisting**.

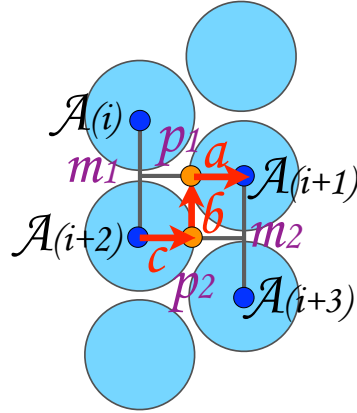


Figure 5.6: Twist: Twist can be calculated for two consecutive trimers, Actin A_i , A_{i+1} , A_{i+2} and Actin A_{i+1} , A_{i+2} , A_{i+3} . The blue dots, A , represent the center of mass (COM) for each protomer. The orange dots, p represent the axis points. Red arrows a , b , and c are vectors.

The **bend** ϕ is defined as the angle between two axis units

$$\overrightarrow{\text{axis}1} = \overrightarrow{p_1 p_2} \quad (5.5)$$

$$\overrightarrow{\text{axis}2} = \overrightarrow{p_2 p_3} \quad (5.6)$$

$$\text{bend } \phi = 180 - \cos^{-1}(\overrightarrow{\text{axis}1} \cdot \overrightarrow{\text{axis}2}) \quad (5.7)$$

as seen in Figure 5.5.

The **axis length** is described as the summation of each axis unit. This is a better measure than the filament length, which we define here as the distance between the first and last protomer's COM. Note both measures are shorter than the actual length that a filament spans.

The **fluctuation of twist** (or any other measure) is defined by the average of 10 ns sliding window ahead of a given time point. This helps determine how much change in motion (either smoothness or disorder) is occurring within the filament in a short amount of time.

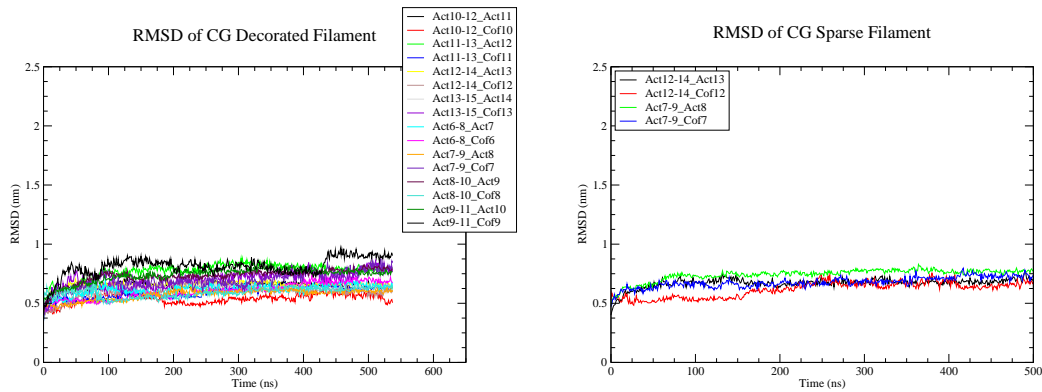
5.3 Results

5.3.1 Maintaining Contacts (Relative RMSD)

Just as in Chapter 4, where Relative RMSD was used to evaluate binding contacts, it is used again here to determine how well the cofilin remain bound. Values for both decorated and sparse filaments remain below 10 Å, which is lower than the average AA MD. Since this is CG, we expected to be more generous with binding distance, but it seems that the cofilin stay close to the actin and do not disconnect. See Fig 5.7 for RMSD of decorated and sparse filament. Only Simulation 2 of both models is shown as an example of this analysis.

5.3.2 Twist

In looking for a trend in the numbers, it appears there is not an obvious one, as will become clear in the following results. Initially, each of the filament models were run as one simulation, Sim 1a. These results were very promising in terms of the twist angles having a clear signature for each model. The goal of the trifurcation at 250 ns was to collect more statistics, with the assumption that simulating long enough after this break-point, with new velocities, could generate new conformations; however,



(a) Decorated Filament

(b) Sparse Filament

Figure 5.7: RMSD of CG Decorated and Sparse Filament: RMSD remain below 1.0 nm for decorated and below 8.5 nm for sparse. (Flanking actins, Actin i and Actin $i+2$, are fitted with least squares and the RMSD of the bound Cofilin i or Actin $i+1$ on the opposing side is calculated over the course of the trajectory.) Note that the RMSD scale is scaled to be comparable to RMSD plots in Chapter 4. All frames are sampled at every 0.02 ns.

the filaments appeared to be similar. See Figure 5.8. But to increase the statistics and to see how reproducible these results were, Sim 2 and Sim 3 were launched from a perfect filament. Only then did it become apparent that it was actually quite stochastic. Since each simulation takes months to run and yields essentially only one data point (or at least one independent filament structure), there is very limited data, and thus difficult to calculate statistics.

Filament Average

The twist of the filaments was calculated by taking the last 100 ns of each simulation (from 400-500 ns) and averaging them for a single set of values. (In the case of Simulation 1 where there is a trifurcation in the simulation, the last 100 ns of Simulation 1a, 1b, and 1c were combined and averaged.) A graphical view of the results can be seen in Figure 5.10 and the values can be seen in Table 5.2.

On a case by case basis, the bare simulation shows a trend for the first two independent runs. The average twist in the middle of the filament is about 170° for Sim. 1 and Sim. 2. (The issue of twisting not being about the observed 166.4° will be addressed

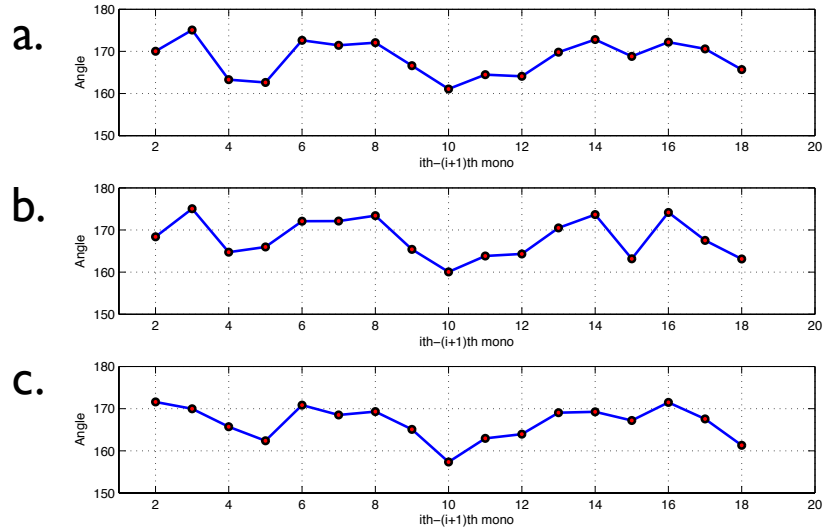


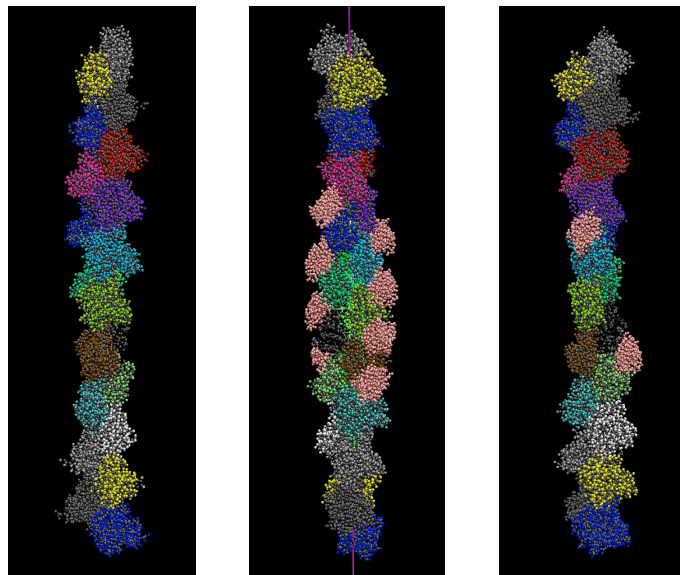
Figure 5.8: Example of Filament Twist from Trifurcating Simulation: For the decorated filament, these are an average of the last 100 ns of (a.) Sim 1a, (b.) Sim 1b, and (c.) Sim 1c.

in Section 5.3.3.) Indeed, the shape of the filament is very similar with consistent and even twisting in the middle and either significant over- or under-twisting on the edges. Sim. 3 seems to be a outlier with a lot of variability and sudden under-twisting (beyond 180°) at the pointed end, followed by over-twisting (to 155°) in the middle of the filament, and finally back to under-twisting, before finishing over-twisted at the barbed end. This roller-coaster twisting is most prominent in Bare Sim. 3, in comparison to all the other simulations. This is perhaps a stability issue.

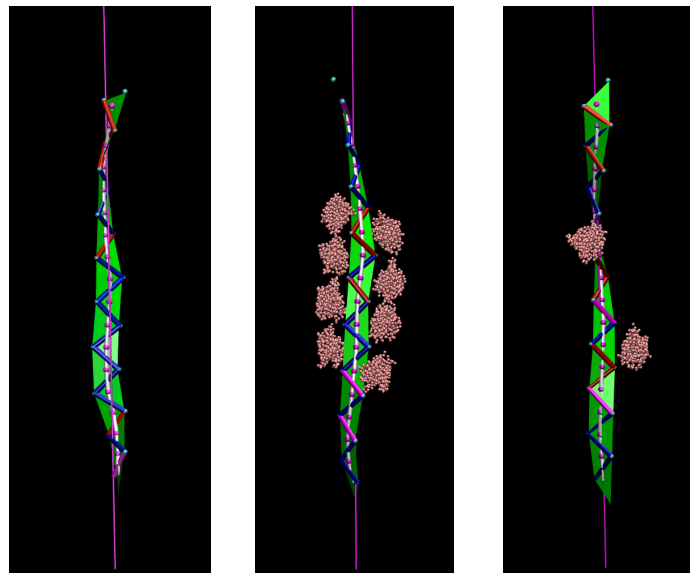
The decorated filament also does not exhibit the same behavior across its three simulations, but does not seem to have as much of an outlier. It ranges from lack of variability (Sim. 2) and roller-coaster characteristics which can be attributed to isolated regions under- or over- twisting and the neighboring sites trying to adjust (Sim. 1 and 3). It cannot be concluded that the filament is overall, under- or over- twisting.

The sparse filament cannot readily be analyzed with averages because of its expected asymmetrical behavior, even though such results are presented here. The shape of the filament that is most prominent in the region between the two cofilin binding sites, in Sim. 2 and 3, where there is a change from high to low values of twisting. This could be attributed to the bound cofilin, but since there are only 3 simulations, the statistics are insufficient to prove that case.

Figure 5.9: Coarse Grain Filaments: The filaments for the 500th ns are shown here, from left to right, bare (Sim. 2), decorated (Sim. 3), and sparse (Sim. 3).



(a) Filament in Full CG Bead Representation



(b) Filaments in Ribbon Representation: The color scale for the twist ranges from red (over-twisting) to blue (under-twisting, flat).

Table 5.2: Average Twist for middle 5 twist values: The last 100 ns of each simulation was averaged for the middle 5 twists (4-5 and 14-15) as denoted by the green lines in Figure 5.10.

Filament	Sim 1	Sim 2	Sim3	Avg	σ
Bare	169.2°	170.4°	163.4°	167.7°	3.7
Decorated	165.1°	172.1°	170.3°	169.2°	3.7
Sparse	168.5°	170.7°	165.8°	168.4°	2.4

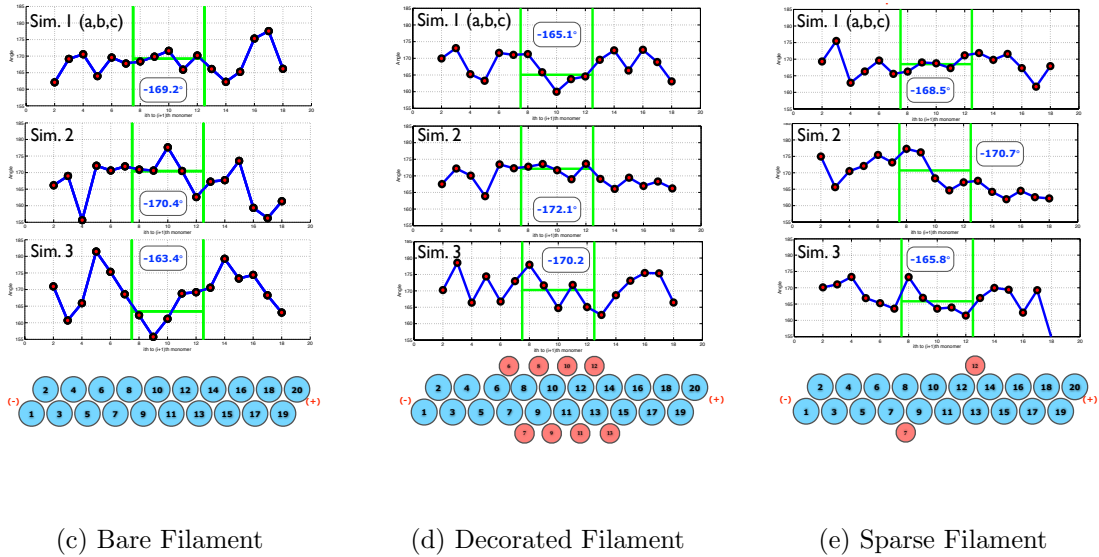


Figure 5.10: Average Twist of 3 Simulations of 3 Filaments: Average values for the middle 5 angle values, to eliminate edge effects.

Figure 5.8 shows the filament twist across a trifurcating simulations (at the 250th ns). The last 100 ns (from 400-500 ns) are averaged for each of the three plots. While there are some differences, the shape is generally the same. This shows that once a CG simulation of this size is underway with a given set of starting velocities, simulating for a long period of time (150 ns) after reinitiating velocities does not greatly change the course in which the dynamics are heading. Namely, the trifurcating simulations are not independent of one another. Twisting may actually be determined by stochastics, whatever the random initial velocities are. Once a simulation has begun, the way it is going to twist is fixed. Although the trifurcation occurred after the filament has equilibrated in filament length, the path of twisting is most likely set even before that point in time.

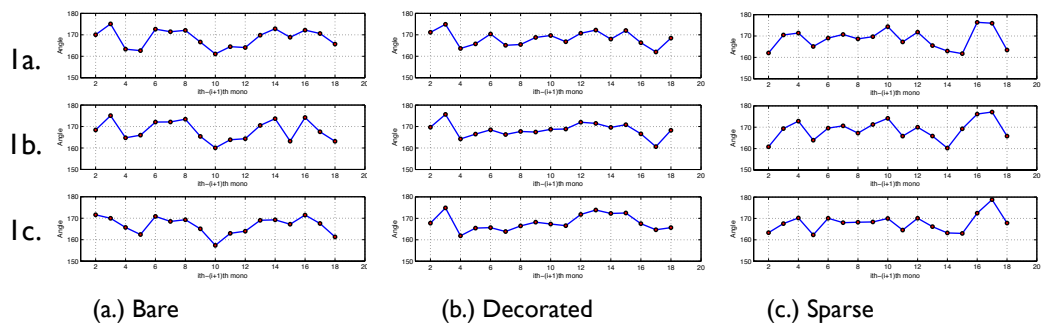


Figure 5.11: Trifurcating Simulation: Sim 1a, 1b, and 1c for the three models. Note the similarity across the trifurcating simulations in each of the filament models.

Distribution

The distribution of twist is perhaps is by far more informative than the values themselves.

The bare filament, in Sim. 1 and 2, have a fairly low distribution of twist angles; Sim. 3 is an outlier with the widest spread out of all simulations—the spread seems to widen with time. But notably through all three simulations, the fluctuations are higher than both decorated and sparse filaments. See Figure 5.13a (right most column for fluctuations). The histogram of the last 200 ns for Sim. 1 and 2 can be seen in Figure 5.12a. (Including Sim. 3, the outlier, as in Figure 5.15, still shows a peak around 169° , but also appears bimodal.) The majority of the twist angles is at 170° .

The decorated filament, on the other hand, has lower fluctuations (Figure 5.13b, right column). It also has a wider spread that is bimodal (Figure 5.12b) with two peaks at about 164° and 172° .

The sparse filament shows higher fluctuations like that of the bare filament, as well as a fairly large spread like that of the decorated filament, although Sim. 1 shows a smaller spread. (Figure 5.13) It appears to have a peak at around 167° .

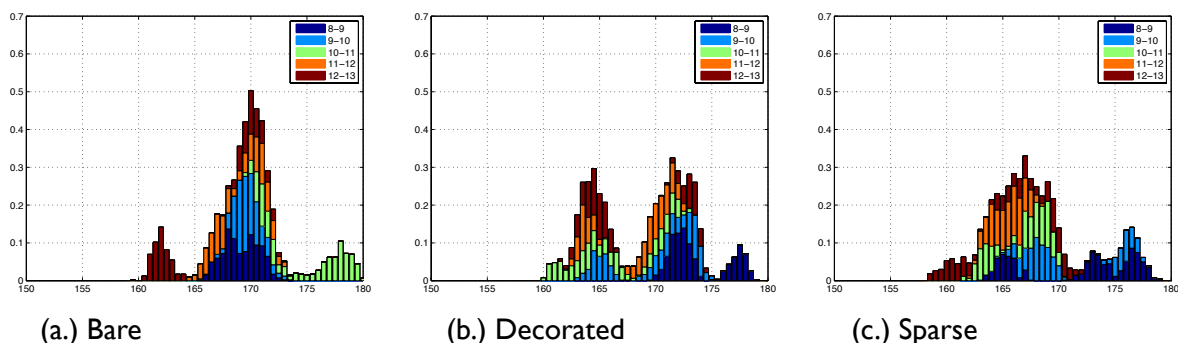


Figure 5.12: Distribution of Twist

Distribution of Twist: These histograms show the distribution of twist angles over the last 200 ns of simulation (from 300 to 500 ns) for the combined trajectories of Sim 1a, 2, and 3. (In the case of the bare filament, Sim 3 has been omitted because it shows some outlier behavior. See Figure 5.15 for a comparison.)

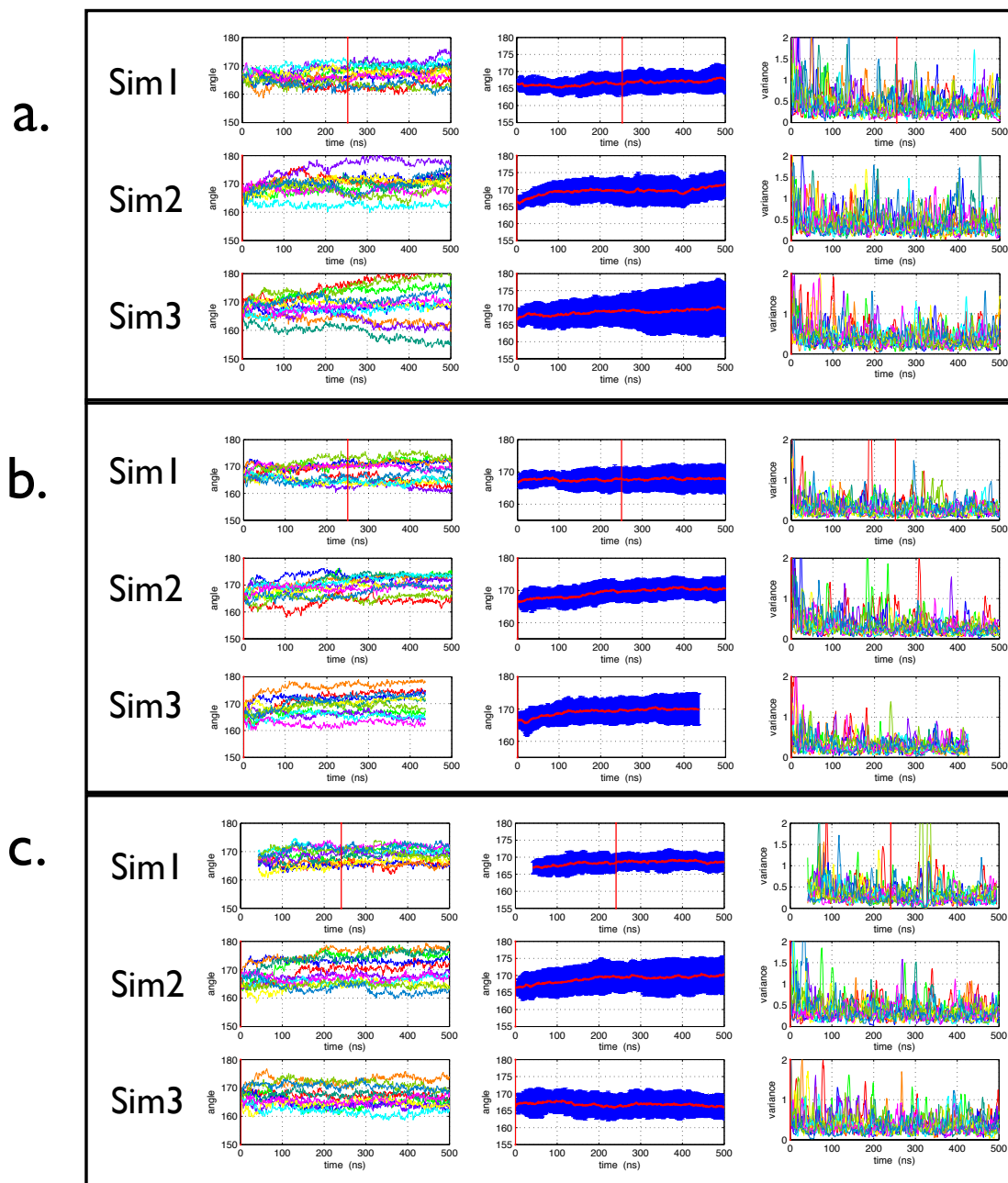


Figure 5.13: Twist Over Time: (a.) Bare, (b.) Decorated, (c.) Sparse. The first column tracks each individual twist (from twist 4-5 to 14-15, omitting the ends). The second column is the average twist of the middle 11 twists in a filament over time and its standard deviation. The third column is the fluctuation of twist for a 10 ns window. Simulations 1a, 2, and 3 are presented for each model. Note how the fluctuations in bare are higher than that of decorated.

5.3.3 Distance Measurements

The measures of axis length, lateral distance, and longitudinal distance over time are plotted in Figure 5.14. There are two major points of this figure. First, the filament seems to shrink approximately 2 Å per protomer, which is actually about a 5% reduction. Initially, it seemed like this effect was due to the coarse graining and the possible interstitial space between the beads, from the AA to CG conversion, that leads to compression. However, the the Oda 2009 and Fuji 2010 structures were stretched for imaging. (Fuji et. al. used blotting conditions that made the filaments straight.) The all-atom filaments from Chapter 4 do not shrink as much. The shrinking in the coarse grain simulations stabilizes after about 250 ns. This may be a reflective of true filaments.

There are fluctuations in the lateral and longitudinal distances, but this does not immediately appear correlated to twist. The most change appears in the longitudinal distance while the lateral distances mostly stay at comparable lengths to one another. Sim. 2 clearly has at least two longitudinal lengths that are much higher than the others, in a split into two populations. The more extreme changes in longitudinal distances, particularly in the sparse model Sim. 2., may be a sign that it is the weaker contact point and thus perhaps the site of severing.

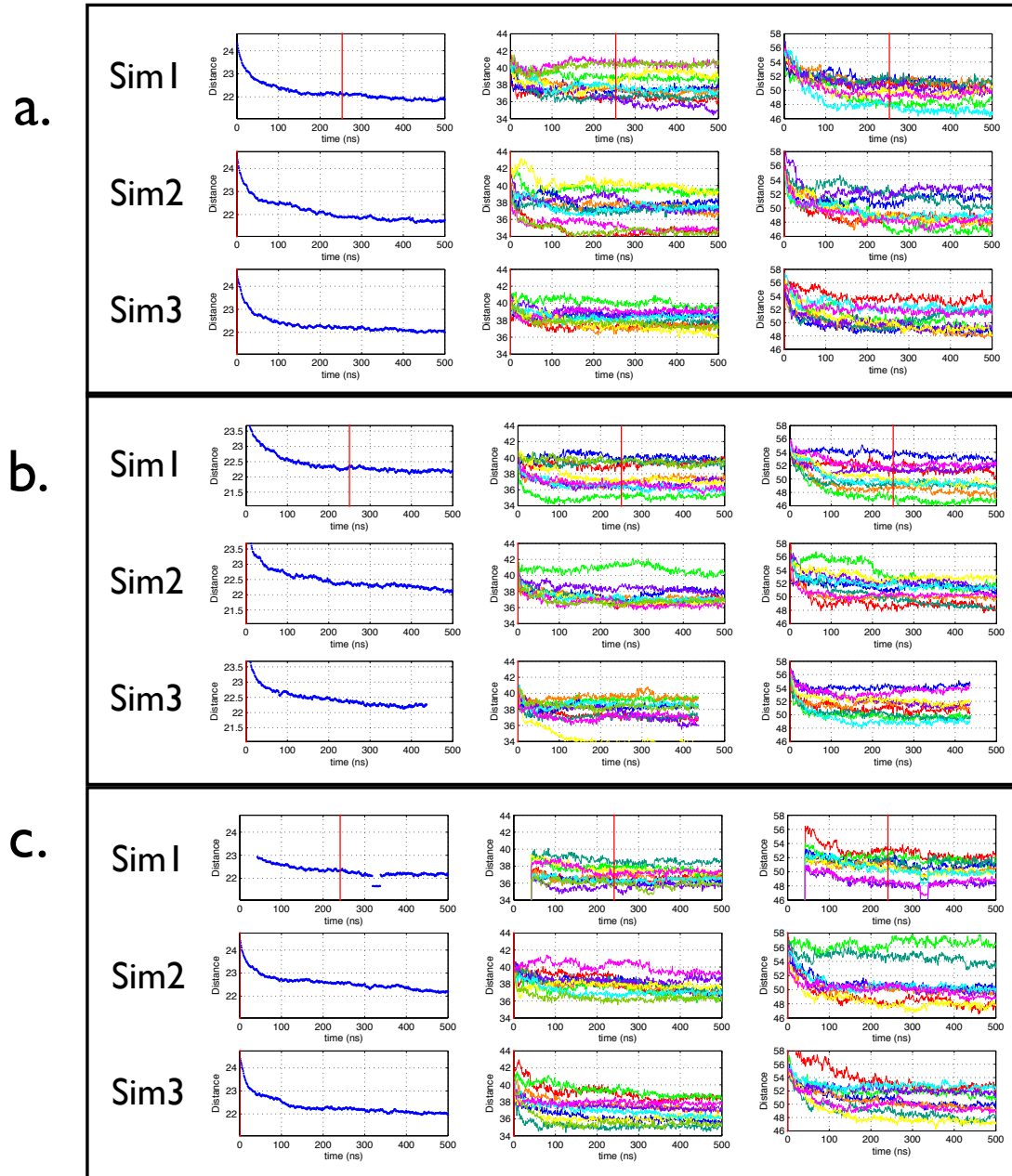


Figure 5.14: Filament Lengths over Time: (a.) Bare, (b.) Decorated, (c.) Sparse. The first column tracks the axis length. The second column is the lateral distance. The third column is the longitudinal distance. Simulations 1a, 2, and 3 are presented for each model.

5.4 Discussion

Much of the twist and distance analysis had been done for the AA simulations, but the filaments proved to be too short for any meaningful conclusions. The CG model seems to have compensated for this shortcoming and has allowed for statistics on more data points.

Because our filaments are of a finite length, they will be free to move. A periodic filament of infinite length has been simulated previously—with a 13 protomer per repeat (or crossover length) in the case of a bare filament, it is possible to connect the ends. (Pfaendtner et al. 2010) However, such a filament would not replicate natural free dynamics and would be expected to have less mobility. Moreover, it would also not be able to twist and sever due to enforced periodicity. While we have not yet seen such an event in our CG model, there is still the hope of it in the unsymmetrical behavior we see between the pointed and barbed ends. The shrinking of the filament length, while somewhat an artifact of CG, also might reflect the fact that the original Oda filament is straightened and possibly also stretched (Galkin et al. 2010), but that stretching notion seems to be debated by people in the field. Unfortunately, time and length scales may still be a hindrance.

The shortening effect in the CG simulation may partially be a result of the coarse grain beads being parameterized for membrane bilayers and therefore may have bead radii that are slightly short. Since the simulations do not fall apart and the protein system still possess their filament characteristics, it is most likely that the radii are not terribly short. It would be interesting to increase the radii in subsequent simulations.

Since the filament is decorated all at once, it still has the characteristics of a bare filament. Even with 500 ns of simulation time, it cannot be expected that the filament can become fully twisted because it takes a lot of time for the twists to propagate out to the ends. Ironically, it was because the All Atom filaments were too short that we saw edge effects, but with these longer filaments, the twists become trapped within the filament. While we cannot see the process of a filament becoming a decorated state, this may cast light on the activity of a true filament.

The simulations show that over-twisting at one point leads to under-twisting at another. With our finite filament, these effects could be propagated out to the ends, which may be possible with simulated annealing if our time scales cannot get that far. With this, the twist angle values would be more meaningful, particularly since the decorated filament is effectively a bare filament with cofilin binding cooperatively in one region.

Another interesting discovery, concerning these simulations is how important initial velocities seem to be. Once each simulation is launched from a perfectly symmetrical filament, the course of how the filament changes conformation may be established. The 250 ns time point was chosen as a point of trifurcation because the filaments appeared to mostly stop shrinking and had overall been equilibrated. That apparently is too late of a time to reinitialize velocities because the structures, with an additional 250 ns of simulation, do not appear to be vastly different. With this respect, it may be wiser to start many simulations for about 150-200 ns each in order to obtain a better sampling of conformations.

This realization may also be relevant to the bare filament and its outlier Sim. 3. It could be that Sim. 3 is not an outlier and that a bare filament simply has the ability to be more flexible (or at least more wildly behaved). In such a case, perhaps it twists wildly (with the right conditions) and allows a cofilin to bind in such a state. In order to see if the bare model has high or low spread, it may need more simulations of shorter time. This would resolve the confusion as to whether Sim. 3 should be included in analysis or not (5.15).

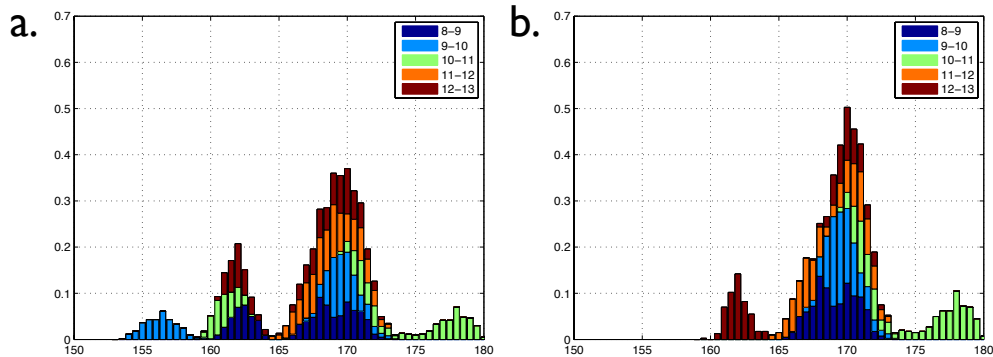


Figure 5.15: Distribution of Bare Filament Twist: Histogram of bare filament, the last 200 ns of (a.) all three simulations, and (b.) removing the outlier Sim 3 data.

The sparse filament must be analyzed differently than that of the bare and decorated filaments. The twist distributions show a shift, which shows that there is a difference against the other filament models. We have looked for a trend of twisting up and down stream of bound cofilin, but the results are currently incomplete.

In an attempt to look for a severing event, or even sever twisting, we plan to use simulated annealing methods to reach more conformations. This will be relevant for all three filament models. It may also help in ironing out the over- and under-twisting. Additionally, all the filament cases need many shorter (~ 200 ns) simulations so that there will be more statistics and better histograms of the data.

In the F-actin polymorphism paper (Galkin et al. 2010) and from personal discussion, the author claims that filaments must first twist into a conformation where the D-loop is disordered (mode 4 or 5 in Figure 1.10) before cofilin can bind. In recent discussions during the March 2011 Biophysical Society Meeting, Galkin stated that the Oda structure is not proper for cofilin binding simulations because of its structured D-loop. He suggested either deleting the D-loop all-together, because of its disordered structure, or using his fitted structure (to one of his bare/native filament modes, possibly with deleted D-loops, with greater twist like that of decorated cofilactin) would be a better representation and starting point of decorated system. Our all-atom simulations, however, do not form helices and in observing them seem to under take very random coil forms, with little correlation to one another (at least during trajectory visualization). In coarse graining the filaments, the secondary structure seems to lose its importance as the surface generated by side chain beads (with electrostatic and Lennard-Jones parameters defining the different types of residues) begin to be more prominent alongside the general globular structure of each protomer or cofilin. It might be interesting to use a pre-twisted filament to see how the twisting distributions change, especially since it is hard to guarantee sampling such conformations even with CG and may be worth trying. However, deleting the D-loop may be unnecessary and possibly detrimental. The D-loop is very dynamic and many studies have already shown that its reactivity and importance is high; one would think that its presence is vital for a believable model. With CG, the D-loop further loses its secondary structure and deleting it would introduce a large gap. This would probably introduce a large warping of the filament and the resulting twist and bending may not actually be credited to the cofilin. However, it might be entertaining to try

since it just might at least result in a severing event (even if it might not be real or correct).

Another characteristic that would be very interesting is the energy of a twist. This would be difficult to calculate since using the simulation to calculate such a property would require only one twist angle change at one site on the filament in a before and after twist snapshot. This may still be possible if we only consider trimers using either the all-atom simulation or the coarse-grain snapshots converted back to all-atom structures. Such analysis would be interesting, juxtaposed with some new and unpublished work presented by De La Cruz (also at the March 2011 Biophysical Society Meeting), where he calculated the energies associated with twisting and bending of cofilactin regions next to bare ones. His data suggests that bending energy is insufficient to break a filament, but that twist energy at the boundaries is approximately equivalent to the energy needed to hold subunits together. With a sampling of conformations from the all-atom and/or coarse grain simulations, calculating energies of different states of twist/bend may be possible.

Chapter 6

Conclusions and Future Work

6.1 Part 1: The Interaction of Cofilin with the Actin Filament

In this section, we have built a binding model for how cofilin interacts with F-actin, with the aid of mutagenesis and biochemical data as well as docking and molecular dynamics tools. This model is also in agreement with structural EM data as well. From this model we have found residues of importance that not only matches previous data, but also found new residues that could be of interest.

6.1.1 Future Work

The new residues need to be experimentally verified. Once that work is done, I can refine the model.

Additionally, there are the loops where human cofilin α -2 and α -3 are located, as seen in the structural alignment of the structures (Figure 3.1) where they are colored in red. Since a mutation in α -2 renders yeast cofilin unstable, it would be interesting to see how that loop affects human and other ADF/Cofilins as well as other structurally similar proteins.

6.2 Part 2: Short-Ranged Dynamics of Cofilin-Bound Actin Filaments:

An All-Atom MD Simulation of Filament Models

Bare, decorated, sparse, and split filament models were built from the model created in Part 1. In this section, I more carefully examined the cofilin-actin interactions by running all-atom MD simulations of all three filaments. The cofilin binding contacts are well maintained for the decorated and sparse models, but I could not obtain a clear dynamics signature to distinguish between all three models. This is due to the limited time-scale for so large a system (with so many waters) as well as the short filament that computational resources allow us to simulate. This work was still important to lay basis for coarse graining work in the next section.

6.2.1 Future Work

Some of the PCA work can be redone using the basis set of only the bare trajectory.

Although not the best use of time, bootstrap analysis can be done to show statistical significance in the RMSF analysis.

6.3 Part 3: Long-Ranged Dynamics of Cofilin-Bound Actin Filaments

A Coarse Grain MD Simulation of Filament Models

To reach longer time scales and filament lengths, I ran simulations of bare, decorated, and sparse filament models using coarse graining techniques in Part 3. Here, the characteristics of twist as well as other length measurements were more obvious. Decorated filaments may have a wider spread of angles and lower fluctuations than most of the bare model simulations. Also, the distributions differ between the filaments.

6.3.1 Future Work

To be more statistically confident in our results, I would like to run more simulations for shorter periods of time. Additionally, using simulated annealing will shake up the system and perhaps reach these conformations more quickly. Additionally, I would like to explore the idea of increasing the bead radii for CG in a water (as opposed to lipid membranes). Finally, though I wish I had done this in time for the dissertation, Kolmogorov-Smirnov test can be used to compare the histograms of the existing data to see if they are significantly different.

Per peer request, I would also like to use different filament models as the starting point of CG simulations. While I would not go as far to say these alternative states should have been used *instead* of the Oda filament, using them may put certain peers at ease, although perhaps a poor allocation of time. Because CG does not depend so much on contacts, fitting the current model to a new filament should yield filaments that are reasonable. Using a pre-twisted filament will probably not have a comparable distribution to the filaments we are currently using since they represent a different population. Also, such a condition would replicate binding that has occurred for a while; this is scenario where a filament first twists before cofilin binds, which has not been definitively proven to be true yet. It may be worth trying a filament without the D-loop and seeing if there is greater twisting and possible severing.

Finally, it would interesting to explore the energy aspects of twisting (and possibly bending). That will require additional preparation.

Although these studies are worth looking into, there is still a possibility that this CG model may be insufficient to find the severing event for which everyone is searching. However, any coarser of a model in which the characteristics of certain residues, and thus surfaces, would be lost may not necessarily result in finding an answer. This fine balance between the detail of an all-atom model that cannot reach long time or length scales and a coarse model that cannot pick up molecular subtleties has as of yet been unreached.

In summary, while I have completed much work in this thesis, there is still tirelessly more work to be done.

References

- B J Agnew, L S Minamide, and J R Bamburg. Reactivation of phosphorylated actin depolymerizing factor and identification of the regulatory site. *J Biol Chem*, 270 (29), Jul 1995.
- Ernesto Andrianantoandro and Thomas D Pollard. Mechanism of actin filament turnover by severing and nucleation at different concentrations of adf/cofilin. *Mol Cell*, 24(1), Oct 2006.
- S Arber, F A Barbayannis, H Hanser, C Schneider, C A Stanyon, O Bernard, and P Caroni. Regulation of actin dynamics through phosphorylation of cofilin by lim-kinase. *Nature*, 393(6687), Jun 1998.
- A Arkhipov, P Freddolino, and K Schulten. Stability and dynamics of virus capsids described by coarse-grained modeling. *Structure*, Jan 2006.
- S Asakura. The interaction between g-actin and atp. *Arch Biochem Biophys*, 92, Jan 1961.
- J R Bamburg. Proteins of the adf/cofilin family: essential regulators of actin dynamics. *Annu Rev Cell Dev Biol*, 15, Jan 1999.
- J R Bamburg, A McGough, and S Ono. Putting a new twist on actin: Adf/cofilins modulate actin dynamics. *Trends Cell Biol*, 9(9), Sep 1999.
- J R Bamburg, B W Bernstein, R C Davis, K C Flynn, C Goldsbury, J R Jensen, M T Maloney, I T Marsden, L S Minamide, C W Pak, A E Shaw, I Whiteman, and O Wiggan. Adf/cofilin-actin rods in neurodegenerative diseases. *Curr Alzheimer Res*, 7(3), May 2010.
- James R Bamburg and Barbara W Bernstein. Roles of adf/cofilin in actin polymerization and beyond. *F1000 Biol Rep*, 2, Jan 2010.
- Sabrina A Benchaar, Yongming Xie, Martin Phillips, Rachel R Ogorzalek Loo, Vitolto E Galkin, Albina Orlova, Mario Thevis, Andras Muhrad, Steven C Almo, Joseph A Loo, Edward H Egelman, and Emil Reisler. Mapping the interaction of cofilin with subdomain 2 on actin. *Biochemistry*, 46(1), Jan 2007.
- Ora Bernard. Lim kinases, regulators of actin dynamics. *Int J Biochem Cell Biol*, 39 (6), Jan 2007.

- B W Bernstein and J R Bamburg. Tropomyosin binding to f-actin protects the f-actin from disassembly by brain actin-depolymerizing factor (adf). *Cell Motil*, 2(1), Jan 1982.
- B W Bernstein, W B Painter, H Chen, L S Minamide, H Abe, and J R Bamburg. Intracellular pH modulation of adf/cofilin proteins. *Cell Motil Cytoskeleton*, 47(4), Dec 2000.
- Barbara W Bernstein and James R Bamburg. Adf/cofilin: a functional node in cell biology. *Trends in Cell Biology*, 20(4), Apr 2010.
- Barbara W Bernstein, Hui Chen, Judith A Boyle, and James R Bamburg. Formation of actin-ADF/cofilin rods transiently retards decline of mitochondrial potential and ATP in stressed neurons. *Am J Physiol, Cell Physiol*, 291(5), Nov 2006.
- L Blanchoin and T D Pollard. Mechanism of interaction of Acanthamoeba actophorin (ADF/cofilin) with actin filaments. *J Biol Chem*, 274(22), May 1999.
- Andrey A Bobkov, Andras Muhrad, Kaveh Kokabi, Sergey Vorobiev, Steven C Almo, and Emil Reisler. Structural effects of cofilin on longitudinal contacts in f-actin. *J Mol Biol*, 323(4), Nov 2002.
- Andrey A Bobkov, Andras Muhrad, Alexander Shvetsov, Sabrina Benchaar, Damon Scoville, Steven C Almo, and Emil Reisler. Cofilin (ADF) affects lateral contacts in f-actin. *J Mol Biol*, 337(1), Mar 2004.
- A A Bogan and K S Thorn. Anatomy of hot spots in protein interfaces. *J Mol Biol*, 280(1), Jul 1998.
- A Bonvin. Flexible protein-protein docking. *Curr Opin Struct Biol*, 16(2), 2006.
- M F Carlier and D Pantaloni. Control of actin dynamics in cell motility. *J Mol Biol*, 269(4), Jun 1997.
- A E Carlsson. Stimulation of actin polymerization by filament severing. *Biophys J*, 90(2), Jan 2006.
- Chikio Chan, Christopher C Beltzner, and Thomas D Pollard. Cofilin dissociates Arp2/3 complex and branches from actin filaments. *Current Biology*, 19(7), Jan 2009.
- Hui Chen, Barbara W Bernstein, Judith M Sneider, Judith A Boyle, Laurie S Minamide, and James R Bamburg. In vitro activity differences between proteins of the ADF/cofilin family define two distinct subgroups. *Biochemistry*, 43(22), Jun 2004.

- Jason B Cross, David C Thompson, Brajesh K Rai, J Christian Baber, Kristi Yi Fan, Yongbo Hu, and Christine Humblet. Comparison of several molecular docking programs: pose prediction and virtual screening accuracy. *J Chem Inf Model*, 49(6), Jun 2009.
- Maxwell D Cummings, Renee L DesJarlais, Alan C Gibbs, Venkatraman Mohan, and Edward P Jaeger. Comparison of automated docking programs as virtual screening tools. *J Med Chem*, 48(4), Feb 2005.
- Richard C Davis, Michael T Maloney, Laurie S Minamide, Kevin C Flynn, Matthew A Stonebraker, and James R Bamburg. Mapping cofilin-actin rods in stressed hippocampal slices and the role of cdc42 in amyloid-beta-induced rods. *J Alzheimers Dis*, 18(1), Jan 2009.
- E M De la Cruz, A Mandinova, M O Steinmetz, D Stoffler, U Aebi, and T D Pollard. Polymerization and structure of nucleotide-free actin filaments. *J Mol Biol*, 295(3), Jan 2000.
- EM De la Cruz. Cofilin binding to muscle and non-muscle actin filaments: isoform-dependent cooperative interactions. *J Mol Biol*, 346(2), Feb 2005.
- EM De la Cruz. How cofilin severs an actin filament. *Biophysical reviews*, 1(2), May 2009.
- EM De la Cruz and David Sept. The kinetics of cooperative cofilin binding reveals two states of the cofilin-actin filament. *Biophys J*, 98(9), May 2010.
- EM De la Cruz, Jeremy Roland, Brannon R McCullough, Laurent Blanchoin, and Jean-Louis Martiel. Origin of twist-bend coupling in actin filaments. *Biophysical Journal*, 99(6), Sep 2010.
- Irina V Dedova, Olga P Nikolaeva, Valeria V Mikhailova, Cris G Dos Remedios, and Dmitrii I Levitsky. Two opposite effects of cofilin on the thermal unfolding of f-actin: a differential scanning calorimetric study. *Biophys Chem*, 110(1-2), Jul 2004.
- D Didry, M F Carlier, and D Pantaloni. Synergy between actin depolymerizing factor/cofilin and profilin in increasing actin filament turnover. *J Biol Chem*, 273(40), Oct 1998.
- C Dominguez, R Boelens, and A Bonvin. Haddock: a protein-protein docking approach based on biochemical or biophysical information. *J Am Chem Soc*, 125(7), 2003.
- R F Doolittle. The origins and evolution of eukaryotic proteins. *Philos Trans R Soc Lond, B, Biol Sci*, 349(1329), Sep 1995.

- A A Fedorov, P Lappalainen, E V Fedorov, D G Drubin, and S C Almo. Structure determination of yeast cofilin. *Nat Struct Biol*, 4(5), May 1997.
- Robert D Finn, Jaina Mistry, John Tate, Penny Coggill, Andreas Heger, Joanne E Pollington, O Luke Gavin, Prasad Gunasekaran, Goran Ceric, Kristoffer Forslund, Liisa Holm, Erik L L Sonnhammer, Sean R Eddy, and Alex Bateman. The pfam protein families database. *Nucleic Acids Res*, 38(Database issue), Jan 2010.
- Christian Frantz, Gabriela Barreiro, Laura Dominguez, Xiaoming Chen, Robert Eddy, John Condeelis, Mark J S Kelly, Matthew P Jacobson, and Diane L Barber. Cofilin is a ph sensor for actin free barbed end formation: role of phosphoinositide binding. *J Cell Biol*, 183(5), Dec 2008.
- P Freddolino, A Shih, A Arkhipov, and K Schulten. 20 application of residue-based and shape-based coarse-graining to biomolecular simulations. *Coarse-graining of . . .*, Jan 2008.
- R Friesner, J Banks, R Murphy, T Halgren, J Klicic, D Mainz, M Repasky, E Knoll, M Shelley, J Perry, D Shaw, P Francis, and P Shenkin. Glide: a new approach for rapid, accurate docking and scoring. 1. method and assessment of docking accuracy. *J Med Chem*, 47(7), 2004.
- Takashi Fujii, Atsuko H Iwane, Toshio Yanagida, and Keiichi Namba. Direct visualization of secondary structures of f-actin by electron cryomicroscopy. *Nature*, Sep 2010.
- V E Galkin, A Orlova, N Lukoyanova, W Wriggers, and E H Egelman. Actin depolymerizing factor stabilizes an existing state of f-actin and can change the tilt of f-actin subunits. *J Cell Biol*, 153(1), Apr 2001.
- Vitold E Galkin, Albina Orlova, Margaret S VanLoock, Alexander Shvetsov, Emil Reisler, and Edward H Egelman. Adf/cofilin use an intrinsic mode of f-actin instability to disrupt actin filaments. *J Cell Biol*, 163(5), Dec 2003.
- Vitold E Galkin, Albina Orlova, Olga Cherepanova, Marie-Christine Lebart, and Edward H Egelman. High-resolution cryo-em structure of the f-actin-fimbrin/plastin abd2 complex. *Proc Natl Acad Sci USA*, 105(5), Feb 2008.
- Vitold E Galkin, Albina Orlova, Gunnar F Schröder, and Edward H Egelman. Structural polymorphism in f-actin. *Nat Struct Mol Biol*, 17(11), Nov 2010.
- D Goodsell and A Olson. Automated docking of substrates to proteins by simulated annealing. *Proteins*, 8(3), 1990.
- Vitaliy Y Gorbatyuk, Neil J Nosworthy, Scott A Robson, Naresh P S Bains, Mark W Maciejewski, Cris G Dos Remedios, and Glenn F King. Mapping the

- phosphoinositide-binding site on chick cofilin explains how pip2 regulates the cofilin-actin interaction. *Mol Cell*, 24(4), Nov 2006.
- J Gray, S Moughon, C Wang, O Schueler-Furman, B Kuhlman, C Rohl, and D Baker. Protein-protein docking with simultaneous optimization of rigid-body displacement and side-chain conformations. *J Mol Biol*, 331(1), 2003.
- Elena E Grintsevich, Sabrina A Benchaar, Dora Warshaviak, Pinmanee Boonthung, Frédéric Halgand, Julian P Whitelegge, Kym F Faull, Rachel R Ogorzalek Loo, David Sept, Joseph A Loo, and Emil Reisler. Mapping the cofilin binding site on yeast g-actin by chemical cross-linking. *J Mol Biol*, 377(2), Mar 2008.
- T Halgren, R Murphy, R Friesner, H Beard, L Frye, W Pollard, and J Banks. Glide: a new approach for rapid, accurate docking and scoring. 2. enrichment factors in database screening. *J Med Chem*, 47(7), 2004.
- M Hawkins, B Pope, S K Maciver, and A G Weeds. Human actin depolymerizing factor mediates a ph-sensitive destruction of actin filaments. *Biochemistry*, 32(38), Sep 1993.
- S M Hayden, P S Miller, A Brauweiler, and J R Bamberg. Analysis of the interactions of actin depolymerizing factor with g- and f-actin. *Biochemistry*, 32(38), Sep 1993.
- Emmanuèle Helfer, Elisa M Nevalainen, Perttu Naumanen, Stéphane Romero, Dominique Didry, Dominique Pantaloni, Pekka Lappalainen, and Marie-France Carlier. Mammalian twinfilin sequesters adp-g-actin and caps filament barbed ends: implications in motility. *EMBO J*, 25(6), Mar 2006.
- Maud Hertzog, Carine van Heijenoort, Dominique Didry, Martin Gaudier, Jérôme Coutant, Benoît Gigant, Gérard Didelot, Thomas Prémat, Marcel Knossow, Eric Guittet, and Marie-France Carlier. The beta-thymosin/wh2 domain; structural basis for the switch from inhibition to promotion of actin assembly. *Cell*, 117(5), May 2004.
- K C Holmes, D Popp, W Gebhard, and W Kabsch. Atomic model of the actin filament. *Nature*, 347(6288), Sep 1990.
- Kenneth C Holmes, Isabel Angert, F Jon Kull, Werner Jahn, and Rasmus R Schröder. Electron cryo-microscopy shows how strong binding of myosin to actin releases nucleotide. *Nature*, 425(6956), Sep 2003.
- Niu Huang, Brian K Shoichet, and John J Irwin. Benchmarking sets for molecular docking. *J Med Chem*, 49(23), Nov 2006.
- W Humphrey, A Dalke, and K Schulten. Vmd: visual molecular dynamics. *Journal of molecular graphics*, Jan 1996.

- J Irwin. Community benchmarks for virtual screening. *J Comput Aided Mol Des*, 22 (3-4), 2008.
- A Jain. Scoring functions for protein-ligand docking. *Curr Protein Pept Sci*, 7(5), 2006.
- Ajay N Jain. Virtual screening in lead discovery and optimization. *Curr Opin Drug Discov Devel*, 7(4), Jul 2004.
- G Jones, P Willett, and R Glen. A genetic algorithm for flexible molecular overlay and pharmacophore elucidation. *J Comput Aided Mol Des*, 9(6), 1995.
- W Kabsch and J Vandekerckhove. Structure and function of actin. *Annu Rev Biophys Biomol Struct*, 21, Jan 1992.
- W Kabsch, H G Mannherz, D Suck, E F Pai, and K C Holmes. Atomic structure of the actin:dnase i complex. *Nature*, 347(6288), Sep 1990.
- J K Amisha Kamal, Sabrina A Benchaar, Keiji Takamoto, Emil Reisler, and Mark R Chance. Three-dimensional structure of cofilin bound to monomeric actin derived by structural mass spectrometry data. *Proc Natl Acad Sci USA*, 104(19), May 2007.
- Sofia Yu Khaitlina and Hanna Strzelecka-Gołaszewska. Role of the dnase-i-binding loop in dynamic properties of actin filament. *Biophysical Journal*, 82(1 Pt 1), Jan 2002.
- Changhoon Kim and Byungkook Lee. Accuracy of structure-based sequence alignment of automatic methods. *BMC Bioinformatics*, 8, Jan 2007.
- E Kim, C J Miller, M Motoki, K Seguro, A Muhrad, and E Reisler. Myosin-induced changes in f-actin: fluorescence probing of subdomain 2 by dansyl ethylenediamine attached to gln-41. *Biophysical Journal*, 70(3), Mar 1996.
- E Kim, W Wriggers, M Phillips, K Kokabi, P A Rubenstein, and E Reisler. Cross-linking constraints on f-actin structure. *J Mol Biol*, 299(2), Jun 2000.
- Douglas B Kitchen, Hélène Decornez, John R Furr, and Jürgen Bajorath. Docking and scoring in virtual screening for drug discovery: methods and applications. *Nat Rev Drug Discov*, 3(11), Nov 2004.
- Fábio Klamt, Stéphanie Zdanov, Rodney L Levine, Ashley Pariser, Yaqin Zhang, Baolin Zhang, Li-Rong Yu, Timothy D Veenstra, and Emily Shacter. Oxidant-induced apoptosis is mediated by oxidation of the actin-regulatory protein cofilin. *Nat Cell Biol*, 11(10), Oct 2009.

- Martin Klemke, Guido H Wabnitz, Faustina Funke, Beate Funk, Henning Kirchgessner, and Yvonne Samstag. Oxidation of cofilin mediates t cell hyporesponsiveness under oxidative stress conditions. *Immunity*, 29(3), Sep 2008.
- Maria Kontoyianni, Prakash Madhav, Eric Suchanek, and William Seibel. Theoretical and practical considerations in virtual screening: a beaten field? *Curr Med Chem*, 15(2), Jan 2008.
- D S Kudryashov, V E Galkin, A Orlova, M Phan, E H Egelman, and E Reisler. Cofilin cross-bridges adjacent actin protomers and replaces part of the longitudinal f-actin interface. *J Mol Biol*, 358(3), May 2006.
- Hao Yuan Kueh, William M Briehner, and Timothy J Mitchison. Dynamic stabilization of actin filaments. *Proc Natl Acad Sci USA*, 105(43), Oct 2008.
- Jeffrey R Kuhn and Thomas D Pollard. Real-time measurements of actin filament polymerization by total internal reflection fluorescence microscopy. *Biophysical Journal*, 88(2), Feb 2005.
- T B Kuhn, P J Meberg, M D Brown, B W Bernstein, L S Minamide, J R Jensen, K Okada, E A Soda, and J R Bamberg. Regulating actin dynamics in neuronal growth cones by adf/cofilin and rho family gtpases. *J Neurobiol*, 44(2), Aug 2000.
- Thomas B Kuhn and James R Bamberg. Tropomyosin and adf/cofilin as collaborators and competitors. *Adv Exp Med Biol*, 644, Jan 2008.
- F Lanni, D L Taylor, and B R Ware. Fluorescence photobleaching recovery in solutions of labeled actin. *Biophysical Journal*, 35(2), Aug 1981.
- P Lappalainen, E V Fedorov, A A Fedorov, S C Almo, and D G Drubin. Essential functions and actin-binding surfaces of yeast cofilin revealed by systematic mutagenesis. *EMBO J*, 16(18), Sep 1997.
- P Lappalainen, M M Kessels, M J Cope, and D G Drubin. The adf homology (adf-h) domain: a highly exploited actin-binding module. *Mol Biol Cell*, 9(8), Aug 1998.
- A Leach, B Shoichet, and C Peishoff. Prediction of protein-ligand interactions. docking and scoring: successes and gaps. *J Med Chem*, 49(20), 2006.
- Andrew Leach. *Molecular Modelling: Principles and Applications (2nd Edition)*. 2001.
- M Lensink, R Mendez, and S Wodak. Docking and scoring protein complexes: Capri 3rd edition. *Proteins*, 69(4), 2007.
- Meng-Chi Lin, Brian J Galletta, David Sept, and John A Cooper. Overlapping and distinct functions for cofilin, coronin and aip1 in actin dynamics in vivo. *J Cell Sci*, 123(Pt 8), Apr 2010.

- S K Maciver, B J Pope, S Whytock, and A G Weeds. The effect of two actin depolymerizing factors (adf/cofilins) on actin filament turnover: ph sensitivity of f-actin binding by human adf, but not of *acanthamoeba* actophorin. *Eur J Biochem*, 256(2), Sep 1998.
- Michael T Maloney, Laurie S Minamide, Andrew W Kinley, Judith A Boyle, and James R Bamberg. Beta-secretase-cleaved amyloid precursor protein accumulates at actin inclusions induced in neurons by stress or amyloid beta: a feedforward mechanism for alzheimer's disease. *J Neurosci*, 25(49), Dec 2005.
- Hans Georg Mannherz, Edda Ballweber, Marco Galla, Sylvie Villard, Claude Granier, Clemens Steegborn, Anja Schmidtman, Kornelia Jaquet, Brian Pope, and Alan G Weeds. Mapping the adf/cofilin binding site on monomeric actin by competitive cross-linking and peptide array: evidence for a second binding site on monomeric actin. *J Mol Biol*, 366(3), Feb 2007.
- S Marrink and A de Vries. . . . Coarse grained model for semiquantitative lipid simulations. *J. Phys. Chem. B*, Jan 2004.
- Brannon R McCullough, Laurent Blanchoin, Jean-Louis Martiel, and EM De la Cruz. Cofilin increases the bending flexibility of actin filaments: implications for severing and cell mechanics. *J Mol Biol*, 381(3), Sep 2008.
- A McGough and W Chiu. Adf/cofilin weakens lateral contacts in the actin filament. *J Mol Biol*, 291(3), Aug 1999.
- A McGough, B Pope, W Chiu, and A Weeds. Cofilin changes the twist of f-actin: implications for actin filament dynamics and cellular function. *J Cell Biol*, 138(4), Aug 1997.
- P J McLaughlin, J T Gooch, H G Mannherz, and A G Weeds. Structure of gelsolin segment 1-actin complex and the mechanism of filament severing. *Nature*, 364(6439), Aug 1993.
- P J Meberg, S Ono, L S Minamide, M Takahashi, and J R Bamberg. Actin depolymerizing factor and cofilin phosphorylation dynamics: response to signals that regulate neurite extension. *Cell Motil Cytoskeleton*, 39(2), Jan 1998.
- R Mendez, R Leplae, M Lensink, and S Wodak. Assessment of capri predictions in rounds 3-5 shows progress in docking procedures. *Proteins*, 60(2), 2005.
- Yanghong Meng, Hisaaki Takahashi, Jinsong Meng, Yu Zhang, Guijin Lu, Suhail Asrar, Toshikazu Nakamura, and Zhengping Jia. Regulation of adf/cofilin phosphorylation and synaptic function by lim-kinase. *Neuropharmacology*, 47(5), Oct 2004.

- Alphée Michelot, Julien Berro, Christophe Guérin, Rajaa Boujemaa-Paterski, Christopher J Staiger, Jean-Louis Martiel, and Laurent Blanchoin. Actin-filament stochastic dynamics mediated by adf/cofilin. *Current Biology*, 17(10), May 2007.
- L S Minamide, A M Striegl, J A Boyle, P J Meberg, and J R Bamberg. Neurodegenerative stimuli induce persistent adf/cofilin-actin rods that disrupt distal neurite function. *Nat Cell Biol*, 2(9), Sep 2000.
- Laurie S Minamide, Sankar Maiti, Judith A Boyle, Richard C Davis, Judith A Copping, Yunhe Bao, Timothy Y Huang, John Yates, Gary M Bokoch, and James R Bamberg. Isolation and characterization of cytoplasmic cofilin-actin rods. *J Biol Chem*, 285(8), Feb 2010.
- N Moitessier, P Englebienne, D Lee, J Lawandi, and C R Corbeil. Towards the development of universal, fast and highly accurate docking/scoring methods: a long way to go. *Br J Pharmacol*, 153 Suppl 1, Mar 2008.
- K Moriyama and I Yahara. Two activities of cofilin, severing and accelerating directional depolymerization of actin filaments, are affected differentially by mutations around the actin-binding helix. *EMBO J*, 18(23), Dec 1999.
- K Moriyama, N Yonezawa, H Sakai, I Yahara, and E Nishida. Mutational analysis of an actin-binding site of cofilin and characterization of chimeric proteins between cofilin and destrin. *J Biol Chem*, 267(11), Apr 1992.
- K Moriyama, K Iida, and I Yahara. Phosphorylation of ser-3 of cofilin regulates its essential function on actin. *Genes Cells*, 1(1), Jan 1996.
- Kenji Moriyama and Ichiro Yahara. The actin-severing activity of cofilin is exerted by the interplay of three distinct sites on cofilin and essential for cell viability. *Biochem J*, 365(Pt 1), Jul 2002.
- James B Moseley, Kyoko Okada, Heath I Balcer, David R Kovar, Thomas D Pollard, and Bruce L Goode. Twinfilin is an actin-filament-severing protein and promotes rapid turnover of actin structures in vivo. *J Cell Sci*, 119(Pt 8), Apr 2006.
- A Muhrad, P Cheung, B C Phan, C Miller, and E Reisler. Dynamic properties of actin. structural changes induced by beryllium fluoride. *J Biol Chem*, 269(16), Apr 1994.
- Andras Muhrad, Dmitry Pavlov, Y Michael Peyser, and Emil Reisler. Inorganic phosphate regulates the binding of cofilin to actin filaments. *FEBS J*, 273(7), Apr 2006.
- M Nelson, W Humphrey, and A Gursoy. . . . Namd: a parallel, object-oriented molecular dynamics program. . . . *Journal of High . . .*, Jan 1996.

- E Nishida, S Maekawa, and H Sakai. Cofilin, a protein in porcine brain that binds to actin filaments and inhibits their interactions with myosin and tropomyosin. *Biochemistry*, 23(22), Oct 1984.
- Toshiro Oda, Mitsusada Iwasa, Tomoki Aihara, Yuichiro Maéda, and Akihiro Narita. The nature of the globular- to fibrous-actin transition. *Nature*, 457(7228), Jan 2009.
- P J Ojala, V Paavilainen, and P Lappalainen. Identification of yeast cofilin residues specific for actin monomer and pip2 binding. *Biochemistry*, 40(51), Dec 2001.
- Pauli J Ojala, Ville O Paavilainen, Maria K Vartiainen, Roman Tuma, Alan G Weeds, and Pekka Lappalainen. The two adf-h domains of twinfilin play functionally distinct roles in interactions with actin monomers. *Mol Biol Cell*, 13(11), Nov 2002.
- Voytek Okreglak and David G Drubin. Cofilin recruitment and function during actin-mediated endocytosis dictated by actin nucleotide state. *J Cell Biol*, 178(7), Sep 2007.
- Shoichiro Ono. Regulation of actin filament dynamics by actin depolymerizing factor/cofilin and actin-interacting protein 1: new blades for twisted filaments. *Biochemistry*, 42(46), Nov 2003.
- A Orlova and E H Egelman. A conformational change in the actin subunit can change the flexibility of the actin filament. *J Mol Biol*, 232(2), Jul 1993.
- Albina Orlova, Alexander Shvetsov, Vitold E Galkin, Dmitry S Kudryashov, Peter A Rubenstein, Edward H Egelman, and Emil Reisler. Actin-destabilizing factors disrupt filaments by means of a time reversal of polymerization. *Proc Natl Acad Sci USA*, 101(51), Dec 2004.
- Matthew Oser and John Condeelis. The cofilin activity cycle in lamellipodia and invadopodia. *J Cell Biochem*, 108(6), Dec 2009.
- L R Otterbein, P Graceffa, and R Dominguez. The crystal structure of uncomplexed actin in the adp state. *Science*, 293(5530), Jul 2001.
- C Owen and D DeRosier. A 13-a map of the actin-scrutin filament from the limulus acrosomal process. *J Cell Biol*, 123(2), Oct 1993.
- Ville O Paavilainen, Enni Bertling, Sandra Falck, and Pekka Lappalainen. Regulation of cytoskeletal dynamics by actin-monomer-binding proteins. *Trends in Cell Biology*, 14(7), Jul 2004.
- Ville O Paavilainen, Maarit Hellman, Emmanuèle Helfer, Miia Bovellan, Arto Annala, Marie-France Carlier, Perttu Permi, and Pekka Lappalainen. Structural basis and evolutionary origin of actin filament capping by twinfilin. *Proc Natl Acad Sci USA*, 104(9), Feb 2007.

- Ville O Paavilainen, Esko Oksanen, Adrian Goldman, and Pekka Lappalainen. Structure of the actin-depolymerizing factor homology domain in complex with actin. *J Cell Biol*, 182(1), Jul 2008.
- Dmitry Pavlov, Andras Muhrad, John Cooper, Martin Wear, and Emil Reisler. Severing of f-actin by yeast cofilin is ph-independent. *Cell Motil Cytoskeleton*, 63(9), Sep 2006.
- Dmitry Pavlov, Andras Muhrad, John Cooper, Martin Wear, and Emil Reisler. Actin filament severing by cofilin. *J Mol Biol*, 365(5), Feb 2007.
- E Pettersen, T Goddard, C Huang, G Couch, D Greenblatt, E Meng, and T Ferrin. Ucsf chimera—a visualization system for exploratory research and analysis. *J Comput Chem*, 25(13), 2004.
- Jim Pfaendtner, EM De la Cruz, and Gregory A Voth. Actin filament remodeling by actin depolymerization factor/cofilin. *Proc Natl Acad Sci USA*, 107(16), Apr 2010.
- J Pfannstiel, M Cyrklaff, A Habermann, S Stoeva, G Griffiths, R Shoeman, and H Faulstich. Human cofilin forms oligomers exhibiting actin bundling activity. *J Biol Chem*, 276(52), Dec 2001.
- T D Pollard, S Almo, S Quirk, V Vinson, and E E Lattman. Structure of actin binding proteins: insights about function at atomic resolution. *Annu Rev Cell Biol*, 10, Jan 1994.
- Thomas D Pollard and Gary G Borisy. Cellular motility driven by assembly and disassembly of actin filaments. *Cell*, 112(4), Feb 2003.
- Thomas D Pollard and John A Cooper. Actin, a central player in cell shape and movement. *Science*, 326(5957), Nov 2009.
- B J Pope, S M Gonsior, S Yeoh, A McGough, and A G Weeds. Uncoupling actin filament fragmentation by cofilin from increased subunit turnover. *J Mol Biol*, 298(4), May 2000.
- Brian J Pope, Karen M Zierler-Gould, Ronald Kühne, Alan G Weeds, and Linda J Ball. Solution structure of human cofilin: actin binding, ph sensitivity, and relationship to actin-depolymerizing factor. *J Biol Chem*, 279(6), Feb 2004.
- Y A Puius, N M Mahoney, and S C Almo. The modular structure of actin-regulatory proteins. *Curr Opin Cell Biol*, 10(1), Feb 1998.
- M Rarey, B Kramer, and T Lengauer. Time-efficient docking of flexible ligands into active sites of proteins. *Proc Int Conf Intell Syst Mol Biol*, 3, 1995.

- D Ritchie. Recent progress and future directions in protein-protein docking. *Curr Protein Pept Sci*, 9(1), 2008.
- R C Robinson, K Turbedsky, D A Kaiser, J B Marchand, H N Higgs, S Choe, and T D Pollard. Crystal structure of arp2/3 complex. *Science*, 294(5547), Nov 2001.
- A A Rodal, J W Tetreault, P Lappalainen, D G Drubin, and D C Amberg. Aip1p interacts with cofilin to disassemble actin filaments. *J Cell Biol*, 145(6), Jun 1999.
- Akansha Saxena, Diana Wong, Karthikeyan Diraviyam, and David Sept. The basic concepts of molecular modeling. *Meth Enzymol*, 467, Jan 2009.
- O Schueler-Furman, C Wang, and D Baker. Progress in protein-protein docking: atomic resolution predictions in the capri experiment using rosettaDock with an improved treatment of side-chain flexibility. *Proteins*, 60(2), 2005a.
- O Schueler-Furman, C Wang, P Bradley, K Misura, and D Baker. Progress in modeling of protein structures and interactions. *Science*, 310(5748), 2005b.
- T Schulz-Gasch and M Stahl. Binding site characteristics in structure-based virtual screening: evaluation of current docking tools. *J Mol Model*, 9(1), 2003.
- N Selve and A Wegner. Rate of treadmilling of actin filaments in vitro. *J Mol Biol*, 187(4), Feb 1986.
- A Shih, A Arkhipov, P Freddolino, and K Schulten. Coarse grained protein lipid model with application to lipoprotein particles. *J. Phys. Chem. B*, Jan 2006a.
- Amy Y Shih, Anton Arkhipov, Peter L Freddolino, and Klaus Schulten. Coarse grained protein-lipid model with application to lipoprotein particles. *The Journal of Physical Chemistry B*, 110(8), Mar 2006b.
- AY Shih, A Arkhipov, PL Freddolino, SG Sligar, and K Schulten. Assembly of lipids and proteins into lipoprotein particles. *J. Phys. Chem. ...*, Jan 2007.
- B Shoichet. Virtual screening of chemical libraries. *Nature*, 432(7019), 2004.
- Alexander Shvetsov, Vitold E Galkin, Albina Orlova, Martin Phillips, Sarah E Bergeron, Peter A Rubenstein, Edward H Egelman, and Emil Reisler. Actin hydrophobic loop 262-274 and filament nucleation and elongation. *J Mol Biol*, 375(3), Jan 2008.
- Xiaoyan Song, Xiaoming Chen, Hideki Yamaguchi, Ghassan Mouneimne, John S Condeelis, and Robert J Eddy. Initiation of cofilin activity in response to egf is uncoupled from cofilin phosphorylation and dephosphorylation in carcinoma cells. *J Cell Sci*, 119(Pt 14), Jul 2006.

- S Sousa, P Fernandes, and M Ramos. Protein-ligand docking: current status and future challenges. *Proteins*, 65(1), 2006.
- H Strzelecka-Gołaszewska, M Mossakowska, A Woźniak, J Moraczewska, and H Nakayama. Long-range conformational effects of proteolytic removal of the last three residues of actin. *Biochem J*, 307 (Pt 2), Apr 1995.
- R L Tellam. Gelsolin inhibits nucleotide exchange from actin. *Biochemistry*, 25(19), Sep 1986.
- R Tiwari, K Mahasenan, R Pavlovicz, C Li, and W Tjarks. Carborane clusters in computational drug design: a comparative docking evaluation using autodock, flexx, glide, and surflex. *J Chem Inf Model*, 49(6), 2009.
- Marleen Van Troys, Lynn Huyck, Shirley Leyman, Stien Dhaese, Joël Vandekerckhove, and Christophe Ampe. Ins and outs of adf/cofilin activity and regulation. *Eur J Cell Biol*, 87(8-9), Sep 2008.
- S Vajda and D Kozakov. Convergence and combination of methods in protein-protein docking. *Curr Opin Struct Biol*, 19(2), 2009.
- Jacco van Rheenen, Xiaoyan Song, Wies van Roosmalen, Michael Cammer, Xiaoming Chen, Vera Desmarais, Shu-Chin Yip, Jonathan M Backer, Robert J Eddy, and John S Condeelis. Egf-induced pip2 hydrolysis releases and activates cofilin locally in carcinoma cells. *J Cell Biol*, 179(6), Dec 2007.
- J Voigt, B Bienfait, S Wang, and M Nicklaus. Comparison of the nci open database with seven large chemical structural databases. *J Chem Inf Comput Sci*, 41(3), 2001.
- G Warren, C Andrews, A Capelli, B Clarke, J LaLonde, M Lambert, M Lindvall, N Nevins, S Semus, S Senger, G Tedesco, I Wall, J Woolven, C Peishoff, and M Head. A critical assessment of docking programs and scoring functions. *J Med Chem*, 49(20), 2006.
- K F Wertman, D G Drubin, and D Botstein. Systematic mutational analysis of the yeast act1 gene. *Genetics*, 132(2), Oct 1992.
- Ineka T Whiteman, Othon L Gervasio, Karen M Cullen, Gilles J Guillemin, Erica V Jeong, Paul K Witting, Shane T Antao, Laurie S Minamide, James R Bamberg, and Claire Goldsbury. Activated actin-depolymerizing factor/cofilin sequesters phosphorylated microtubule-associated protein during the assembly of alzheimer-like neuritic cytoskeletal striations. *J Neurosci*, 29(41), Oct 2009.
- W Wriggers, J X Tang, T Azuma, P W Marks, and P A Janmey. Cofilin and gelsolin segment-1: molecular dynamics simulation and biochemical analysis predict a similar actin binding mode. *J Mol Biol*, 282(5), Oct 1998.

- N Yang, O Higuchi, K Ohashi, K Nagata, A Wada, K Kangawa, E Nishida, and K Mizuno. Cofilin phosphorylation by lim-kinase 1 and its role in rac-mediated actin reorganization. *Nature*, 393(6687), Jun 1998.
- Sharon Yeoh, Brian Pope, Hans G Mannherz, and Alan Weeds. Determining the differences in actin binding by human adf and cofilin. *J Mol Biol*, 315(4), Jan 2002.
- N Yonezawa, E Nishida, and H Sakai. pH control of actin polymerization by cofilin. *J Biol Chem*, 260(27), Nov 1985.
- N Yonezawa, E Nishida, K Iida, I Yahara, and H Sakai. Inhibition of the interactions of cofilin, destrin, and deoxyribonuclease i with actin by phosphoinositides. *J Biol Chem*, 265(15), May 1990.
- V Zoete, A Grosdidier, and O Michielin. Docking, virtual high throughput screening and in silico fragment-based drug design. *J Cell Mol Med*, 13(2), 2009.

Curriculum vitae

Diana Yi Fei Wong

dianaywong@gmail.com

Degrees

- Bioengineering Engineering. University of California, Berkeley. B.S. May 2004.
- Biomedical Engineering. Washington University in St Louis, St. Louis, MO. M.S. December 2006.
- Biomedical Engineering. Washington University in St Louis, St. Louis, MO. Ph.D. May 2011.

Employment

- Visiting Research Investigator. University of Michigan, Ann Arbor, MI. 2009–2011.
- Research Assistant. University of California, San Francisco, CA. 2003.
- Research Assistant. University of California, Berkeley/San Francisco, CA. 2001–2002.

Leadership and Service

- Public Affairs Committee Member, Biophysical Society, 2010–2012.
- Committee Member, Center for Computational Biology (CCB) Colloquium Series at Washington University, 2008–2009.
- Children's Aikido Class Teaching Assistant, St. Louis Ki Society, 2009.
- Undergraduate Study Committee Student Representative, UC Berkeley College of Engineering, 2003-2004.
- Bioengineering Curriculum Committee Student Member, UC Berkeley Bioengineering Department, 2002-2004.

- Vice Chair and Office of Public Information Director, Berkeley Model United Nations, 2000-2004.
- Treasurer and EMBS 2004 San Francisco conference student representative, Engineers in Medicine and Biology Society (EMBS), 2001-2004.
- High School Outreach Officer, Engineers' Joint Council, 2002-2003.
- Board of Directors Member and Administrative Committee Representative, University Students' Cooperative Association (USCA), 2003.

Teaching and Mentoring

- Substitute Lecturer. Washington University in St. Louis. 2007-2009.
- Scholarship Advisor. Northern California Scholarship Foundation (NCSF). 2004-2008.
- Teaching Assistant. Washington University in St. Louis. 2006.

Awards

- National Science Foundation Graduate Research Fellow (NSF GRFP), 2005.
- IEEE 4th International Summer School on Biocomplexity from System to Gene Scholarship, 2004.
- Cal Alumni Leadership Scholarship, 2002-03, 2003-04.
- Society of Women Engineers Scholarships, 2000, 2002.
- Chinese American Institute of Engineers and Scientists Scholarship, 2001.
- Northern California Scholarship Foundation Scholar (NCSF), 2000-2004.

Publications

D.Y. Wong and D. Sept. "The Interaction of Cofilin with the Actin Filament." (Submitted)

D.Y. Wong and D. Sept. "Insights of Twist by Coarse Grain Modeling of Cofilin and Actin Filaments." (In preparation)

A. Saxena, **D. Wong**, K. Diraviyam, and D. Sept. “The Basic Concepts of Molecular Modeling”, *Methods Enzymol.* 2009; 467:307- 34.

Conferences

D.Y. Wong, D. Sept. “Observations of twist and disorder in F-actin from cofilin binding.” Abstract presented at Biophysical Society Meeting, Baltimore, MD, March 2011.

D.Y. Wong, D. Sept. “Molecular Interaction of Cofilin with F-actin.” Abstract presented at Biophysical Society Meeting, San Francisco, CA, March 2010.

D.Y. Wong, D. Sept. “Structural Binding Model of Cofilin and F-actin.” Abstract presented at Biophysical Society Meeting, Boston, MA, March 2009.

D.Y. Wong, D. Sept. “Energy calculations using a polarizable force field.” Abstract presented at Biophysical Society Meeting, Long Beach, CA, Feb 2008 and Biomedical Engineering Society (BMES), Saint Louis, MO, Oct 2008.

D.Y. Wong, D. Sept. “Reparameterizing scoring functions for protein-protein complexes.” Abstract presented at Biophysical Society Meeting, Baltimore, MD, March 2007.

D.Y. Wong, A. Qutub, and C. A. Hunt. “Modeling Transport Kinetics with Star-Logo.” Proceedings of the 26th Annual International Conference IEEE Engineering in Medicine and Biology Society (EMBS), San Francisco, CA, Sept 2004.

M. Keehner, **D. Wong**, and F. Tendick, “Effects of Viewing Angle, Spatial Ability, and Sight of Own Hand on Accuracy of Movements Performed Under Simulated Laparoscopic Conditions.” Proc. Human Factors and Ergonomics Society Annual Meeting, New Orleans, LA, Sept 2004.

Professional Societies

Biophysical Society

Biomedical Engineering Society

May 2011

Interactions of Cofilin & F-actin, Wong, Ph.D. 2011